International Journal of Physical Sciences

Volume 8 Number 34 16 September, 2013

ISSN 1992-1950

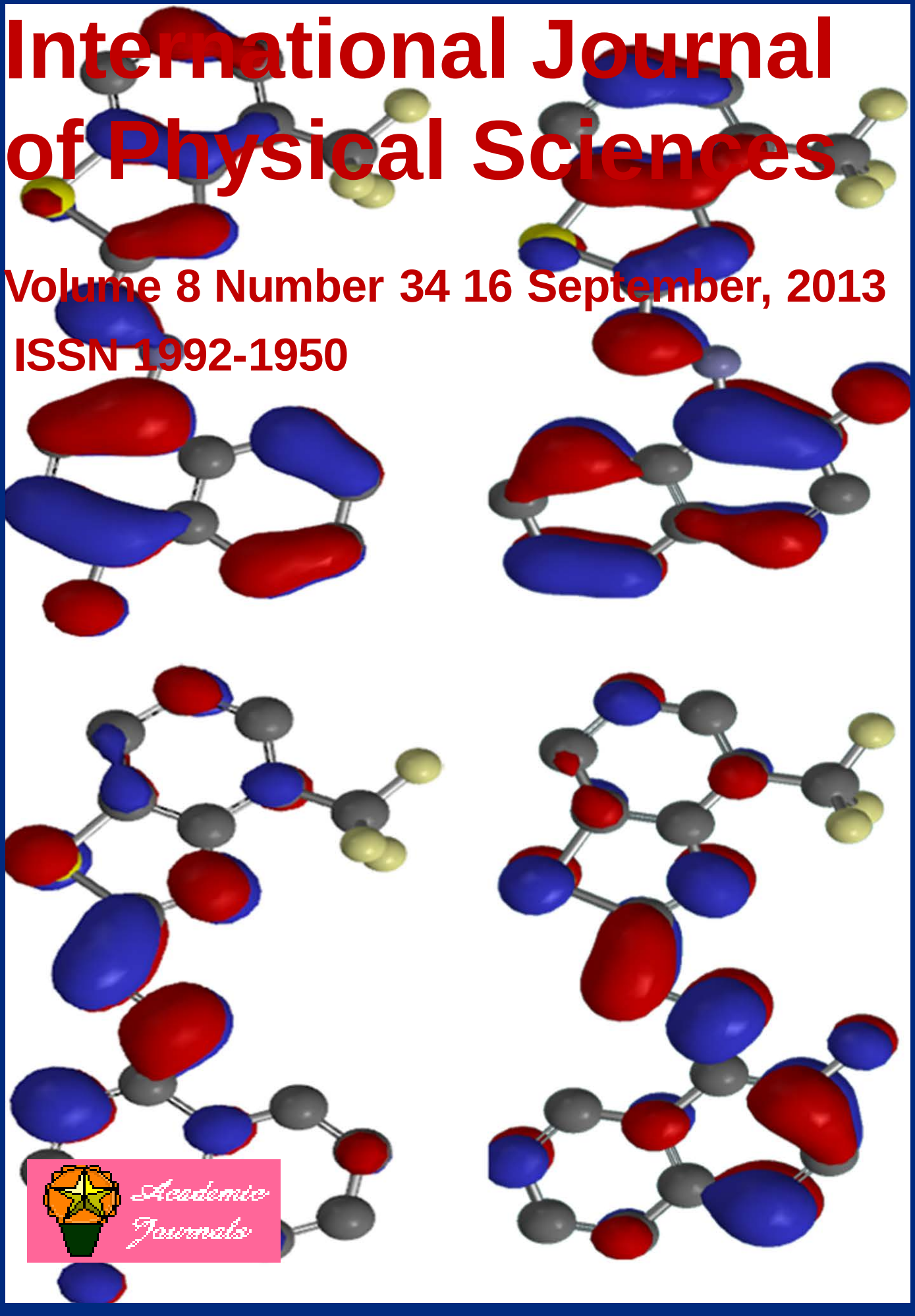

Academic Journals

ABOUT IJPS

The **International Journal of Physical Sciences (IJPS)** is published weekly (one volume per year) by Academic Journals.

International Journal of Physical Sciences (IJPS) is an open access journal that publishes high-quality solicited and unsolicited articles, in English, in all Physics and chemistry including artificial intelligence, neural processing, nuclear and particle physics, geophysics, physics in medicine and biology, plasma physics, semiconductor science and technology, wireless and optical communications, materials science, energy and fuels, environmental science and technology, combinatorial chemistry, natural products, molecular therapeutics, geochemistry, cement and concrete research, metallurgy, crystallography and computer-aided materials design. All articles published in IJPS are peer-reviewed.

Submission of Manuscript

Submit manuscripts as e-mail attachment to the Editorial Office at: ijps@academicjournals.org. A manuscript number will be mailed to the corresponding author shortly after submission.

For all other correspondence that cannot be sent by e-mail, please contact the editorial office (at ijps@academicjournals.org).

The International Journal of Physical Sciences will only accept manuscripts submitted as e-mail attachments.

Please read the **Instructions for Authors** before submitting your manuscript. The manuscript files should be given the last name of the first author.

Editorial Board

Instructions for Author

Electronic submission of manuscripts is strongly encouraged, provided that the text, tables, and figures are included in a single Microsoft Word file (preferably in Arial font).

The **cover letter** should include the corresponding author's full address and telephone/fax numbers and should be in an e-mail message sent to the Editor, with the file, whose name should begin with the first author's surname, as an attachment.

Article Types

Three types of manuscripts may be submitted:

Regular articles: These should describe new and carefully confirmed findings, and experimental procedures should be given in sufficient detail for others to verify the work. The length of a full paper should be the minimum required to describe and interpret the work clearly.

Short Communications: A Short Communication is suitable for recording the results of complete small investigations or giving details of new models or hypotheses, innovative methods, techniques or apparatus. The style of main sections need not conform to that of full-length papers. Short communications are 2 to 4 printed pages (about 6 to 12 manuscript pages) in length.

Reviews: Submissions of reviews and perspectives covering topics of current interest are welcome and encouraged. Reviews should be concise and no longer than 4-6 printed pages (about 12 to 18 manuscript pages). Reviews are also peer-reviewed.

Review Process

All manuscripts are reviewed by an editor and members of the Editorial Board or qualified outside reviewers. Authors cannot nominate reviewers. Only reviewers randomly selected from our database with specialization in the subject area will be contacted to evaluate the manuscripts. The process will be blind review.

Decisions will be made as rapidly as possible, and the journal strives to return reviewers' comments to authors as fast as possible. The editorial board will re-review manuscripts that are accepted pending revision. It is the goal of the IJPS to publish manuscripts within weeks after submission.

Regular articles

All portions of the manuscript must be typed double-spaced and all pages numbered starting from the title page.

The Title should be a brief phrase describing the contents of the paper. The Title Page should include the authors' full names and affiliations, the name of the corresponding author along with phone, fax and E-mail information. Present addresses of authors should appear as a footnote.

The Abstract should be informative and completely self-explanatory, briefly present the topic, state the scope of the experiments, indicate significant data, and point out major findings and conclusions. The Abstract should be 100 to 200 words in length.. Complete sentences, active verbs, and the third person should be used, and the abstract should be written in the past tense. Standard nomenclature should be used and abbreviations should be avoided. No literature should be cited.

Following the abstract, about 3 to 10 key words that will provide indexing references should be listed.

A list of non-standard **Abbreviations** should be added. In general, non-standard abbreviations should be used only when the full term is very long and used often. Each abbreviation should be spelled out and introduced in parentheses the first time it is used in the text. Only recommended SI units should be used. Authors should use the solidus presentation (mg/ml). Standard abbreviations (such as ATP and DNA) need not be defined.

The Introduction should provide a clear statement of the problem, the relevant literature on the subject, and the proposed approach or solution. It should be understandable to colleagues from a broad range of scientific disciplines.

Materials and methods should be complete enough to allow experiments to be reproduced. However, only truly new procedures should be described in detail; previously published procedures should be cited, and important modifications of published procedures should be mentioned briefly. Capitalize trade names and include the manufacturer's name and address. Subheadings should be used. Methods in general use need not be described in detail.

Results should be presented with clarity and precision. The results should be written in the past tense when describing findings in the authors' experiments. Previously published findings should be written in the present tense. Results should be explained, but largely without referring to the literature. Discussion, speculation and detailed interpretation of data should not be included in the Results but should be put into the Discussion section.

The Discussion should interpret the findings in view of the results obtained in this and in past studies on this topic. State the conclusions in a few sentences at the end of the paper. The Results and Discussion sections can include subheadings, and when appropriate, both sections can be combined.

The Acknowledgments of people, grants, funds, etc should be brief.

Tables should be kept to a minimum and be designed to be as simple as possible. Tables are to be typed double-spaced throughout, including headings and footnotes. Each table should be on a separate page, numbered consecutively in Arabic numerals and supplied with a heading and a legend. Tables should be self-explanatory without reference to the text. The details of the methods used in the experiments should preferably be described in the legend instead of in the text. The same data should not be presented in both table and graph form or repeated in the text.

Figure legends should be typed in numerical order on a separate sheet. Graphics should be prepared using applications capable of generating high resolution GIF, TIFF, JPEG or Powerpoint before pasting in the Microsoft Word manuscript file. Tables should be prepared in Microsoft Word. Use Arabic numerals to designate figures and upper case letters for their parts (Figure 1). Begin each legend with a title and include sufficient description so that the figure is understandable without reading the text of the manuscript. Information given in legends should not be repeated in the text.

References: In the text, a reference identified by means of an author‘s name should be followed by the date of the reference in parentheses. When there are more than two authors, only the first author‘s name should be mentioned, followed by ’et al‘. In the event that an author cited has had two or more works published during the same year, the reference, both in the text and in the reference list, should be identified by a lower case letter like ’a‘ and ’b‘ after the date to distinguish the works.

Examples:

Abayomi (2000), Agindotan et al. (2003), (Kelebeni, 1983), (Usman and Smith, 1992), (Chege, 1998; 1987a,b; Tijani, 1993,1995), (Kumasi et al., 2001)

References should be listed at the end of the paper in alphabetical order. Articles in preparation or articles submitted for publication, unpublished observations, personal communications, etc. should not be included in the reference list but should only be mentioned in the article text (e.g., A. Kingori, University of Nairobi, Kenya, personal communication). Journal names are abbreviated according to Chemical Abstracts. Authors are fully responsible for the accuracy of the references.

Examples:

Ogunseitan OA (1998). Protein method for investigating mercuric reductase gene expression in aquatic environments. Appl. Environ. Microbiol. 64:695-702.

Gueye M, Ndoye I, Dianda M, Danso SKA, Dreyfus B (1997). Active N2 fixation in several Faidherbia albida provenances. Ar. Soil Res. Rehabil. 11:63-70.

Charnley AK (1992). Mechanisms of fungal pathogenesis in insects with particular reference to locusts. In: Lomer CJ, Prior C (eds) Biological Controls of Locusts and Grasshoppers: Proceedings of an international workshop held at Cotonou, Benin. Oxford: CAB International, pp 181-190.

Mundree SG, Farrant JM (2000). Some physiological and molecular insights into the mechanisms of desiccation tolerance in the resurrection plant Xerophyta viscasa Baker. In Cherry et al. (eds) Plant tolerance to abiotic stresses in Agriculture: Role of Genetic Engineering, Kluwer Academic Publishers, Netherlands, pp 201-222.

Short Communications

Short Communications are limited to a maximum of two figures and one table. They should present a complete study that is more limited in scope than is found in full-length papers. The items of manuscript preparation listed above apply to Short Communications with the following differences: (1) Abstracts are limited to 100 words; (2) instead of a separate Materials and Methods section, experimental procedures may be incorporated into Figure Legends and Table footnotes; (3) Results and Discussion should be combined into a single section.

Proofs and Reprints: Electronic proofs will be sent (e-mail attachment) to the corresponding author as a PDF file. Page proofs are considered to be the final version of the manuscript. With the exception of typographical or minor clerical errors, no changes will be made in the manuscript at the proof stage.

International Journal of Physical Sciences

Table of Contents: Volume 8 Number 34 16 September, 2013

ARTICLES

academicJournals

Vol. 8(34), pp. 1694-1702, 16 September, 2013
DOI: 10.5897/IJPS11.1327
ISSN 1992 - 1950 © 2013 Academic Journals
http://www.academicjournals.org/IJPS

International Journal of Physical Sciences

Review

Structural health monitoring and damage assessment Part I: A critical review of approaches and methods

Burcu Gunes[1] and Oguz Gunes[2]*

[1]Department Civil of Engineering, Atilim University, Ankara, Turkey.
[2]Department Civil of Engineering, Cankaya University, Ankara, Turkey.

Accepted 5 December, 2011

Aging and deterioration of existing structures and the need for rapid assessment and evaluation of these structures for hazard mitigation have significantly expanded the research efforts in the field of structural health monitoring (SHM). SHM involves monitoring of a structure using periodically sampled measurements, extraction of damage sensitive features from these measurements, and assessment of the current health state/integrity of the system. Extraction of damage signatures that allows one to distinguish between the undamaged and the damaged structure from the measured vibration response is the area of SHM that receives the most attention. This paper presents a critical review of the damage assessment methodologies based on the research and applications reported in the literature. Challenges and research gaps in SHM are emphasized. These challenges include optimization of the number and location of sensors, identification of features sensitive to small damage levels, ability to discriminate changes in these features caused by damage from those caused by changing environmental or test conditions, and development of statistical methods to discriminate features from structures in undamaged and damaged states. A companion paper presents an application on the vibration data obtained from the ASCE benchmark structure.

Key words: Vibration based structural health monitoring, global methods, damage assessment.

INTRODUCTION

Structural health monitoring (SHM) is the process of implementing a damage identification strategy for civil infrastructures. Damage identification problem involves detection, localization and assessment of the extent of damage in a structure so that its remaining life can be predicted and possibly extended. SHM encompasses both local and global methods of damage identification. The local methods include visual inspections and non-destructive evaluation tools such as acoustic emission, ultrasonic, magnetic particle inspection, radiography and eddy current. All these techniques, however, require apriori localization of the damaged zone and easy access to the portion of the structure under inspection. As an alternative that overcomes these limitations, global vibration based methods have been widely developed over the years (Farrar et al., 1994; Salawu, 1997; Doebling et al., 1998; Sohn et al., 2003; Chang et al., 2003; Farrar and Worden, 2007). SHM based on vibration measurements involves temporal observation of a structure using periodically sampled vibration measurements, extraction of damage sensitive features from these measurements and assessment of the current health state/integrity of the system. The basic premise of the vibration-based techniques is that the vibration characteristics or the so-called modal parameters (frequencies, mode shapes and modal damping) are functions of the physical properties of the structure (mass, energy dissipation mechanisms and stiffness) and changes in these physical properties cause changes in the modal properties. This postulation, however,

*Corresponding author. E-mail: ogunes@cankaya.edu.tr.

is compromised by the fact that temperature changes, moisture and other environmental factors also produce changes in dynamic characteristics. If the causes of changes in dynamic characteristics other than damage are considered to be noise in the measurement, then the changes due to damage must be significantly larger than the noise in order for the techniques to work. Usually four different levels of damage identification are studied (Rytter, 1993): damage detection (Level 1), damage localization (Level 2), damage quantification (Level 3), and prediction of the remaining service life of the damaged structure, or the acceptable load level to reach the intended service life (Level 4).

The scope of the paper is limited to the global damage strategies based on measured vibration data, excluding local SHM techniques and damage prognosis. The SHM applications using these strategies reported in the literature are summarized with the emphasis on the challenges and research gaps between the theory and SHM practice.

DAMAGE IDENTIFICATION APPROACHES

Most of the existing global damage identification methods can be classified into two groups: model-based and non-model or feature-based methods. The model-based methods are essentially model updating procedures in which the mathematical model or the physical parameters of a structure is calibrated or updated using vibration measurements from the physical structure (Zimmerman and Kaouk, 1992; Fritzen et al., 1998). Analytical sensitivities of response parameters to changes in physical properties are used to update modeling assumptions, physical sizing, elastic moduli, etc. The feature-based approaches detect structural changes by detecting damage features in the measured data without the need for an analytical model of the structure. The main task here is the extraction of damage features sensitive to structural changes so that damage can be identified from the measured vibration response of civil engineering structures.

The civil engineering community has been studying the vibration-based damage assessment of bridge and building structures since the early 1980s. The ASCE Benchmark structure of a 4-story 2-bay by 2-bay steel frame scale-model structure built and tested in the Earthquake Engineering Research Laboratory at the University of British Columbia, Canada (Dyke et al., 2003); the 2-story 8 by 9 m building structure of the STEELQUAKE project constructed and tested at the European Laboratory for Structural Assessment (ELSA) at the Joint Research Centre (JRC) at Ispra, Italy; the Z24 prestressed bridge, with three spans, two lanes and 60 m overall length of the SIMCES project in Switzerland (Worden, 2003); and the ANCRISST structural health monitoring problem of a cable-stayed bridge constructed in mainland China comprising a main span of 260 m and two side spans of 25.15+99.85 m each (http://smc.hit.edu.cn) can be listed among major research initiatives in this field.

Both model-based and non-model based approaches utilizing the measured data in time-domain, frequency domain or modal domain were investigated. While measurements were always performed in the time domain, data could be analyzed in any of the three domains. Although conversion between domains involves some data compression, Friswell and Penny (1997) argued that loss of information during conversion was minimal for linear systems and that the frequency domain may be more advantageous in reducing the effects of random noise. Modal domain introduces further reduction of the measured data since only the modes within a frequency band are considered. Friswell and Penny (1997) find this acceptable unless the out of band modes are very close, that is, the response is dominated by the in-band modes. Lee and Shin (2002) disagree with this argument pointing out the fact that the modal data can be contaminated by modal extraction error which the frequency response function data does not possess.

FEATURE-BASED METHODS

The following methods were proposed in the literature for feature-based damage detection in civil engineering structures (Doebling et al., 1996; Sohn et al., 2003; Randall et al., 2004a, b):

1. Natural frequency based metrics.
2. Mode shape based metrics.
3. Structural damping based metrics.
4. Modal strain energy based metrics.
5. Flexibility based methods and other matrix perturbation approaches.
6. Pattern Recognition, neural networks and other statistical approaches.
7. Non-linear methods based on advanced time-variant transforms.
8. Other methods.

Natural frequency based metrics

Damage detection based on changes or shifts in natural frequency has been the topic of numerous research studies (Salawu, 1997). These studies have revealed that changes in frequencies alone may not provide enough information for damage detection, especially in the case of large structures, for the following reasons:

(a) Damage is a local phenomenon and may not significantly influence the global low-frequency response behavior of structures typically measured during vibration

tests. Hence, high damage levels are often required for noticeable frequency shifts (Doebling et al., 1998; Salawu, 1997; Sohn et al., 2003). Tests on the I-40 Bridge conducted by Farrar et al. (1994) showed that a 96.4% reduction in the cross-sectional stiffness at the center of a main plate girder causing a 21% reduction in the bending stiffness of the overall bridge cross-section resulted in no significant reductions in the modal frequencies. The first four fundamental frequencies of a steel channel studied by Chen et al. (2005) exhibited no shifts greater than 5% due to a single notch severe enough to cause the channel to fail at its design load.
(b) The spatial wavelengths of the low-frequency modes are typically far larger than the extent of damage, which makes its detection difficult.
(c) Structures usually behave in a (weakly) nonlinear and time-varying fashion, which reduces the effectiveness of the approaches that are based on linear system modeling.
(d) Dynamic characteristics of structures, especially bridges, can be significantly affected by the environmental temperature.
(e) Data measured from actual structures are inevitably contaminated by noise. The distinction between damage and noise may be fuzzy.
(f) Different damage cases may provide similar frequency-change characteristics. In case of symmetric structures, for instance, the change in natural frequency due to damage at two symmetric locations is exactly the same.
(g) The identification of multiple damage scenarios using frequency shifts is a challenge even for simple laboratory structures.
(h) If a member is not strained in its fundamental mode, loss of that member has no effect on the fundamental frequency.
(i) In reinforced concrete structures where most of the stiffness is provided by the concrete, deterioration of the reinforcing steel was shown to have little influence on the natural frequency of the structure (Friswell and Penny, 1997).
(j) In highly redundant structures such as shells, damage in the form of a notch does not produce measurable changes in the dynamic characteristics of the structure (Srinivasan and Kot, 1992).
(k) Some forms of damage such as the loss of a bolt in the connection with several bolts may not affect the frequency at low levels of vibration (Chang et al., 2003).
(l) Chen et al. (2005) investigated steel space structures subjected to atmospheric corrosion and showed that the atmospheric corrosion does not lead to a perceptible change in the natural frequencies of the structure.

The success of the algorithms using frequency shifts for detecting damage is generally limited to small laboratory structures with a single or a few damage locations. The use of frequency changes alone for identifying damage in applications to full-scale structures does not seem promising with the exception of the work done by De Roeck et al. (2000). Following a progressive damage-testing program on the Z24 Bridge in Switzerland, the effects of air temperature, humidity, rain, wind speed and wind direction were monitored through hourly readings from 16 accelerometers placed on the bridge. It was demonstrated that once the effects of environmental influences were filtered out, stiffness changes could be detected if the corresponding frequency shifts were more than 1%.

Mode shape based metrics

In formulating the eigenvalue problem, assuming that structural damage only affects the stiffness matrix and not the mass matrix, the undamaged and damaged conditions of a structure can be represented by the following expressions, respectively:

$$([K]-\lambda_i[M])\{\phi_i\}=0 \quad (1)$$

$$([K^*]-\lambda_i^*[M])\{\phi_i^*\}=0 \quad (2)$$

where $[K]$ and $[M]$ are the stiffness and the mass matrices, λ_i and ϕ_i are the ith eigenvalue and eigenvector corresponding to the undamaged condition, respectively, and the asterisk denotes the damaged condition. The pre- and post-damage eigenvectors are used as the basis for damage detection (Law et al., 1998; Shi et al., 2000a; Hu et al., 2001; Siringoringo and Fujino, 2008).

Mode shape curvatures which can be estimated numerically from derivatives of the displacement mode shapes have also been used for damage detection purposes. The use of mode shape curvatures in damage identification is based on the assumption that the changes in the curvatures of mode shapes are highly localized to the region of damage and that they are more pronounced than changes in the displacement mode shapes. Alampalli et al. (1997), however, showed that this is not necessarily the case, particularly for structures with redundancy since the curvature is often calculated from the measured displacement mode shapes using a central difference approximation. The challenges associated with mode shape based methods can be summarized as follows:

(a) Mode shape based methods generally require measurements at many locations on the structure, which requires a dense sensor resolution.
(b) No changes in a mode shape can be detected if the mode has a node point at the location of damage.
(c) These methods require data with high signal to noise ratio and although they are well verified with simulated data, noise and measurement errors, which are inevitable,

can be major drawbacks in practical applications.
(d) These methods require an accurate and a well correlated model of the structure.
(e) Environmental effects have to be monitored and changes due to environmental conditions need to be distinguished from changes due to damage.

Studies by Kim and Stubbs (1995), Salawu and Williams (1995) and Shi et al. (2000a) suggest that methods based on mode shapes are more robust than those based on natural frequency shifts. While Ren and De Roeck (2002) cast doubts on the use of mode shapes for damage detection in large structures, Wahab and De Roeck (1999) presented promising results from a bridge application.

Structural damping based metrics

Damping properties have seldom been used for damage detection due to the high errors involved in estimating damping values and the existence of various definitions of damping. A review of the existing literature, however, suggests that crack detection in a structure based on damping may prove to be more advantageous than detection schemes based on frequency and mode shapes. The study by Modena et al. (1999) on identification of manufacturing defects causing structural damage in precast members revealed that visually undetectable cracks cause very little change in resonant frequencies and require higher mode shapes to be detected, while the same cracks cause larger changes in damping. Kawiecki (2000) suggests that damping as a damage-sensitive indicator can be useful for especially lightweight structures and microstructures. Zonta et al. (2000) showed that cracking of prestressed reinforced concrete hollow panels produces a frequency splitting in the frequency domain and the beat phenomenon of the free decay signals in time domain. It is claimed that the crack formation in prestressed concrete causes a non viscous dissipative mechanism, making damping more sensitive to damage. Curadelli et al. (2008) developed a damage detection strategy with the instantaneous damping coefficients identified using wavelet transforms. The experimental results obtained from a simply supported reinforced concrete beam and a one-bay six story aluminum frame suggest that damping reveals more marked variations than frequency upon damage.

The limitations of using damping properties for damage detection can be listed as follows:

(a) Consistent measurement and accurate modeling of damping is difficult. Alampalli et al. (1997) and Farrar and Doebling (1999) reported large scatter in the measured damping values from laboratory tests.
(b) For low frequency modes that also have low damping, such as the case for long suspension bridges, damping ratios are overestimated due to bias errors. Littler (1992) reported a 25% increase in the damping ratio of a long span suspension bridge when measurement duration was reduced to 1 h from 13 h. He also showed that there was a pronounced increase in damping value with increasing wind speed.
(c) Even when the damping values are measured with a high level of accuracy, the observed changes may not give any indication of damage. Casas and Aparicio (1994) investigated the identification of cracking in laboratory size concrete beams. Using a model updating technique, it was found that damping was not significantly different in the cracked beams compared to the uncracked beams and that there was no clear relation between crack growth and increase in damping.

Modal strain energy based metrics

The change in the strain energy stored in a particular vibration mode is also investigated as a potential indicator of damage. Kim and Stubbs (1995) developed a damage indicator based on the ratio of modal strain energy of elements before and after damage and applied this algorithm to locate and size a single crack in an experimental plate girder. Stubbs and Kim (1996) used the same indicator to localize and estimate severity of damage in an experimental two-span beam. Farrar and Doebling (1999) also used the same damage index for locating controlled damage in a bridge and found that this method outperformed the direct comparison of the mode shape curvature before and after damage. Park et al. (2001) applied a modal strain energy method to a laboratory space truss with 300 elements. In 17 damage scenarios, 16 of the 22 truly damaged members were identified. Law et al. (1998) developed a modal strain energy based method that is applied successfully to an experimental two-storey plane frame for which damage was simulated with loose joints. Hu et al. (2001) developed a damage assessment methodology using modal strain energy tailored to single damage cases and demonstrated the performance of the developed method on an experimental fixed-fixed beam with a single saw cut. Shi et al. (2000b) were able to locate the loosening of up to two semi rigid bolted joints in an experimental steel frame by calculating the change in the modal strain energy. Peterson et al. (2001a, b) applied a modal strain energy method to locate a saw cut damage in a laboratory timber beam. As the depth of the cut increased, the confidence in the correct localization of damage increased. Cornwell et al. (1999) extended the 1-D strain method to 2-D and applied both methods to an experimental aluminum plate with two saw cuts. Both methods exhibited a tendency to produce false-positive results especially at low levels of damage. Kim et al. (2003) applied both a frequency based and a modal strain energy based method to locate damage in a

simulated beam. The modal strain energy method was found to produce more accurate predictions than the frequency based method. Shi et al. (2000b) stated that modal expansion may be required to successfully locate damage and found that modal truncation error may lead to errors in quantification of damage. Similar to above-mentioned methods, masking effect of noise may have a pronounced effect in the low damage scenarios.

Flexibility based methods

The dynamically measured flexibility matrix, $[\boldsymbol{F}]$, is estimated from:

$$[F] = [\Phi][\Lambda]^{-1}[\Phi]^{T} \quad (3)$$

where $[\Phi]$ is the measured mode-shape matrix, $[\Lambda]$ is the diagonal matrix of the associated measured modal frequencies squared and *T* denotes the transpose operation. A truncated version of the flexibility matrix is generally estimated using only the lower vibration modes due to practical difficulties in measuring the higher modes. The flexibility matrix is most sensitive to changes in the lower frequency modes because of the inverse relationship to the square of the modal frequencies.

Pandey and Biswas (1994) and Li et al. (1999) used the change in flexibility as a damage feature. Bernal (2002) and Bernal and Gunes (2004) developed the Damage Locating Vector (DLV) approach mapping changes in flexibility to the spatial distribution of damage. The principle behind the method is the fact that the null space of the change in flexibility provides vectors that, when treated as loads on the structure, lead to stress fields that are zero over the damaged portion of the domain. An appreciation of why this is so can be gained by noting that the null space of the change in flexibility contains vectors that lead to identical displacements (at the sensors) in the undamaged and damaged states. The DLV localization is in principle carried out by computing the null space of the change in the flexibility matrix upon damage, treating the computed vectors as static loads on the system and identifying the damage as the intersection of the regions of zero stress. The application of the DLV method to the IASC-ASCE structural health monitoring benchmark structure is presented in the companion paper (Gunes and Gunes, 2012). Zhang and Aktan (1995) used the change in curvature (second derivative) of the flexibility matrix at the pre- and post-damage states to determine the location of damage.

Zhao and DeWolf (1999) examined and compared sensitivity coefficients for natural frequencies, mode shapes and modal flexibility. Application to a simulated five DOF spring mass system revealed that the modal flexibility was most sensitive to damage. Farrar and Doebling (1999) compared strain energy, mode shape curvature and the flexibility based methods for locating damage on the I-40 Bridge over the Rio Grande in America. Four controlled damage states were investigated and it was found that the strain energy based method was the most successful one followed by the mode shape curvature based method. In this study, the change in flexibility method could only locate damage in the most severe damage scenario.

Pattern recognition, neural networks and other statistical approaches

The inherent uncertainties in the measured data are recognized as one of the main barriers against the application of vibration based damage detection techniques on real life structures. Farrar and Doebling (1999) suggested that the vibration based damage detection problem is fundamentally one of statistical pattern recognition and that any advancement in the state of the art requires the developments of non-model based pattern recognition methods supplement the existing model based techniques. The objective of pattern recognition in damage detection is to distinguish between different classes of patterns representing damage conditions. Statistical pattern recognition assigns features to different classes using statistical density functions. In recent years, neural networks have been established as a powerful tool for pattern recognition (Mangal et al., 1996; Waszczyszyn and Ziemianski, 2001; Zubaybi et al., 2002). The architecture and the training process of neural networks depend on the required level of damage identification. An unsupervised scheme offers the possibility of novelty detection. Novelty detection is concerned with the identification of any deviations in measured data relative to data measured under normal operating conditions. Features derived from measurements taken from a structure in its undamaged state will have a distribution with an associated mean and variance. If the structure is damaged, then there may be a change in the mean, the variance, or both. A supervised learning scheme is required for determining location and severity of damage. This scheme, however, usually needs a correlated numerical model of the structure for localizing and quantifying the damage.

The main challenge associated with pattern recognition approaches is that they require significant amount of pre-processing. In the case of neural network approaches, pre-processing is needed to extract features for training. Pattern recognition analysis requires feature selection procedures for training. Some advanced pattern recognition approaches require a large number of features, and as the dimensionality of the feature space increases, the design of a good classifier becomes more difficult. Reduction of dimensionality then becomes a major challenge in pattern recognition. Novelty detection schemes provide information only on the existence of damage; however, they do not require any models of damage. They are also suitable for data sets obtained

through ambient excitation only, for example traffic or wind loading on a bridge structure (Siringoringo and Fujino, 2008; Zhang et al., 2009).

Statistical process control provides a framework for monitoring the distribution of the features and identifying new data that is inconsistent with the previous data. If all other variables can be eliminated, then a change in the distribution characteristics of the features will indicate damage. Worden et al. (2000), Fugate et al. (2000) and Carden and Fanning (2004) all considered statistical process control approaches for damage detection. Four waveform recognition techniques to distinguish between frequency response function (FRF) waveforms of intact and damaged bridges were investigated by Samman and Biswas (1994a, b) in two companion papers. INRIA in France recently proposed a statistical model based damage detection and localization method utilizing a subspace based residual and a statistical analysis of aggregated sensitivities of the residual to damage (Basseville, 2002). A disadvantage of these methods is that they are generally limited to Level 1 or possibly Level 2 identification. Hence, the detection of damage, rather than location and quantification, is the objective of using statistical pattern recognition. Ching and Beck (2004) devised a statistical Bayesian updating methodology based on expectation–maximization algorithm that can find the most probable values of the parameter with their probability density functions and applied the approach to the ASCE benchmark structure. Although the approach was found to be reliable in detecting the local damage in the bracing system, the connection is found to be much more difficult to detect.

Non-linear methods based on advanced time-variant transform

The use of linear and non-linear functions and transforms of data is a common way of feature reduction procedure for damage identification. There exist a number of methods based on Fourier analysis. The majority of these methods are based on the assumption that the analyzed data is linear and stationary. Many damage mechanisms such as cracks, however, will produce non-linear effects. Assuming the rest of the structure is linear, there is a very local non-linearity in a predominantly linear structure. Thus it is probable that the small changes due to damage may be more identifiable if the non-linear effects can be separated from the linear effects. Methods using wavelets and other time frequency transformations such as Hilbert-Huang transform and Wigner-Ville distribution show promise due to their ability to examine local data with a zoom effect. The zoom effect can provide multi levels of details and approximations of the original signal (Liew and Wang, 1998; Hou et al., 2000; Yang et al., 2004; Hera and Hou, 2004). Damage and the moment when the damage occurs can be detected by a spike in the time-frequency plot. The spatial distribution of spikes may be used to identify the location of damage.

Other methods

In the literature, there are also techniques that do not fall into any of the categories described above. Sawyer (2000) proposed a fuzzy logic based damage identification system. Sohn and Law (2001) made use of Ritz vectors extracted from measured flexibility. Tan et al. (2001) studied dynamic response of reinforced concrete slabs and showed that plots of measured dynamic strain display unique deflection signatures that varied with the internal state of the slab.

MODEL UPDATING BASED METHODS

Model-based also called parametric methods are based on a model of the structure, some parameters of which are adjusted using vibration measurements, by minimizing the difference between the parameters computed with the model and the ones that are derived from the measurements (Mottershead and Friswell, 1993; Friswell and Mottershead, 1995). Damage, in this context, is viewed as shifting of values in a set of system parameters and damage characterization falls in the realm of model updating as an optimization problem. This optimization problem is often non-convex which may totally miss the real optimum leading to wrong parametric values. Global iterative optimization methods exist to solve this problem, such as coupled local minimizers, genetic algorithms, or simulated annealing. Furthermore, the quality of damage location assessment is critically dependent on the detail and accuracy of the structure's finite element model. It is inevitable that there will be errors even in the model of the undamaged structure. This 'systematic error' problem may be reduced and a reliable model may be produced by updating the model of the undamaged structure using data measured from the undamaged structure. Another alternative that eliminate the systematic errors is to use differences between the damaged and undamaged response data in the damage location algorithm. In either case, however, a fundamental difficulty lies in the fact that the inverse problem posed is typically ill-conditioned and, given the constraints imposed by the available data, generally non-unique (Udwadia 1985). Berman (1989) concluded that there can be no unique corrected dynamic model of a structure as long as the model has fewer degrees-of-freedom (DOF) than the actual structure. He argued that as the true actual structure has an infinite number of DOF, there exist an infinite number of physically reasonable models, which adequately predict the behavior of the structure over an adequate frequency range. When such a model is applied to damage

determination, the true changes in the physical characteristics are required and this represents a far more onerous task than the prediction of model behavior. In the same vein, Baruch (1978) showed that simultaneous changes in the mass and stiffness matrices could not be identified using modal data alone since the mode shapes could not provide a reference basis. Methods that do use mode shapes as a reference basis may determine the stiffness and mass matrices with significant errors since the solution is non-unique.

The model-updating problems are usually solved by iterative methods that require the solution of the analytical problem at least once in each iteration; hence, its application to large models can be very processor intensive. Although the technological advances in speed and memory of computers allow tackling larger and more complex models than ever before, model size is still an issue. Moller and Friberg (1998) proposed a method that reduced the problem by projection onto a subspace spanned by a reduced number of modes leading to substantial computational time savings. Law et al. (2001) presented a damage detection oriented modeling methodology for large structures. To reduce the number of DOFs, super elements were formulated while the modal sensitivities to small physical changes were maintained for use in a sensitivity based updating algorithm. The method was demonstrated on a simulated bridge deck structure where the initial 5370 DOFs were reduced to 211 DOFs with reasonable success.

Updating techniques arrive at the damaged system properties using constrained optimization algorithms that select a particular solution from the set of possible ones. For example, strategies that use matrix perturbations of minimum rank or minimum norm have been widely used (Baruch, 1978; Kabe, 1985). The minimum norm type solutions generally tend to spread the identified damage over a large number of parameters. The physical parameters obtained from these formulations may be unrelated to the actual damage scenarios, although they are consistent with the measured modal data. Using engineering judgment, such as specifying the likely location and form of damage, are key aspects for the success of any model updating project. An alternative approach that reduces the size of the original updating problem is a multivariate regression method that combines a parameter subset selection process (Lallement and Piranda, 1990; Friswell et al., 1997; Titurus et al., 2003), with a damage function (Teughels et al., 2002; Teughels and De Roeck, 2004).

CONCLUSION

Structural damage detection and integrity assessment is the fundamental objective of structural health monitoring. A review of the state of the art in vibration based condition monitoring revealed numerous algorithms that use data in time, frequency and modal domains. Many of the algorithms suggested for damage localization are tested on simulated data or on very controlled experimental data. Although simulations are necessary to test the performance of algorithms for various damage cases, they are not sufficient. Laboratory testing is required to simulate the errors that might be expected in real structures. Most identification schemes are able to cope well with the random noise that is often added to simulated data, but not with systematic type errors that exist between the model and the structure.

The monitoring methods used for civil engineering structures mainly rely on linear models due to complex nature of these structures. Material non-linearity or cracking and other damage mechanisms producing non-linear effects which are often ignored can cause problems in damage identification using linear assumptions. Non stationarity of the structure is another significant problem that must be dealt with since environmental effects such as temperature can change the signals from an undamaged structure significantly. Methods based on novelty detection may prove to be advantageous since they do not require any baseline data. However, these methods provide only Level 1 or 2 damage identification.

Despite the extensive research and progress in SHM of structures, global monitoring methods based on dynamic characteristics are unlikely to have an inherent capability for damage location and quantification of operational civil structures in the short term unless the damage to the structure is substantial. Local monitoring techniques are much more likely to locate and quantify the damage. However, since local monitoring of all infrastructures in a timely manner is not a realistic goal at present, global methods should be combined with the use of local monitoring techniques to obtain a better picture of the structural damage.

REFERENCES

Alampalli S, Fu G, Dillon EW (1997). Signal versus noise in damage detection by experimental modal analysis. J. Struct. Eng. 123(2):237–245.

Baruch M (1978). Optimization procedure to correct stiffness and flexibility matrices using vibration tests. AIAA J. 16 (11):1209-1210.

Basseville M, Mevel L, Goursat M (2002). Statistical model-based damage detection and localization: Subspace-based residuals and damage-to-noise sensitivity ratios. Rapport de Recherche, No. 4645, Theme 4, INRIA, Rennes, France, November ISSN0249-6399.

Berman A (1989). Nonunique structural system identification. Proceedings of the 7th International Modal Analysis Conference, Society for Experimental Mechanics, Las Vegas, Nevada. pp. 355-359.

Bernal D (2002). Load vectors for damage localization. J. Eng. Mech. 128(1):7–14.

Bernal D, Gunes B (2004). A flexibility based approach for the localization and quantification of damage: A benchmark application. J. Eng. Mech. 130:61-70.

Carden EP, Fanning P (2004). Vibration based condition monitoring: A review. Structural Health Monitoring. 3(4):355-377.

Casas JR, Aparicio AC (1994). Structural damage identification from

dynamic-test data. J. Struct. Eng. 120(8):2437–2450.
Chang PC, Flatau A, Liu SC (2003). Review Paper: Health Monitoring of Civil Infrastructure. Structural Health Monitoring. 2(3):257-267.
Chen B, Xu YL, Qu WL (2005). Evaluation of atmospheric corrosion damage to steel space structures in coastal areas. Int J Solids Struct. 42:4673-4694.
Ching J, Beck JL (2004) Bayesian analysis of the phase II IASC–ASCE structural health monitoring experimental benchmark data. J. Eng. Mech. 130(10):1233-1244.
Cornwell P, Doebling SW, Farrar CR (1999). Application of the strain energy damage detection method to plate-like structures. Journal of Sound and Vibration. 224(2):359–374.
Curadelli RO, Riera JD, Ambrosini D, Amani MG (2008). Damage detection by means of structural damage identification. Engineering Structures. 20:3497-3504.
De Roeck G, Peeters B, Maeck J (2000). Dynamic monitoring of civil engineering structures. Computational Methods for Shell and Spatial Structures, IASS-IACM 2000, Chania, Crete, Greece.
Doebling SW, Farrar CR, Prime MB (1998). A summary review of vibration-based damage identification methods. Shock and Vibration Digest. 30:91-105.
Doebling SW, Farrar CR, Prime, MB, Shevitz DW (1996). Damage identification and health monitoring of structural and mechanical systems from changes in their vibration characteristics: A literature review. Technical Report LA-13070-MS, Los Alamos National Laboratory, Los Alamos, NM.
Dyke SJ, Bernal D., Beck JL., Ventura C (2003). Experimental phase of the structural health monitoring benchmark problem. Proc., 16th Engineering Mechanics Conf., ASCE, Reston, VA, USA.
Farrar CR, Worden K (2007). An Introduction to Structural Health Monitoring. Philosophical Transactions of the Royal Society A: Mathematical, Physical and Engineering Sciences. 365:303-315.
Farrar CR, Doebling SW (1999). Damage detection II: field applications to large structures. In: Silva, J.M.M. and Maia, N.M.M. (eds.). Modal Analysis and Testing, Nato Science Series. Dordrecht, Netherlands: Kluwer Academic Publishers.
Farrar CR, Baker WE, Bell TM, Cone KM, Darling TW, Duffey TA, Eklund, A, Miglori A (1994). Dynamic characterization and damage detection in the I-40 bridge over the Rio Grande. Los Alamos National Laboratory Report LA-12767-MS, Los Alamos National Laboratory, P.O. Box 1193, Los Alamos, NM, 87544, USA.
Friswell MI, Mottershead JE (1995). Finite-element model updatingin structural dynamics, Kluwer, Norwell, MA, USA.
Friswell MI, Penny JET (1997). Is damage location using vibration measurements practical, Euromech 365 international workshop: Damas 97, Structural Damage Assessment using Advanced Signal Processing Procedures, Sheffield, UK, June/July.
Friswell MI, Penny JET, Garvey SD (1997). Parameter subset selection in damage location. Inverse Problems in Engineering. 5(3):189–215.
Fritzen CP, Jennewein D, Kiefer T (1998). Damage detection based on model updating methods. Mech. Syst. Signal Process. 12(1):163–86.
Fugate ML, Sohn H, Farrar CR (2000). Unsupervised learning methods for vibration-based damage detection. Proceedings of the 18th International Modal Analysis Conference, February, San Antonio, Texas, USA.
Gunes B, Gunes O (2012). Structural health monitoring and damage assessment, part II: Application of the DLV method to the ASCE benchmark structure experimental data. Int. J. Phy. Sci. Under review. 7(9):1509-1515.
Hera A, Hou Z (2004). Application of wavelet approach for ASCE structural health monitoring benchmark studies. J. Eng. Mech. 130(1):96-104.
Hou Z, Noori M, Amand RSt (2000). Waveletbased approach for structural damage detection. J. Eng. Mech. 126(7):677–683.
Hu N, Wang X, Fukunaga H, Yao ZH., Zhang HX, Wu ZS (2001). Damage assessment of structures using modal test data. International Journal of Solids and Structures. 38:3111–3126.
Kabe AM (1985). Stiffness matrix adjustment using mode data. AIAA J. 23(9):1431-1436.
Kawiecki G (2000). Modal damping measurements for damage detection. European COST F3 conference on system identification and structural health monitoring. Madrid, Spain, pp. 651-658.
Kim J-T, Stubbs N (1995). Model-uncertainty impact and damage-detection accuracy in plate girder. J. Structural Eng. 121(10):1409–1417.
Kim J-T, Ryu Y-S, Cho H-M, Stubbs N (2003). Damage identification in beam-type structures: frequency-based method vs. mode-shape-based method. Eng. Structures. 25:57–67.
Lallement G, Piranda J (1990). Localisation methods for parameter updating of finite-element models in elastodynamics. Proc. 8th Int. Modal Analysis Conf. pp. 579-585.
Law SS, Chan THT, Wu D (2001). Efficient numerical model for the damage detection of large scale engineering structures. Eng. Structures. 23:436-451.
Law SS, Shi ZY, Zhang LM (1998). Structural damage detection from incomplete and noisy modal test data. J. Eng. Mech. 124(11):1280-1288.
Lee U, Shin J (2002). A frequency response function-based structural damage identification method. Computers and Structures. 80:117-132.
Li G-Q, Hao K-C, Chen S-W (1999). A flexibility next term approach for identification of cantilever-type structures with bending and shear deformation. Computers and Structures. 73(6):565-572.
Liew KM, Wang Q (1998). Application of wavelet theory for crack identification in structures. J. Eng. Mech. 124(2):152–157.
Littler JD (1992). Ambient vibration tests on long span suspension bridges. J. Wind Eng. Industrial Aerodynamics. 42:1359-1370.
Mangal L, Idichandy VG, Ganapathy C (1996). ART-based multiple neural networks for monitoring offshore platforms. Applied Ocean Res. 18:137-143.
Modena C, Sonda D, Zonta D (1999) Damage localization in reinforced concrete structures by using damping measurements. Damage assessment of structures. Proceedings of the international conference on damage assessment of structures, DAMAS 99, pp. 132-141.
Mottershead JE, Friswell MI (1993). Model updating in structural dynamics: A survey. J. Sound Vib. 167(2):347-375.
Möller PW, Friberg O (1998). Updating large finite element models in structural dynamics. AIAA J. 36(10):1861-1868.
Pandey AK, Biswas M (1994). Damage detection in structures using changes in flexibility. J Sound Vibration. 169(1):3-17.
Park G, Muntges DE, Inman DJ (2001). Self-monitoring and self-healing jointed structures. In: Damage Assessment of Structures, Proceedings of the 4th International Conference on Damage Assessment of Structures, Cardiff, Wales, UK, June, Key Engineering Materials. pp. 204-205.
Peterson ST, McLean DI, Symans MD, Pollock DG., Cofer WF, Emerson RN, Fridley KJ (2001a). Application of dynamic system identification to timber beams I. J. Struct. Eng. 127(40):418–425.
Peterson ST, McLean DI, Symans MD, Pollock DG, Cofer WF, Emerson RN Fridley KJ (2001b). Application of dynamic system identification to timber beams II. J. Struct. Eng. 127(4):426–432.
Randall BR (2004a). State of the art in monitoring rotating machinery—part 1. Journal of Sound and Vibration. 38:14–21.
Randall BR (2004b). State of the art in monitoring rotating machinery—part 2. Journal of Sound and Vibration. 38:10-17.
Ren W-X, De Roeck G (2002). Structural damage identification using modal data II: Test verification. J. Struct. Eng. 128(1):96-104.
Rytter A (1993). Vibration based inspection of civil engineering structures. Ph.D. Dissertation, Department of Building Technology and Structural Engineering, Aalborg University, Denmark.
Salawu OS (1997). Detection of structural damage through changes in frequency: a review. Engineering Structures. 19(9):718-723.
Salawu OS, Williams C (1995). Bridge assessment using forced-vibration testing. Journal of Structural Engineering. 121(2):161-173.
Samman MM, Biswas M (1994a). Vibration testing for nondestructive evaluation of bridges I: Theory. J. Struct. Eng. 120(1) 269-289.
Samman MM, Biswas M (1994b). Vibration testing for nondestructive evaluation of bridges II: Results. J. Struct. Eng. 120(1):290–306.
Sawyer JP, Rao SS (2000). Structural damage detection and identification using fuzzy logic. AIAA J. 38(12):2328-2334.
Shi ZY, Law SS, Zhang LM (2000a). Damage localization by directly

using incomplete mode shapes. Journal of Engineering Mechanics. 126(6):656–660.
Shi ZY, Law SS, Zhang LM (2000b). Structural damage detection from modal strain energy change. Journal of Engineering Mechanics. 126(12):1216–1223.
Siringoringo DM, Fujino Y (2008). System Identification of Suspension Bridge from Ambient Vibration Response. Engineering Structures. 30(2):462-477.
Sohn H, Farrar CR, Hemez FM, Shunk DD, Stinemates DW, Nadler BR (2003). A review of structural health monitoring literature: 1996-2001, Los Alamos National Laboratory, USA.
Sohn H, Law, KH (2001). Damage diagnosis using experimental Ritz vectors. J. Eng. Mech. 127(11):1184–1192.
Srinivasan MG, Kot CA (1992). Effects of damage on the modal parameters of a cylindrical shell. Proceedings of the 10th International Modal Analysis Conference: pp. 529–535.
Stubbs N, Kim J-T (1996). Damage localization in structures without baseline modal parameters. AIAA J. 34(8):1644–1649.
Tan HC, Olubayo OR, Famiyesin OR, Imbabi MSE (2001). Dynamic deformation signatures in reinforced concrete slabs for condition monitoring. Computers and Structures. 79:2413–2423.
Teughels A, De Roeck G (2004). Structural damage identification of the highway bridge Z24 by FE model updating. J. Sound Vib. 278:589–610.
Teughels A, Maeck J, De Roeck G (2002). Damage assessment by FE model updating using damage functions. Comput. Struct. 80:1869–1879.
Titurus B, Friswell MI., Starek L (2003). Damage detection using generic elements. Part II: Damage detection. Comput. Struct. 81:2287–2299.
Udwadia FE (1985). Some uniqueness results related to soil and building structural identification. SIAM Journal of Applied Mathematics. 45:674-685.
Wahab MMA, De Roeck G (1999). Damage detection in bridges using modal curvatures: applications to a real damage scenario. Journal of Sound and Vibration. 226(2):217–235.
Waszczyszyn Z, Ziemianski L (2001). Neural networks in mechanics of structures and materials – new results and prospects of applications. Computers and Structures. 79:2261–2276.
Worden K, Manson G, Fieller NRJ (2000). Damage detection using outlier analysis. Journal of Sound and Vibration. 229(3):647–667.
Worden K (2003). Cost action F3 on structural dynamics:Benchmarks for working group 2-structural health monitoring. Mechanical Systems and Signal Processing.17(1):73–75.
Yang JN, Lei Y, Lin S, Huang N (2004). Hilbert-Huang Based Approach for Structural Damage Detection. J. Eng. Mech. 130(1):89-95.
Zhang J, Aktan AE (1995). The damage indices for constructed facilities. Proceedings of the 13th International Modal Analysis Conference.
Zhang J, Prader J, Grimmelsman KA, Moon FL, Aktan AE (2009). Mitigation of uncertainty in the structural identification of longspan suspension bridges. The 7th International Workshop on Structural Health Monitoring, Palo Alto, CA.
Zhao J, DeWolf JT (1999). Sensitivity study for vibrational parameters used in damage detection. J. Struct. Eng. 125(4):410–416.
Zimmerman DC, Kaouk M (1992). Eigenstructure assignment approach for structural damage detection. AIAA J. 30(12):1848–55.
Zonta D, Modena C, Bursi OS (2000). Analysis of dispersive phenomena in damaged structures. European COST F3 conference on system identification and structural health monitoring. Madrid, Spain, pp. 801-810.
Zubaybi A, Haddara MR, Swamidas ASJ (2002). Damage identification in a ship's structure using neural networks. Ocean Eng. 29:1187–1200.

academicJournals

Vol. 8(34), pp. 1703-1715, 16 September, 2013
DOI: 10.5897/IJPS2013.3993
ISSN 1992 - 1950 © 2013 Academic Journals
http://www.academicjournals.org/IJPS

International Journal of Physical Sciences

Full Length Research Paper

Singulo oscillatory – stiff rational integrators

Elakhe O. A.* and Aashikpelokhai U. S. U.

Mathematics Department, Ambrose Alli University, Ekpoma, Edo State, Nigeria.

Accepted 4 September, 2013

In this paper, we derive a general singulo oscillatory – stiff rational integrator of order (S+3) for s = 0, 1, 2, 3, 4,… for the solution of initial value problems in ordinary differential systems that are singular, oscillatory or stiff. We compared our integrators with certain maximum order second derivative hybrid multi-step methods, certain Tau and Euler methods, the adaptive implicit and classical Runge-Kutta methods and some existing conventional methods. Our results show good improvement over the existing methods compared with.

Key words: Rational integrator, initial value problems, stability, convergence, consistency.

INTRODUCTION

Many of the problems in real life from physical situation, chemical kinetics, engineering construction work, biological simulations, nuclear reactors and practical realities often lead to initial value ordinary differential equations (Kreider et al., 1968; Birkhoff and Rota, 1969; Burghes and Borries, 1981; Lambert, 1995; Bartels et al., 1996). These types of initial value problems (ivp) are stiff, singular or oscillatory (Luke et al., 1975; Fatunla, 1978, 1980; Niekerk, 1987; Aashikpelokhai, 1991, 2000; Abhulimen and Otunta, 2007; Ademiluyi et al., 2007; Aashikpelokhai and Momodu, 2008; Egbetade et al., 2008). The solutions of these problems sometimes results in large set of linear equations that generate mystical entities called Matrices (Kolman, 1980; Atkinson, 1985; Jacques and Judd, 1987; Billingsley, 1989; Health, 1997). The work of Health (1997) and Parasuram (2001) shows that natural modes and frequencies of vibration of a structure and their stabilities are determined by the locations of the eigenvalues of an appropriate matrix hence their computation is of critical interest in this study. The problem for this research work is to find a suitable numerical solution to the ivp.

$$y^1 = f(x, y), y(x_0) = y_0, \ a \le x \le b \qquad (1)$$

where f(x, y) is defined and continuous in a region D $\subset$ [a,b] of the real line.

This work was motivated by the research work of Lambert and Shaw (1965), Aashikpelokhai (1991) and Momodu (2006). Essentially, Momodu (2006) extended the work of Lambert and Shaw (1965) from linear denominator to Quadratic denominator. Our work here is an extension of Momodu (2006) from Quadratic denominator to a polynomial of degree three. We however used the method of derivation as found in Aashikpelokhai (1991). According to Luke et al. (1975), this area has not been attractive because of the difficulty in deriving these types of integrators. This statement was recently re-echoed by Agbeboh et al. (2007). However because of the excellent accurate results so far recorded in the area and with Aashikpelokhai (2010) hope for attention of more researchers in this area, we are encouraged to extend Momodu (2006) to a polynomial of degree three.

*Corresponding author. E-mail: bssabraela@yahoo.co.uk. Tel: +2348039611725.

2010 AMS Subject Classification: 65Lxx

THE SINGULO OSCILLATORY – STIFF RATIONAL INTEGRATORS

Basic expansion

Let the operator U: R $\rightarrow C^{m+2}$ (x)be defined by

$$U(x)\ Q_3(x) = P_m(x) \tag{2}$$

where $U(x) = \sum_{r=0}^{\infty} c_r x^r$ (3)

is the Taylor's' series of the function whose approximant is sought,

$$P_m(x) = \sum_{i=0}^{m} p_i x^i \tag{4}$$

$$Q_3(x) = 1 + \sum_{i=1}^{3} q_i x^i \tag{5}$$

For the purpose of our integration, U(x) is subject to the constraint

$$U(x_{n+i}) = \begin{cases} y(x_{n+i}) & \text{for } i = 0 \\ y_{n+i} & \text{for } i = 0,1,2 \end{cases} \tag{6}$$

On expansion we have the

$$\left.\begin{aligned} p_0 &= c_0 \\ p_1 &= c_0 q_1 + c_1 \\ p_2 &= c_0 q_2 + c_1 q_1 + c_2 \\ p_3 &= c_0 q_3 + c_1 q_2 + c_2 q_1 + c_3 \\ &\vdots \\ &\vdots \end{aligned}\right\} \tag{7}$$

$$p_m = c_{m-3} q_3 + c_{m-2} q_2 + c_{m-1} q_1 + c_m, \quad \forall\ m \geq 3 \tag{8}$$

By definition of $p_m(x)$ we have $p_s = 0 \ \forall \ s > m$

That is $p_{m+1} = p_{m+2} = \ldots = p_s = 0 \ \ if \ \ s > m.$

We shall be interested in the first three consecutive terms for our simultaneous linear equation to yield $q_1,\ q_2,\ q_3$. Thus for $p_{m+1} = p_{m+2} = p_{m+3} = 0$ we then have,

$c_{m-2}q_3 + c_{m-1}q_2 + c_m q_1 = -c_{m+1}$
$c_{m-1}q_3 + c_m q_2 + c_{m+1}q_1 = -c_{m+2}$
$c_m q_3 + c_{m+1}q_2 + c_{m+2}q_1 = -c_{m+3}$

Rearranging and putting in matrix form, we have

$$\begin{bmatrix} c_{m+2} & c_{m+1} & c_m \\ c_{m+1} & c_m & c_{m-1} \\ c_m & c_{m-1} & c_{m-2} \end{bmatrix} \begin{bmatrix} q_1 \\ q_2 \\ q_3 \end{bmatrix} = - \begin{bmatrix} c_{m+3} \\ c_{m+2} \\ c_{m+1} \end{bmatrix} \tag{9}$$

where (i) m ≥ 0 (ii) $C_\alpha = 0$ whenever $\alpha < 0$,

(iii) $c_r = \dfrac{h^r y_n^{(r)}}{r! x_{n+1}^r}, \quad r = 0,1,2, \ . \ . \ .$ (10)

Reduction to matrix – free form

Employing Crammers rule to obtain q_1, q_2, q_3 we have from Equation 9

$$\text{Det } \mathbf{c} = |\mathbf{c}| = \begin{vmatrix} c_{m+2} & c_{m+1} & c_m \\ c_{m+1} & c_m & c_{m-1} \\ c_m & c_{m-1} & c_{m-2} \end{vmatrix}$$

$$\therefore \quad |\mathbf{c}| = c_{m+2}c_m c_{m-2} - c_{m+2}c_{m-1}^2 - c_{m+1}^2 c_{m-2} + 2c_{m+1}c_m c_{m-1} - c_m^3 \tag{11}$$

Also, to obtain values of q_i, i = 1, 2, 3 we have from Crammers rule

$$q_i = \frac{|\mathbf{c}(q_i)|}{|\mathbf{c}|} \qquad \text{for } i = 1, 2, 3.$$

Hence,

$$\therefore \quad q_1 = \frac{c_{m+3}c_{m-1}^2 - c_{m+3}c_m c_{m-2} + c_{m+2}c_{m+1}c_{m-2} - c_{m+1}^2 c_{m-1} - c_{m+2}c_m c_{m-1} + c_{m+1}c_m^2}{c_{m+2}c_m c_{m-2} - c_{m+2}c_{m-1}^2 + c_{m+1}^2 c_{m-2} + 2c_{m+1}c_m c_{m-1} - c_m^3} \tag{12}$$

Similarly,

$$\therefore\ q_2 = \frac{c_{m+2}c_{m+1}c_{m+1} - c_{m+2}^2 c_{m-2} + c_{m+3}c_{m+1}c_{m-2} - c_{m+3}c_m c_{m-1} - c_m c_{m+1}^2 + c_{m+2}c_m^2}{c_{m+2}c_m c_{m-2} - c_{m+2}c_{m-1}^2 + c_{m+1}^2 c_{m-2} + 2c_{m+1}c_m c_{m-1} - c_m^3} \tag{13}$$

Also,

$$\therefore\ q_3 = \frac{c_{m+2}^2 c_{m-1} + c_{m+1}^3 - 2c_{m+2}c_{m+1}c_m - c_{m+3}c_{m+1}c_{m-1} + c_{m+3}c_m^2}{c_{m+2}c_m c_{m-2} - c_{m+2}c_{m-1}^2 + c_{m+1}^2 c_{m-2} + 2c_{m+1}c_m c_{m-1} - c_m^3} \tag{14}$$

The integration formula

From the works so far, we move on to derive our integration formula from the basic form:

$$y_{n+1} = P_m(x_{n+1})\left[1 + q_1 x_{n+1} + q_2 x_{n+1}^2 + q_3 x_{n+1}^3\right]^{-1} \tag{15}$$

into a form that would not require users to compute for the parameters. Our first step is to recall that the governing equation in matrix-free forms gave rise to:

$$c_r = \begin{cases} \dfrac{h_r y_n^{(r)}}{r! x_{n+1}^r} & r = 0,1,2 \ldots m \\ 0 & r < 0 \end{cases} \quad (16)$$

The explicit formula we derive is the one that would come handy from the values obtained for $p_0, p_1, \ldots p_m$ where $m \geq 1$ as given in Equation 7.
By considering Equations 16, 7, 8, 12, 13 and 14, we obtain values for $\left(p_i x_{n+1}^i\right)_{i=0}^m$, $\left(q_i x_{n+1}^i\right)_{i=1}^3$ which when substituted into Equation 15 yields:

$$y_{n+1} = \frac{\sum_{r=0}^{s} \frac{h^r y_n^{(r)}}{r!} + A\sum_{r=0}^{s-1} \frac{h^r y_n^{(r)}}{r!} + B\sum_{r=0}^{s-2} \frac{h^r y_n^{(r)}}{r!} + C\sum_{r=0}^{s-3} \frac{h^r y_n^{(r)}}{r!}}{1 + A + B + C} \quad (17)$$

where,

$$A = q_1 x_{n+1} = h \frac{\left[\begin{array}{l}\left(s^3+s^2\right)y_n^{(s-2)^2} y_n^{s+3} - \left(s^3-s\right)y_n^{(s)} y_n^{(s-2)} y_n^{s+3} + \left(s^3+2s^2-3s\right)y_n^{(s-2)} y_n^{(s+1)} y_n^{(s+2)} - \\ \left(s^3+5s^2+6s\right)y_n^{(s+1)^2} y_n^{(s-1)} - \left(s^3-4s^2+3s\right)y_n^{(s+2)} y_n^{(s)} y_n^{s-1} + \left(s^3+6s^2+11s+6\right)y_n^{(s+1)} y_n^{(s)^2}\end{array}\right]}{(s+3)\left[\begin{array}{l}\left(s^3-s\right)y_n^{(s+2)} y_n^{(s)} y_n^{(s-2)} - \left(s^3+s^2\right)y_n^{(s+2)} y_n^{(s-2)^2} - \left(s^3+s^2-2s\right)y_n^{(s+1)^2} y_n^{(s-2)} \\ + 2\left(s^3+3s^2+2s\right)y_n^{(s+1)} y_n^{(s)} y_n^{(s-1)} - \left(s^3+4s^2+5s+2\right)y_n^{(s)^3}\end{array}\right]} \quad (18)$$

$$B = q_2 x_{n+1}^2 = h^2 \frac{\left[\begin{array}{l}\left(s^3+5s^2+6s\right)y_n^{(s+2)} y_n^{(s+1)} y_n^{(s-1)} - \left(s^3+2s^2-3s\right)y_n^{(s+2)^2} y_n^{(s-2)} + \left(s^3+s^2+2s\right)y_n^{(s+3)} y_n^{(s+1)} y_n^{(s-2)} - \\ \left(s^3+3s^2+2s\right)y_n^{(s+3)} y_n^{(s)} y_n^{(s-1)} - \left(s^3+7s^2+16s+12\right)y_n^{(s+2)^2} y_n^{(s)} + \left(s^3+6s^2+11s+6\right)y_n^{(s)^2} y_n^{(s+2)}\end{array}\right]}{(s+2)(s+3)\left[\begin{array}{l}\left(s^3-s\right)y_n^{(s+2)} y_n^{(s)} y_n^{(s-2)} - \left(s^3-s^2\right)y_n^{(s+2)} y_n^{(s-1)^2} - \left(s^3+s^2-2s\right)y_n^{(s+1)^2} y_n^{(s-2)} + \\ 2\left(s^3+3s^2+2s\right)y_n^{(s+1)} y_n^{(s)} y_n^{(s-1)} - \left(s^3+4s^2+5s+2\right)y_n^{(s)^3}\end{array}\right]} \quad (19)$$

$$C = q_3 x_{n+1}^3 = h^3 \frac{\left[\begin{array}{l}\left(s^3+4s^2+3s\right)y_n^{(s+2)^2} y_n^{(s-1)} - 2\left(s^3+6s^2+11s+6\right)y_n^{(s+2)} y_n^{(s+1)} y_n^{(s)} + \left(s^3+7s^2+16s+12\right)y_n^{(s+1)^3} - \\ \left(s^3+3s^2+2s\right)y_n^{(s+3)} y_n^{(s+1)} y_n^{(s-1)} + \left(s^3+4s^2+5s+2\right)y_n^{(s+3)} y_n^{(s)^2}\end{array}\right]}{(s+1)(s+2)(s+3)\left[\begin{array}{l}\left(s^3-s\right)y_n^{(s+2)} y_n^{(s)} y_n^{(s-2)} - \left(s^3+s^2\right)y_n^{(s+2)} y_n^{(s-2)^2} - \left(s^3+s^2-2s\right)y_n^{(s+1)^2} y_n^{(s-2)} + \\ 2\left(s^3+3s^2-2s\right)y_n^{(s+1)} y_n^{(s)} y_n^{(s-1)} - \left(s^3+4s^2+5s+2\right)y_n^{(s)^3}\end{array}\right]} \quad (20)$$

For s = 0, 1, 2, 3, . . . and $y_n^{(\alpha)} = \begin{cases} y_n^{(\alpha)} & \text{if } \alpha \geq 0 \\ 0 & \text{otherwise} \end{cases}$

CONVERGENCE AND CONSISTENCY

To establish convergence and consistency, the work of Lambert (1974, 1976, 1995) is usually called into play. Lambert (1976, 1995) asserts that convergence is a minimal property of any given numerical integrator and that convergence must take place for all initial value problems. Lambert (1976, 1995) reports that one-step method is said to be convergent if, for all initial value problem satisfying the Lipschitz then,

$$\lim_{h \to 0} \max_{0 \leq n \leq N} \left\| y(x_n) - y_n \right\| = 0$$

Lambert (1995) went further to conclude that every one-step method is convergent if and only if the one step method is consistent. On consistency, a one-step method is said to be consistent if the increment function is consistent with the initial value problem, that is, $\Phi(x_n, y_n; 0) = f(x_n, y_n)$. Armed with these facts we state and prove the convergence and consistency of our rational general integrator.

Theorem

The general one-step rational integrator

$$y_{n+1} = \frac{\sum_{r=0}^{s} \frac{h^r y_n^{(r)}}{r!} + A\sum_{r=0}^{s-1} \frac{h^r y_n^{(r)}}{r!} + B\sum_{r=0}^{s-2} \frac{h^r y_n^{(r)}}{r!} + C\sum_{r=0}^{s-3} \frac{h^r y_n^{(r)}}{r!}}{1 + A + B + C}$$

where the function A, B and C, are specified by Equations 18, 19 and 20 respectively is consistent and convergent.

Proof

From the integrator (17) we have

$$y_{n+1} - y_n = \frac{\sum_{r=1}^{s} \frac{h^r y_n^{(r)}}{r!} + A\sum_{r=1}^{s-1} \frac{h^r y_n^{(r)}}{r!} + B\sum_{r=1}^{s-2} \frac{h^r y_n^{(r)}}{r!} + C\sum_{r=1}^{s-3} \frac{h^r y_n^{(r)}}{r!}}{1 + A + B + C} \quad (21)$$

hence,

$$\frac{y_{n+1} - y_n}{h} = \frac{\sum_{r=1}^{s} \frac{h^{r-1} y_n^{(r)}}{r!} + A\sum_{r=1}^{s-1} \frac{h^{r-1} y_n^{(r)}}{r!} + B\sum_{r=1}^{s-2} \frac{h^{r-1} y_n^{(r)}}{r!} + C\sum_{r=1}^{s-3} \frac{h^{r-1} y_n^{(r)}}{r!}}{1 + A + B + C} \quad (22)$$

$$= \frac{y_n^{(1)}[1 + A + B + C] + \sum_{r=2}^{s} \frac{h^r y_n^{(r)}}{r!} + A\sum_{r=2}^{s-1} \frac{h^r y_n^{(r)}}{r!} + B\sum_{r=2}^{s-2} \frac{h^r y_n^{(r)}}{r!} + C\sum_{r=2}^{s-3} \frac{h^r y_n^{(r)}}{r!}}{1 + A + B + C} \quad (23)$$

Note that from Equations 18, 19 and 20

$$\lim_{h \to 0} A = 0, \qquad \lim_{h \to 0} B = 0, \qquad \lim_{h \to 0} C = 0$$

Hence $$\lim_{h \to 0} \left[\frac{y_{n+1} - y_n}{h}\right] = \frac{y_n^{(1)}[1+0+0+0] + 0+0+0+0}{1+0+0+0}$$

$$= y_n^{(1)}$$

$$\therefore \quad \lim_{h \to 0} \left[\frac{y_{n+1} - y_n}{h}\right] = y_n^{(1)} = f(x_n, y_n)$$

as required.

Thus our new rational integrator (17) is consistent with

the initial value problem (1). But (1) was chosen arbitrarily. Hence our integrator is convergent (Lambert, 1976).

STABILITY CONSIDERATION

By employing $y^1 = \lambda y \; and \; \bar{h} = \lambda h$ we obtain our stability function as

$$\varsigma(\bar{h}) = \frac{(s+1)(s+2)(s+3)\sum_{r=0}^{s}\frac{h^r}{r!} - 3(s+1)(s+2)\sum_{r=0}^{s-1}\frac{h^{r+1}}{r!} + 3(s+1)\sum_{r=0}^{s-2}\frac{h^{r+2}}{r!} - \sum_{r=0}^{s-3}\frac{h^{r+3}}{r!}}{(s+1)(s+2)(s+3) - 3(s+1)(s+2)\bar{h} + 3(s+1)\bar{h}^{-2} - \bar{h}^{-3}}$$

for s = 0, 1, 2, 3, . . .
In analyzing our stability functions to determine the type of stability properties they posses, we shall analyse the first three cases that is for s = 0, 1, 2.

Case 1: s = 0

The Stability function for s = 0 on simple substitution is given as

$$\zeta(\bar{h}) = \frac{6}{6 - 6\bar{h} + 3\bar{h}^{-2} - \bar{h}^{-3}}$$

By setting $\bar{h} = u + iv, \; i^2 = -1$, we get $\left|\zeta(\bar{h})\right| \le 1$

this holds after expansion, simplification, rearranging and collecting terms $\Leftrightarrow$

$$\left(u^2+v^2\right)^3 - 6u\left(u^2+v^2\right)^2 + 9\left(u^2+v^2\right) + 12\left(u^2+v^2\right)\left(u^2-v^2\right) - 24u\left(2u^2-3u+3\right) \ge 0$$

Observe that:

i. Our preference is for: $\left(u^2+v^2\right)^3, \; 9\left(u^2+v^2\right)^2$ $\forall \; u, \; v \; we \; have$

$\left(u^2+v^2\right)^3 \ge 0, \; 9\left(u^2+v^2\right)^2 \ge 0$

Hence Region of Instability (RIS) from this set is empty, by this contribution.
ii. Preference is for:

$-6u\left(u^2+v^2\right)^2 \; and \; 24u\left(2u^2-3u+3\right)$
$\forall \; u \le 0, and \; \forall \; v$
$-6u\left(u^2+v^2\right)^2 \ge 0$
$-24u\left(2u^2-3u+3\right) \ge 0$

Hence our RIS from this set is the right half of the complex plane, by this our RAS will be the entire left half of the complex plane.
iii. Preference is for:

$$12\left(u^2+v^2\right)\left(u^2-v^2\right)$$

$(i) \;\; \forall \; u, \; v \; we \; have:$
$\left(u^2+v^2\right) \ge 0,$
$(ii) \;\; \left(u^2-v^2\right) \ge 0$
$\Leftrightarrow u \ge v \ge 0 \; or \; u \le v \le 0,$
$Hence \;\; 12\left(u^2+v^2\right)\left(u^2-v^2\right) \ge 0 \;\; \forall \;\; u \le 0$

For easy actualization of the nature of the RAS we shall employ the polar form where,

$u = R\,Cos\,\theta, \; v = R\,Sin\theta,$
$u^2+v^2 = R^2\left(Cos^2\theta + Sin^2\theta\right) = R^2,$
$u^2-v^2 = R^2\left(Cos^2\theta - Sin^2\theta\right) = R^2 Cos2\theta$

Consequently our inequality becomes,
$R^6 - 6R^5 Cos\theta + 9R^4 + 12R^3 Cos2\theta - 24RCos\theta\left(2R^2Cos^2\theta - 3RCos\theta + 3\right) \ge 0$
Which gives a vast span of Region of Absolute stability on plotting $\theta \in \left[0^0, 360^0\right]$

Figure 1 shows that our integrator is A-stable and so the Region of Absolute Stability of the integrator is the entire left – half of the complex plane and the exterior part of the region of Instability shaded in the figure. Our Singulo Oscillatory – Stiff integrator is L- Stable since by direct substitution of $\zeta(\bar{h})$,

$$\underset{\mathrm{Re}(\bar{h}) \to -\infty}{Limit} \left|\zeta(\bar{h})\right| = 0$$

Case 2: s = 1

Our stability function is given as

$$\zeta(\bar{h}) = \frac{24 + 6\bar{h}}{24 - 18\bar{h} + 6\bar{h}^{-2} - \bar{h}^{-3}}$$

By setting $\bar{h} = u + iv, \; i^2 = -1$, we get $\left|\zeta(\bar{h})\right| \le 1 \Leftrightarrow$

$\left(u^2+v^2\right)^3 - 12u\left(u^2+v^2\right)^2 + 72u^2\left(u^2+v^2\right) - 72u\left(u^2+v^2\right) - 48u\left(4u^2-12u+24\right) \ge$
Observe that:

i. Our preference is for: $\left(u^2+v^2\right)^3, \; 9\left(u^2+v^2\right)^2$ $\forall \; u, \; v \; we \; have$

$\left(u^2+v^2\right)^3 \ge 0 \; \text{and} \; 72u^2\left(u^2+v^2\right)^3 \ge 0$

Hence RIS for this set is empty.
ii. Preference is for

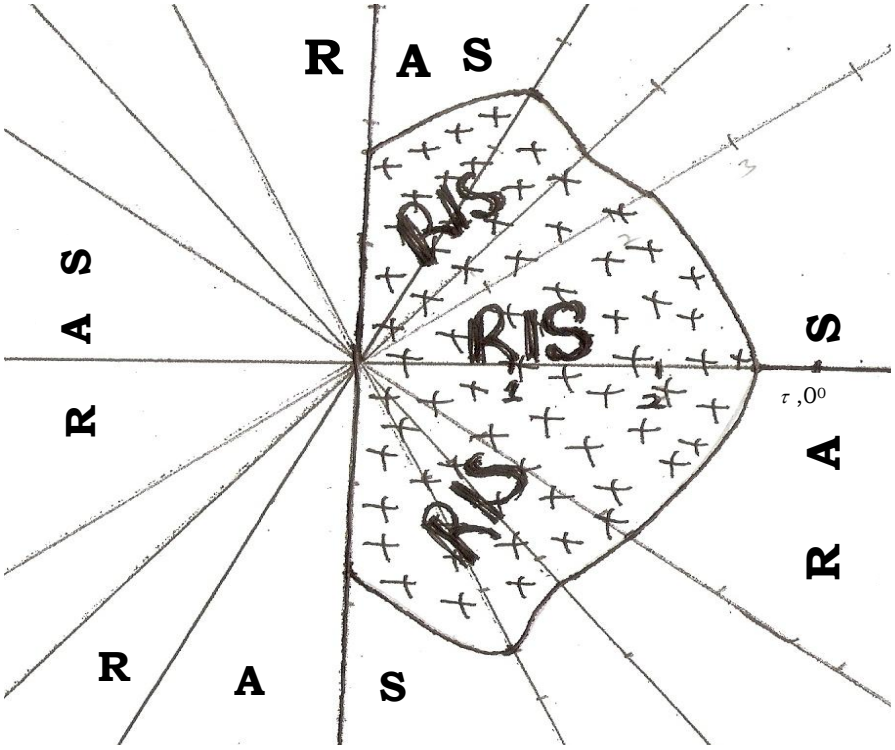

Figure 1. Region of absolute stability (RAS) for our new method for s = 0, $\tau = 2.55$.

$$-12u\left(u^2+v^2\right)^2-72u\left(u^2+v^2\right)-48u\left(4u^2-12u+24\right)$$

$\forall\ u \le 0\ and\ \forall\ v$ we have that

$$-12u\left(u^2+v^2\right)^2 \ge 0,$$
$$-72u\left(u^2+v^2\right)^2 \ge 0$$
$$-48u\left(4u^2-12u+24\right) \ge 0$$

Hence our RAS will be the entire left half of the complex plan.

On employing the polar form where u = R cos θ, v = R sin θ our inequality becomes

$$R^6-12R^5\cos\theta+72R^4\cos^2\theta-72R^3\cos\theta-48R\cos\theta\left[4R^2\cos^2\theta-12R\cos\theta+24\right]\ge 0$$

On plotting $\theta \in \left[0^0, 360^0\right]$ we obtain our Region of Absolute Stability as given in Figure 2, which shows that the integrator is A-stable and the Region of Absolute Stability is the entire left – half of the complex plane and the space outside the Region of Instability.

The Integrator is L – Stable as by direct substitution of $\zeta\left(\bar{h}\right)$

$$\lim_{\mathrm{Re}\left(\bar{h}\right)\to-\infty} \left|\zeta\left(\bar{h}\right)\right| = 0$$

Case 3: s = 2

Our stability function as $\zeta\left(\bar{h}\right) = \dfrac{60+24\bar{h}+3\bar{h}^2}{60-36\bar{h}+9\bar{h}^2-\bar{h}^3}$

By setting $\bar{h} = u+iv,\ i^2=-1$, we get $\left|\zeta\left(\bar{h}\right)\right| \le 1 \Leftrightarrow$

$$\left(u^2+v^2\right)^3-18u\left(u^2+v^2\right)^2+144u^2\left(u^2+v^2\right)-432u\left(u^2+v^2\right)-480u\left(u^2-3u+15\right)\ge 0\ \forall\ u<0$$

$ie\ \left|\zeta(u,v)\right| \le 1\ \forall\ u,v \in \{(u+iv): u<0\}$

Observe that

i. $\left(u^2+v^2\right)^3 \ge 0,\ 144u^2\left(u^2+v^2\right) \ge 0\ \forall\ u,v$

ii. $-18u\left(u^2+v^2\right)^2 \ge 0, -432u\left(u^2+v^2\right) \ge 0,\ -480u\left(u^2-3u+15\right) \ge 0\ \forall\ u<0$

Since our Stability function for S = 2 is equivalent to Aashikpelokhai (1991) for k = 3, the polar form and RAS will be the same. We simply quote the polar form and hence the RAS as follows:

$$R^6-18R^5\cos\theta+144R^4\cos^2\theta-48R^3\cos\theta\left(19\cos^2\theta+9\sin^2\theta\right)+1440R^2\cos^2\theta-7280R\cos\theta\ge 0$$

The RAS is given in Figure 3 which is equivalent to Aashikpelokhai (1991) for k = 3. Hence the integrator is A-stable and so the Region of Absolute Stability of the integrator is the entire left – half of the complex plane.

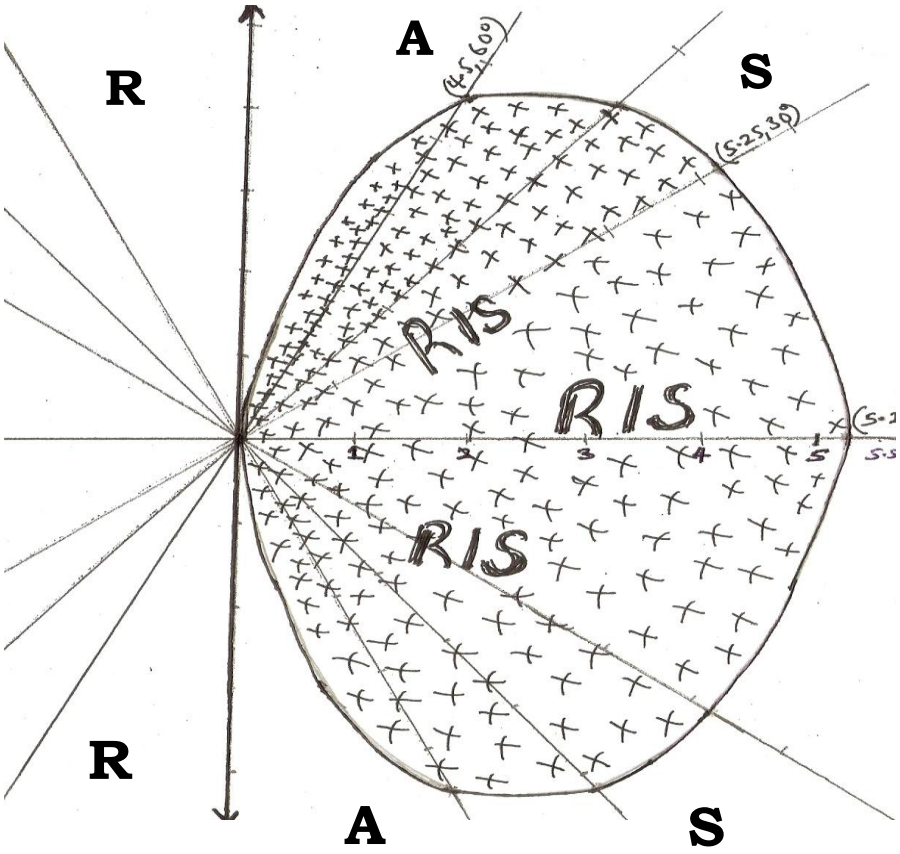

Figure 2. Showing RAS for our new method for s = 1.

We easily confirm that the method is L – Stable, since on simple application of $\zeta(\bar{h})$,

$$\lim_{\mathrm{Re}(\bar{h})\to-\infty} \left|\zeta(\bar{h})\right| = 0$$

NUMERICAL EXPERIMENT

We shall be concerned with the application of our new integrator in solving a number of problems in this section. Our interest is to select problems in the three classes of problems, this integrator have been designed for. A number of comparisons are made with the respective exact solution where such exact solutions exist and also compared with recent research work in that area.

Example 1

$y^1 = -100y$, $y(x_0) = 1$, $x \in [0, 1]$ Exact solution $y(x) = \ell^{-100x}$ Ademiluyi and Kayode (2001). A variable Step Size was used starting with h = 0.10.

Table 1 shows the performance of our integrator. The convergence rate is very high as s increases from 0 to 2 and then from s = 5 the convergence is excellent. Our new integrator performs better than the maximum order second derivative hybrid multi-step methods of Ademiluyi and Kayode (2001) and converges quickly to the analytic solution than its counterpart.

Example 2

$y^1(x) + 2xy(x) = 0$, $0 \le x \le 1$, $y(0) = 1$ Exact solution $y(x) = \ell^{-x^2}$ Egbetade et al. (2008).

Uniform mesh-size h = 0.1 was used. Table 2 shows that our new numerical integrator gives a better approximation than the Euler but next to Tau for case s = 0 and s = 1. For s = 2, our integrator gives a better approximation than Tau and Euler. The table shows that our integrator converges quickly to the analytic solution at each corresponding mesh point than Tau and Euler methods.

Example 3

$2(1 + x)\, y^1(x) + y(x) = 0$, $0 \le x \le 1$, $y(0) = 1$ Exact solution $y(x) = (1+x)^{-1/2}$ Egbetade et al. (2008).

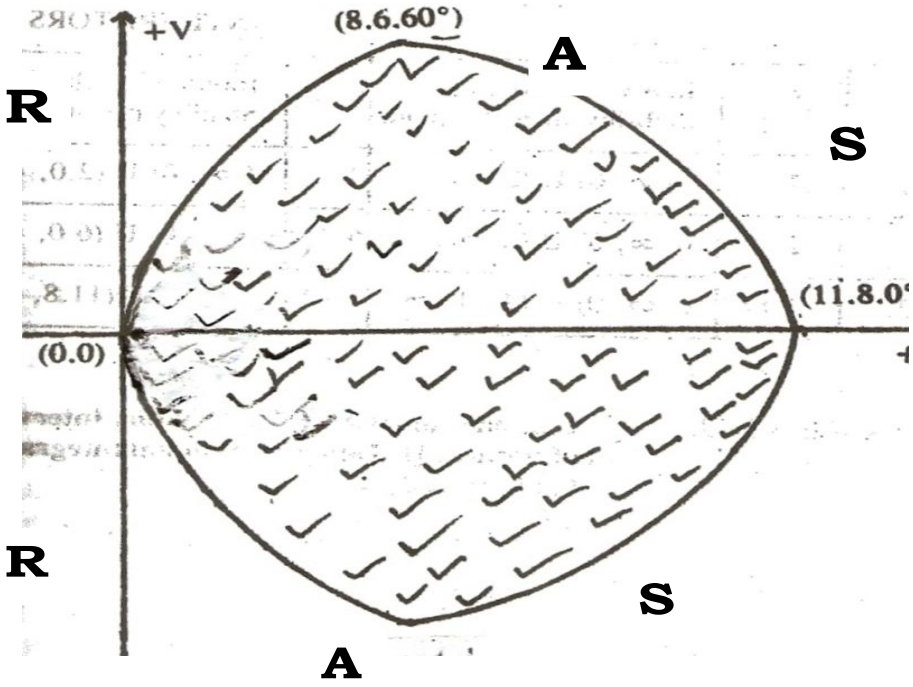

Figure 3. Shows RAS for our new method of s = 2 ≡ Aashikpelokhai (1991) for k = 3.

Uniform mesh-size h = 0.1 was used. Table 3 shows that our new integrator performs better than the Tau and Euler methods proposed by Egbetade et al. (2008).

The Table shows that our integrator converges quickly to the analytic solution at each corresponding mesh point than the given Tau and Euler method.

Example 4

$y^1 = 1 + y^2$, $y(0) = 1$ $0 \le x \le 1$ Exact solution $y = \tan\left(x + \frac{\pi}{4}\right)$ Aashikpelokhai (1991) and Fatunla (1982).

Uniform mesh – size h = 0.05 was used. From Table 4, the trend shows that for a given mesh point, the errors in numerical integrator decreases as s increases from 0 to 2 and also shows that the accuracy in the computed results falls as we approach the point of singularity. Our new numerical integrator compete fairly well with known conventional methods like Lambert and Shaw (1965), Fatunla (1982), Niekerk (1987) and Aashikpelokhai (1991). Our integrator converges quickly to the analytic solutions as s increases and performs better than those compared with.

Example 5

$x^1 = 5x - 2y$, $x(0) = 1$

$y^1 = 3x$ $y(0) = 2$, $h = 0.01$

Exact solutions: $x = 2e^{2t} - e^{3t}$, $y = 3e^{2t} - e^{3t}$ Ademiluyi et al. (2007).

Tables 5 and 6 shows that our integrators compete favourably well with Ademiluyi et al. (2007).

Example 6

$$y_1^{(1)} = -2000y_1 + 999.75y_2 + 1000.25$$
$$y_2^{(1)} = y_1 - y_2$$
$$y_1(0) = 0$$
$$y_2(0) = -2 \qquad x \in [0,10] \quad h = 0.50$$

Ademiluyi and Kayode (2001).

Exact solutions: $y_1 = -1.499875\exp(-0.5x) + 0.499875\exp(-20005x) + 1$

$y_2 = -2.99975\exp(-0.5x) - 0.00025\exp(-20005x) + 1$

Tables 7 and 8 show the performance of our integrators compared with Ademiluyi and Kayode (2001).

Example 7

$y' = \begin{bmatrix} 0 & 1 \\ -1 & 5(1-y_1^2) \end{bmatrix} y$, $y(0) = \begin{bmatrix} 2 \\ 0 \end{bmatrix}$ $0 \le x \le 1$. Fatunla (1980) and Aashikpelokhai (1991).

Exact solutions: Unknown.

Table 1. Error in Numerical Integrators on Example 1.

h	Value of x	Analytic solution	Ademiluyi, and Kayode (2001)	Rational integrator, order = S + 3						
				S = 0	S = 1	S = 2	S = 3	S = 4	S = 5	S = 6
1.00000D-01	1.00000D-01	-1.68748D+02	2.14454D-02	-4.3469870000D-03	2.0001050000D-02	-5.1678738001D-02	1.68748D+02	-1.11022D-16	0.00000D+00	0.00000D+00
5.00000D-02	1.50000D-01	-5.09314D-04	2.00536D-02	-8.4833320000D-07	1.0061580000D-06	-8.4833318193D-07	5.09620D-04	1.11022D-16	-1.11022D-16	0.00000D+00
2.50000D-02	1.75000D-01	-1.01713D-07	1.97436D-02	-8.0351810000D-09	2.5665250000D-09	-7.4090876666D-10	1.26823D-07	5.96046D-08	0.00000D+00	0.00000D+00
1.25000D-02	1.87500D-01	6.97190D-09	1.68208D-02	-2.8626790000D-10	2.9542090000D-11	-3.3080616716D-12	2.22223D-10	1.11022D-16	-5.96046D-08	0.00000D+00
6.25000D-03	1.93750D-01	3.84976D-09	1.24074D-02	-1.4987770000D-11	6.0145620000D-13	-2.9159240580D-14	9.79550D-13	-5.96046D-08	5.96046D-08	0.00000D+00
3.12500D-03	1.96875D-01	2.81725D-09	7.84083D-03	-8.7327870000D-13	1.5429890000D-14	-3.4695157775D-16	7.59669D-15	0.00000D+00	5.96046D-08	0.00000D+00
1.56250D-03	1.98438D-01	2.40973D-09	4.43528D-03	-5.2832730000D-14	4.3859390000D-16	-4.7468516322D-18	-1.52056D-15	5.96046D-08	0.00000D+00	0.00000D+00
7.81250D-04	1.99219D-01	2.22864D-09	2.36270D-03	-3.2499840000D-15	1.3083900000D-17	-6.9469936565D-20	-8.87885D-16	-5.96046D-08	-1.11022D-16	0.00000D+00
3.90625D-04	1.99609D-01	2.14326D-09	1.21590D-03	-2.0153060000D-16	3.9957290000D-19	-1.0513465586D-21	1.33227D-15	1.11022D-16	0.00000D+00	0.00000D+00
1.95313D-04	1.99805D-01	2.10180D-09	6.19892D-04	-1.2546370000D-17	1.2344020000D-20	-1.6543612251D-23	6.66134D-16	1.11022D-16	0.00000D+00	0.00000D+00
9.76563D-05	1.99902D-01	2.08138D-09	Not stated	-7.8260720000D-19	3.9084280000D-22	7.0310352067D-24	-1.33227D-15	2.22045D-16	0.00000D+00	0.00000D+00

Table 2. Error in numerical integrators on Example 2.

Value of x	Analytic solution	Egbetade et al. (2008)		Rational integrator, order = S + 3		
		Tau	Euler	S = 0	S = 1	S = 2
0.10	9.9004983375D-01	4.72D-02	9.95D-03	-4.917615D-05	0.000000D+00	8.2505386967D-08
0.20	9.6078943915D-01	1.32D-02	1.92D-02	-4.960649D-05	1.577458D-06	8.4904185682D-08
0.30	9.1393118527D-01	2.17D-03	2.69D-02	-5.253809D-05	6.306041D-06	9.5526001109D-08
0.40	8.5214378897D-01	1.03D-03	3.22D-02	-5.735429D-05	3.684451D-06	1.1631798935D-07
0.50	7.7880078307D-01	1.48D-04	3.48D-02	-6.331738D-05	2.489074D-06	1.5519120644D-07
0.60	6.9767632607D-01	6.97D-05	3.45D-02	-6.963457D-05	1.85956D-06	2.4763663675D-07
0.70	6.1262639418D-01	6.03D-05	3.17D-02	-7.552774D-05	1.522491D-06	8.3757392144D-07
0.80	5.2729242404D-01	6.40D-06	2.69D-02	-8.030164D-05	1.353403D-06	-4.1282457863D-07
0.90	4.4485806622D-01	8.00D-07	2.06D-02	-8.340400D-05	1.280778D-06	-1.3945307575D-07
1.00	3.6787944117D-01	2.00D-07	4.51D-03	-8.447050D-05	1.257789D-06	-7.5853677450D-08

Problem type

Van Der Pol's oscillator problem. Nonlinear Stiff in some regions and non – stiff in other regions.

Tables 9 and 10 shows the performance of our integrator at s = 2 when compared with Aashikpelokhai (1991), Fatunla (1978, 1980) and Norelli (1985).

CONCLUSION AND RECOMMENDATIONS

In this work, we have been able to derive a family of rational integrator having its members A-stable

Table 3. Error in numerical integrators on Example 3.

Value of x	Analytic solution	Egbetale et al. (2008)		Rational integrator, order = S + 3				
		Tau method	Euler method	S = 0	S = 1	S = 2	S = 3	S = 4
0.1	9.534626D-01	4.69D-03	3.40D-03	3.351720D-06	9.485746D-09	3.2235009217D-08	-9.5341701444D-01	-9.5341701444D-01
0.2	9.128709D-01	1.10D-04	6.05D-03	2.128150D-06	-7.834597D-08	-6.4574900649D-08	-4.3465059489D-05	-4.3465059489D-05
0.3	8.770580D-01	1.07D-04	8.02D-03	1.504906D-06	-3.893317D-09	4.8008580444D-09	-1.9801983859D-09	-1.9801983859D-09
0.4	8.451542D-01	3.26D-05	9.54D-03	1.070653D-06	7.889883D-09	1.3577405422D-08	-9.0168061594D-14	-9.0168061594D-14
0.5	8.164966D-01	3.05D-05	1.07D-02	7.475101D-07	-2.029751D-08	-1.6461896735D-08	-4.1041068680D-18	-4.1041068680D-18
0.6	7.905694D-01	1.55D-05	1.17D-02	5.984675D-07	3.145635D-08	3.4112142000D-08	-1.8674165387D-22	-1.8674165387D-22
0.7	7.669650D-01	3.30D-06	1.23D-02	3.980663D-07	-2.875809D-08	-2.6876332382D-08	-8.4946652258D-27	-8.4946652258D-27
0.8	7.453560D-01	2.20D-06	2.21D-02	3.223554D-07	-4.409917D-09	-3.0492284253D-09	-3.8632620036D-31	-3.8632620036D-31
0.9	7.254763D-01	8.00D-07	2.24D-02	2.867425D-07	3.280389D-08	3.3805727995D-08	-1.7566313688D-35	-1.7566313688D-35

Table 4. Error in numerical integrators on Example 4.

Value of x	Analytic solution	Lambert and Shaw (1965)	Luke et al. (1975)	Fatunla order 4 K = 4 (1982)	Niekerk Order 2 (1987)	Aashikpelokhai (1991)		Rational integrator, order = S + 3		
						Order 3 K - 2	Order 5 K = 3	S = 0	S = 1	S = 2
0.10	1.1053555921D+00	9(-9)	1(-5)	-	2(-6)	2(-6)	2(-10)	-2.3922899373D-05	3.4389746828D-08	-1.5467094272D-10
0.20	1.2230488842D+00	2(-7)	2(-5)	6(-5)	8(-6)	3(-6)	2(-10)	-2.1573281999D-05	9.7985064507D-09	-1.5691825617D-10
0.30	1.3560878681D+00	4(-7)	3(-5)	5(-5)	2(-5)	5(-6)	2(-10)	-1.9837158535D-05	1.6594276397D-08	-1.6103607337D-10
0.40	1.5084976569D+00	7(-7)	3(-5)	2(-4)	5(-5)	1(-5)	2(-10)	-1.8660567270D-05	-1.1544370793D-08	-1.6727819130D-10
0.50	1.6857964172D+00	1(-6)	7(-5)	2(-4)	1(-4)	2(-5)	2(-10)	-1.7899054741D-05	-8.7192120191D-10	-1.7604917524D-10
0.60	1.8957651776D+00	4(-6)	2(-4)	7(-4)	5(-4)	8(-5)	2(-10)	-1.7366474947D-05	2.0532583034D-07	-1.8799828361D-10
0.65	2.1497477742D+00	8(-6)	4(-3)	1(-3)	1(-3)	2(-4)	2(-10)	-1.7488961197D-05	1.9269808504D-07	-2.0412205259D-10
0.70	2.4649630098D+00	2(-5)	1(-2)	3(-3)	3(-3)	6(-4)	1(-9)	-1.8098347009D-05	1.9229756232D-07	-2.2602453242D-10
0.75	2.8688844682D+00	1(-4)	1(-1)	1(-2)	2(-2)	5(-3)	4(-9)	-1.9083213533D-05	4.5660165604D-07	-2.5640156665D-10

$a(b) = ax10^{b}$

and at least three of its members L-stable, leaving its users for easy choice of s for use as all the p_i *and* q_j, $(i = 1\ (1)\ s)$, $(j = 1\ (1)\ 3)$ have been fully derived. This integrator can cope effectively well with the three classes of problems, namely Stiff, mildly Stiff and non-stiff, singular and non-singular and oscillating and non-oscillatory initial value problems in ordinary differential equations.

The integrator compared favourably well with

Table 5. Error in numerical integrators first component on Example 5.

Values of TI	Ademiluyi et al. (2007)	New Integrator (Order = S + 3)						
		S = 2	S = 3	S = 4	S = 5	S = 6	S = 7	S = 8
3.00000000D-02	0.3238292541D-04	-4.01897400D-10	-6.15099061D-09	-6.15099061D-09	-6.15099061D-09	-6.15099061D-09	-6.15099061D-09	-6.15099061D-09
6.00000000D-02	0.2995808673D-04	-3.56716000D-10	-1.11073899D-07	-1.11073899D-07	-1.11073899D-07	-1.11073899D-07	-1.11073899D-07	-1.11073899D-07
9.00000000D-02	0.2787104097D-04	-1.89672700D-09	-1.15763126D-07	-1.15763126D-07	-1.15763126D-07	-1.15763126D-07	-1.15763126D-07	-1.15763126D-07
1.20000000D-01	0.2605580892D-04	1.23133400D-09	-1.05589737D-09	-1.05589737D-09	-1.05589737D-09	-1.05589737D-09	-1.05589737D-09	-1.05589737D-09
1.50000000D-01	0.2446254221D-04	-4.03830900D-09	-1.62302885D-07	-1.62302885D-07	-1.62302885D-07	-1.62302885D-07	-1.62302885D-07	-1.62302885D-07
1.80000000D-01	0.2305287807D-04	1.01706500D-09	3.51731264D-08	3.51731264D-08	3.51731264D-08	3.51731264D-08	3.51731264D-08	3.51731264D-08
2.10000000D-01	0.2179681180D-04	8.98252400D-10	-4.33673466D-08	-4.33673466D-08	-4.33673466D-08	-4.33673466D-08	-4.33673466D-08	-4.33673466D-08
2.40000000D-01	0.2067053833D-04	7.26404000D-10	-6.53996413D-08	-6.53996413D-08	-6.53996413D-08	-6.53996413D-08	-6.53996413D-08	-6.53996413D-08
2.70000000D-01	0.196542975D-04	-1.23739400D-09	-1.62053748D-08	-1.62053748D-08	-1.62053748D-08	-1.62053748D-08	-1.62053748D-08	-1.62053748D-08
3.00000000D-01	0.1873444048D-04	3.30105100D-10	4.25262905D-08	4.25262905D-08	4.25262905D-08	4.25262905D-08	4.25262905D-08	4.25262905D-08
3.30000000D-01	0.1789630619D-04	6.88611400D-11	-1.37350189D-08	-1.37350189D-08	-1.37350189D-08	-1.37350189D-08	-1.37350189D-08	-1.37350189D-08
3.60000000D-01	0.1712994847D-04	-2.37488500D-10	-8.42760395D-08	-8.42760395D-08	-8.42760395D-08	-8.42760395D-08	-8.42760395D-08	-8.42760395D-08
3.90000000D-01	0.1712994847D-04	-5.64629500D-10	-9.86133362D-08	-9.86133362D-08	-9.86133362D-08	-9.86133362D-08	-9.86133362D-08	-9.86133362D-08
4.20000000D-01	0.1642652616D-04	-1.00651400D-09	-9.38846805D-08	-9.38846805D-08	-9.38846805D-08	-9.38846805D-08	-9.38846805D-08	-9.38846805D-08
4.50000000D-01	0.1577859276D-04	-1.43394400D-09	4.70074202D-10	4.70074202D-10	4.70074202D-10	4.70074202D-10	4.70074202D-10	4.70074202D-10
4.80000000D-01	0.1517983194D-04	-1.99811000D-09	-9.95356952D-08	-9.95356952D-08	-9.95356952D-08	-9.95356952D-08	-9.95356952D-08	-9.95356952D-08
5.10000000D-01	0.1462485089D-04	-2.54803700D-09	-5.62501530D-08	-5.62501530D-08	-5.62501530D-08	-5.62501530D-08	-5.62501530D-08	-5.62501530D-08
5.40000000D-01	0.1410901759D-04	9.74980300D-08	2.95151725D-09	2.95151725D-09	2.95151725D-09	2.95151725D-09	2.95151725D-09	2.95151725D-09
5.69999900D-01	0.13628331113D-04	1.17562200D-07	-2.83948820D-08	-2.83948820D-08	-2.83948820D-08	-2.83948820D-08	-2.83948820D-08	-2.83948820D-08
5.99999900D-01	0.1275894717D-04	1.40095800D-07	1.67908905D-08	1.67908905D-08	1.67908905D-08	1.67908905D-08	1.67908905D-08	1.67908905D-08
6.29999900D-01	0.1236456325D-04	1.65635400D-07	2.52512509D-08	2.52512509D-08	2.52512509D-08	2.52512509D-08	2.52512509D-08	2.52512509D-08
6.59999800D-01	0.1199382870D-04	1.94263200D-07	-1.15564580D-08	-1.15564580D-08	-1.15564580D-08	-1.15564580D-08	-1.15564580D-08	-1.15564580D-08
6.89999800D-01	0.1164467828D-04	2.26304200D-07	5.60328139D-09	1.53459467D-11	1.53459467D-11	1.53459467D-11	1.53459467D-11	1.53459467D-11
7.19999800D-01	0.1131528043D-04	2.62465000D-07	4.31058034D-09	4.31058034D-09	4.31058034D-09	4.31058034D-09	4.31058034D-09	4.31058034D-09
7.49999800D-01	0.1070939677D-04	3.02850300D-07	-1.91763583D-08	-1.91763583D-08	-1.91763583D-08	-1.91763583D-08	-1.91763583D-08	-1.91763583D-08
7.79999700D-01	0.1016509888D-04	3.47702700D-07	-1.72803656D-08	-1.72803656D-08	-1.72803656D-08	-1.72803656D-08	-1.72803656D-08	-1.72803656D-08
8.09999700D-01	0.9913183923D-05	3.98191800D-07	-4.51632189D-08	-4.51632189D-08	-4.51632189D-08	-4.51632189D-08	-4.51632189D-08	-4.51632189D-08
8.39999700D-01	0.9673451145D-05	4.54307000D-07	1.03405924D-08	1.03405924D-08	1.03405924D-08	1.03405924D-08	1.03405924D-08	1.03405924D-08
8.69999600D-01	0.9445040210D-05	5.17281900D-07	-1.83549945D-07	-1.83549945D-07	-1.83549945D-07	-1.83549945D-07	-1.83549945D-07	-1.83549945D-07
8.99999600D-01	0.1043015177D-04	5.86612800D-07	-4.18202735D-08	-4.18202735D-08	-4.18202735D-08	-4.18202735D-08	-4.18202735D-08	-4.18202735D-08

other conventional methods like Lambert and Shaw (1965), Luke et al. (1975), Fatunla (1978, 1980, 1982), Norelli (1985), Niekek (1987) and Aashikpelokhai (1991). The new integrator also compared favourably well with recent work in the area like Ademiluyi and Kayode (2001), Egbetale et al. (2008) and Ademiluyi et al. (2007).

The integrator can effectively cope with ivp arising from mechanical oscillation, chemical

Table 6. Error in numerical integrators second component on Example 5.

Values of TI	Ademiluyi et al. (2007)	New integrator (Order = S + 3)						
		S = 2	S = 3	S = 4	S = 5	S = 6	S = 7	S = 8
3.00000000D-02	0.000000000D+00	-4.53041826D-09	2.97802411D-07	2.97718588D-07	2.97718588D-07	2.97718588D-07	2.97718588D-07	2.97718588D-07
6.00000000D-02	0.000000000D+00	3.74003140D-09	2.12429478D-08	2.11451257D-08	2.11451257D-08	2.11451257D-08	2.11451257D-08	2.11451257D-08
9.00000000D-02	0.000000000D+00	-6.74308609D-09	-9.77442065D-08	-9.78790471D-08	-9.78790471D-08	-9.78790471D-08	-9.78790471D-08	-9.78790471D-08
1.20000000D-01	0.000000000D+00	5.04410380D-09	-2.56280690D-08	-2.58062087D-08	-2.58062087D-08	-2.58062087D-08	-2.58062087D-08	-2.58062087D-08
1.50000000D-01	0.000000000D+00	-2.04006416D-08	1.23085502D-07	1.22857956D-07	1.22857956D-07	1.22857956D-07	1.22857956D-07	1.22857956D-07
1.80000000D-01	0.000000000D+00	4.88393992D-09	1.06220372D-07	1.05937690D-07	1.05937690D-07	1.05937690D-07	1.05937690D-07	1.05937690D-07
2.10000000D-01	0.000000000D+00	4.87973262D-09	-5.71917855D-08	-5.75347849D-08	-5.75347849D-08	-5.75347849D-08	-5.75347849D-08	-5.75347849D-08
2.40000000D-01	0.000000000D+00	4.90586283D-09	-1.05662416D-07	-1.06070213D-07	-1.06070213D-07	-1.06070213D-07	-1.06070213D-07	-1.06070213D-07
2.70000000D-01	0.000000000D+00	-4.79951656D-08	2.09875879D-07	2.09359915D-07	2.09359915D-07	2.09359915D-07	2.09359915D-07	2.09359915D-07
3.00000000D-01	0.1096978240D-05	4.91908336D-09	-1.54067350D-07	-1.54657053D-07	-1.54657053D-07	-1.54657053D-07	-1.54657053D-07	-1.54657053D-07
3.30000000D-01	0.1109145273D-05	4.90235097D-09	-1.97239157D-07	-1.97948710D-07	-1.97948710D-07	-1.97948710D-07	-1.97948710D-07	-1.97948710D-07
3.60000000D-01	0.1109145273D-05	4.91438845D-09	1.98260945D-08	1.89917504D-08	1.89917504D-08	1.89917504D-08	1.89917504D-08	1.89917504D-08
3.90000000D-01	0.1121585230D-05	4.85971352D-09	-1.44263610D-08	-1.53889994D-08	-1.53889994D-08	-1.53889994D-08	-1.53889994D-08	-1.53889994D-08
4.20000000D-01	0.1134307399D-05	4.74913797D-09	-1.46154218D-07	-1.47247327D-07	-1.47247327D-07	-1.47247327D-07	-1.47247327D-07	-1.47247327D-07
4.50000000D-01	0.1147321494D-05	4.63128025D-09	4.15880099D-08	4.04549403D-08	4.04549403D-08	4.04549403D-08	4.04549403D-08	4.04549403D-08
4.80000000D-01	0.1160637680D-05	4.45390658D-09	3.70378901D-07	3.69060326D-07	3.69060326D-07	3.69060326D-07	3.69060326D-07	3.69060326D-07
5.10000000D-01	0.1174266597D-05	4.23985869D-09	2.77000748D-07	2.75495756D-07	2.75495756D-07	2.75495756D-07	2.75495756D-07	2.75495756D-07
5.40000000D-01	0.1188219395D-05	-7.07429284D-08	-6.21336675D-08	-6.38247699D-08	-6.38247699D-08	-6.38247699D-08	-6.38247699D-08	-6.38247699D-08
5.69999900D-01	0.1217143933D-05	-6.10936928D-08	-1.18398513D-08	-1.37702192D-08	-1.37702192D-08	-1.37702192D-08	-1.37702192D-08	-1.37702192D-08
5.99999900D-01	0.1232140783D-05	-4.95526433D-08	-1.14634431D-07	-1.16802906D-07	-1.16802906D-07	-1.16802906D-07	-1.16802906D-07	-1.16802906D-07
6.29999900D-01	0.1247511805D-05	-3.58115599D-08	1.93723432D-07	1.91263741D-07	1.91263741D-07	1.91263741D-07	1.91263741D-07	1.91263741D-07
6.59999800D-01	0.1263271177D-05	-1.96332968D-08	-2.21608700D-08	-2.49093537D-08	-2.49093537D-08	-2.49093537D-08	-2.49093537D-08	-2.49093537D-08
6.89999800D-01	0.1279433808D-05	-6.77740974D-10	2.33782189D-08	2.02886157D-08	2.02886157D-08	2.02886157D-08	2.02886157D-08	2.02886157D-08
7.19999800D-01	0.1296015373D-05	2.13456812D-08	-7.31643777D-08	-7.65913257D-08	-7.65913257D-08	-7.65913257D-08	-7.65913257D-08	-7.65913257D-08
7.49999800D-01	0.1313032376D-05	4.66411394D-08	-4.04818419D-08	-4.42973263D-08	-4.42973263D-08	-4.42973263D-08	-4.42973263D-08	-4.42973263D-08
7.79999700D-01	0.1330502196D-05	7.59433001D-08	2.21412357D-07	2.17343559D-07	2.17343559D-07	2.17343559D-07	2.17343559D-07	2.17343559D-07
8.09999700D-01	0.1348443152D-05	1.09458130D-07	2.99723895D-07	2.95165076D-07	2.95165076D-07	2.95165076D-07	2.95165076D-07	2.95165076D-07
8.39999700D-01	0.1366874563D-05	1.47845335D-07	2.23335017D-07	2.18292594D-07	2.18292594D-07	2.18292594D-07	2.18292594D-07	2.18292594D-07
8.69999600D-01	0.1385816818D-05	1.91262203D-07	-1.04686314D-07	-1.10260577D-07	-1.10260577D-07	-1.10260577D-07	-1.10260577D-07	-1.10260577D-07
8.99999600D-01	0.1405291455D-05	2.40932396D-07	-1.40836560D-07	-1.46990015D-07	-1.46990015D-07	-1.46990015D-07	-1.46990015D-07	-1.46990015D-07

kinetics, electrical networks, nuclear reactor control, tunnel switching problems and reversible enzyme kinetics. Our RAS of the integrator covers the whole of the left half of the complex plane. Hence, this integrator is fully recommended for users who are currently working in this area of research.

Table 7. Error in numerical integrators first component on Example 6.

Values of TI	Ademiluyi and Kayode (2001)	New integrator (Order = S + 3)		
		S = 2	S = 3	S = 4
0.5	0.62546D+10	-1.8597990000D-01	-4.1791014417D+08	1.0733593395D+11
1.0	-0.164725D-4	-2.5982120000D-06	7.0350798400D-06	4.4114315832D-04
1.5	0.884654D-5	2.7616450000D-06	5.4594691825D-06	3.2616226040D-04
2.0	0.285650D-4	5.7546770000D-06	4.2456011141D-06	2.6516493362D-04
2.5	0.439218D-4	8.1974730000D-06	3.1322937279D-06	-1.7729331943D-05
3.0	0.558816D-4	7.6845330000D-06	2.8370901596D-06	4.3121567216D-04
3.5	0.651960D-4	7.4236880000D-06	2.2622175933D-06	4.2652807910D-04
4.0	0.724500D-4	6.7186670000D-06	1.7225585679D-06	2.3561118467D-04
4.5	0.780994D-4	5.7379170000D-06	1.1743983170D-06	1.0220427121D-04
5.0	0.824992D-4	5.1037650000D-06	1.2824719999D-06	4.2256810127D-04
5.5	0.859258D-4	4.2722520000D-06	1.0587345097D-06	3.9742962227D-04
6.0	0.885944D-4	3.4621620000D-06	6.4438750580D-07	1.0882681777D-04

Table 8. Error in numerical integrators second component on Example 6.

Values of TI	Ademiluyi and Kayode (2001)	New integrator (Order = S + 3)		
		S = 2	S = 3	S = 4
0.5	-0.195980D-3	-2.3362080000D+00	2.0796841379D+05	-5.3681289336D+07
1.0	-0.130935D-3	-1.4621490000D-03	7.9457824294D-06	-4.5847248398D-07
1.5	-0.802970D-4	5.8857820000D-03	5.6141249800D-06	-3.4633949753D-07
2.0	-0.406600D-4	9.3650730000D-03	4.7584613492D-06	-2.8558171494D-07
2.5	-0.101465D-4	1.7823120000D-02	-1.0350207275D-05	-2.4721998593D-07
3.0	0.137732D-4	-8.0727550000D-03	4.2436688444D-06	-1.6707486894D-07
3.5	0.32401D-4	-1.0290480000D-03	3.4515515805D-06	-9.4924783589D-08
4.0	0.46910D-4	3.7119820000D-04	2.5510474640D-06	-7.1556906067D-08
4.5	0.58208D-4	6.9258230000D-04	1.6931455414D-06	-9.4993801825D-08
5.0	0.670084D-4	3.2224520000D-04	1.7304789729D-06	-5.7660370367D-08
5.5	0.738615D-4	2.8508780000D-04	1.3426086373D-06	-2.8298192567D-08
6.0	0.791987D-4	4.1747570000D-04	9.9075178761D-07	-2.2527173571D-08

Table 9. Error in numerical integrators first component on Example 7.

h	S = 2	Aashikpelokhai (1991)	Fatunla (1980)	Fatunla (1978)	Norelli (1985)	N_I
0.0125	1.8695066367D+00	1.8694389	1.8694388	1.8694389	N = 5:1. 8692929	80
0.0250	1.8660314693D+00	1.8694387	1.8694389	1.8694387	N = 5:1.8691415	40
0.0500	1.8636132555D+00	1.8694846	1.8694380	1.8694357	N = 5:1.8688354	20
0.1000	1.8712469008D+00	1.8695057	1.8705973	1.8693953	N = 5:1.8682097	10

Table 10. Error in numerical integrators second component on Example 7.

h	S = 2	Aashikpelokhai (1991)	Fatunla (1980)	Fatunla (1978)	Norelli (1985)	N_I
0.0125	-1.4822680915D-01	-0.14823588	-0.14823588	-0.14823587	N = 5:-0.1495268	80
0.0250	-1.4870613284D-01	-0.14823589	-0.14823587	-0.14823589	N = 5:-0.1497309	40
0.0500	-1.4904503196D-01	-0.14822960	-0.14823599	-0.14823631	N = 5:-0.1501113	20
0.1000	-1.4735968362D-01	-0.14822671	-0.14610294	-0.14824187	N = 5:-0.1507630	10

REFERENCES

Aashikpelokhai USU (1991). A Class of Non Linear One-Step Rational Integrators, Ph.D thesis, University of Benin, Benin city, Nigeria.

Aashikpelokhai USU (1996). On the Sensitivity and Accuracy of Two Pade Sequences. Nig. Ann. Nat. Sci. 3:71-78.

Aashikpelokhai USU (2000). A variable Order Numerical Integration based on Rational Interpolants. J. Nig. Mathe. Soc. 19:27-38.

Aashikpelokhai USU (2010). A General [L, M] One-Step Integrator for Initial Value Problems. Int. J. Comput. Mathe. 1-12.

Aashikpelokhai USU, Momodu B (2008). A quadratic based integration scheme for the solution of Singulo-stiff differential equations. IJPS, 3(4):97–103.

Abhulimen CE, Otunta FO (2007). A family of Two-step exponentially fitted multi derivable methods for the numerical integration of Stiff ivps in ODE. Int. J. Num. motion. 2:1-21.

Ademiluyi RA, Kayode SJ (2001). Maximum Order Second derivative hybrid multi-step methods for integration of initial value problems in Ordinary Differential Equations. J. Nig. Ass. Maths. Phys. 5:251–262.

Ademiluyi RA, Babatola PO, Areo EO (2007). Adaptive Runge-Kutta Method for solution of initial value problems in ode. Int. J. Num-Maths. 2(1):135–157.

Agbeboh GU, Aashikpelokhai USU, Aigbedion I (2007). Implementation of a new 4th Order Runge – Kutta Formula for solving Initial value problems (ivps). IJPS, 2(4):089–098. Online at http://www.academicjournals.org/IJPS. ISSN 1992 - 1950 © 2007 Academic Journals.

Atkinson K (1985). Elementary Numerical Analysis, John Wiley and Sons, New York.

Bartels R, Gautschi W, Witzgal C (1996). Introduction to Numerical Analysis, second edition, Donnelley & Sons, Harrisonburg, USA.

Burghes DN, Borries MS (1981). Modelling with Differential Equations, Ellis Horwood Limited, Chi Chester, London.

Birkhoff G, Rota G (1969). Ordinary Differential Equations, Blaisdell Publishing Company, USA.

Billingsley J (1989). Controlling with Computers, McGraw Hill Book Company, England.

Egbetade SA, Ajila RA, Oladeji FA, Odetunde OS (2008). On the Comparison of the Tau and Euler methods for the Numerical solution to initial value problems. Int. J. Num. Maths. 3(1):42–55.

Fatunla SO (1978). An Implicit Two – point Numerical Integration Formula for Linear and Nonlinear Stiff systems of Ordinary Differential Equations. Maths. Comp. 32(141):1–11.

Fatunla SO (1980). Numerical Integrators for Stiff and Highly Oscillatory Differential Equations. Maths. Comp. 34:373–390.

Fatunla SO (1982). "Non-Linear Multi-step Methods for ivps, Compt. Maths. Application. 18:231-239.

Health MT (1997). Scientific Computing: An Introduction Survey McGraw-Hill Companies, Inc, USA.

Jacques I, Judd CJ (1987). Numerical Analysis, Chapman and Hall Limited, New York.

Kolman B (1980). Introduction to Linear Algebra with Application, Macmillan Publisher Co Inc.

Kreider DL, Kuller RG, Ostberg DR (1968). Elementary Differential Equation, Addison – Wesley Publishing Company, Canada.

Lambert JD (1974). "Two Conventional Classes of Methods for Stiff Systems" (Ed Willoughby, R.A), Wildbad W. Germany, 171–186.

Lambert JD (1976). "Convergence and Stability", (Ed Hall G. and Watt, J.M), Oxford, 20–44.

Lambert JD (1995). Numerical Methods for Ordinary Differential Systems, John Wiley & Sons Ltd., England.

Lambert JD, Shaw B (1965). "On the Numerical Solution of $y^1 = f(x, y)$ by a class of formulae Based on Rational Approximation". Mathematics of Computation, 19:456–462.

Luke VL, Fair W, Wimp J (1975). "Predictor-Corrector Formulae based on Rational Interpolants", Computers and Mathematics with Applications. 1:3–12.

Momodu IBA (2006). Solution of Singulo-stiff Ordinary Differential Equation. PhD Thesis, AAU, Ekpoma.

Niekerk VFD (1987). Nonlinear one – step methods for Initial Value Problems, Comput. Maths. Application. 13:367–371.

Norelli F (1985). "High-Accuracy Explicit Spectral solvers for Stiff, Non-stiff and Highly Oscillatory Differential Systems", ENEA-Dipartiments Reattori Veloci, Centro ricerche energia Casaccia. pp. 1–62.

Parasuram S (2001). Handout M.3-Eigenvalues and Eigen Vector: http://www.mengritamu.edu/aparlos/MEEN651/EigenvaluesEigenvectors.pdf.

academicJournals

Vol. 8(34), pp. 1716-1721, 16 September, 2013
DOI: 10.5897/IJPS2013.3850
ISSN 1992 - 1950 © 2013 Academic Journals
http://www.academicjournals.org/IJPS

International Journal of Physical Sciences

Full Length Research Paper

Effect of dielectric constant on energy losses in lead sulphide thin films grown by solution method at room temperature

Mosiori, Cliff Orori

Department of Physics, School of Pure and Applied Sciences, Kenyatta University, Kenya.

Accepted 8 August, 2013

Thin films of lead sulphide (PbS) were deposited using chemical bath deposition (CBD) at different lead ion concentrations. A mixture of sodium hydroxide, varied concentrations of lead nitrate, triethanolamine (TEA), ammonia solution, thiourea, di-ionized and distilled water were used. A dip time of 120 min and pH of 9 at room temperature were maintained. It was found out that dielectric constants of the films varied from a maximum value of 12 to a minimum value of 2.3 in the photon energy range of 1.0 to 4.8 eV. Energy losses in the thin films were also found to be dependent on the concentration of lead ions in the bath and also this energy losses decreased as dielectric constants increased. It was concluded that the films could be used in photoconductivity, capacitance and solar cell absorber applications.

Key words: dielectric constant, thin films, lead sulphide, temperature.

INTRODUCTION

Semiconducting thin films and particularly lead chalcogenides have been widely studied owing to their interesting switching property (Prakash and Ashokan, 2004). These materials are used to fabricate a variety of electronic devices, which arises when the material is cast into thin film form. It is also observed that most physical properties reported on chalcogenides have been investigated using polycrystalline pellets or electrodeposits (Bresser et al., 1996; Lade et al., 1994). A good amount of work on DC conduction (Sagbo et al., 1994), contact capacitance (Simashkevin et al., 1994), spectral properties (Vidourek et al., 1995), AC conduction (Giuntini et al., 1995), and structural and magnetic properties (Dauoudi and Ekpunobi, 1996) has also been reported. However, dielectric constant behaviour as a function of energy loss and photon energy (frequency) has been over looked to some extent. In semiconductor thin film IR detector integrated circuits (for which high capacitance in small area is required), capacitors are grown by either evaporation or sputter techniques. When large-area capacitors are required, then the appropriate method of choice of growing them could be chemical bath method (CBD). To use lead sulphide thin film circuits, it is necessary that their dielectric and energy losses be understood so as they have appropriate value ranges. The dielectric coefficient of a thin film (capacitance) is an important practical parameter for assessing the expected behaviour of any thin film device. This makes it necessary to study the effect of energy, dielectric losses and (photon energy) frequency on thin films for any device fabrication. The dielectric behavior of thin film devices depends not only on their material properties but also on the method and conditions of preparation. Fringing effects at the edges of thin film dielectrics is usually negligible because the thickness of the dielectric is usually very small and uniform compared to its lateral

E-mail: cliffmosiori@gmail.com

Table 1. Parameters for depositing PbS thin films.

Conc. Pb^{+2} (mol.)	Vol. Pb^{+2} (cm^3)	Vol. 1M NaOH (cm^3)	Vol. 1M TU (cm^3)	Vol TEA (cm^3)
0.3	5	5	6	2
0.4	5	5	6	2
0.5	5	5	6	2
0.6	5	5	6	2
0.7	5	5	6	2

dimensions. The magnitude of its geometrics and measured influence of dielectric capacitance gains or losses may differ if the electric field at the thin film/metal insulator interface varies with the insulator over a certain region. For given material the film thickness alone establishes the capacitance density which in turn can be used to determine the area needed for a particular capacitance value. Since most capacitors utilize constant and uniform thickness then much concern is not only based on thickness but also on dielectric and energy losses in capacitor performance. The dielectric loss as part of the energy of an electric field is dissipated without recovery as heat in the dielectric material and is comprised of two parts; the first part arises due to lead resistance and electrode resistance. This part is frequency dependent. It is effective and very influential at higher frequencies or photon energies. It is minimized using high conducting metal electrodes. The other part arises due to material property and is also frequency dependent (Maissel and Glang, 1970). Dielectric strength is found to reduce rapidly below about 100 nm wavelength as the presence of pinholes or discrete defects in thin films increases. To the best of our knowledge, little or no reports is available on the study of dielectric properties of lead sulphide (PbS) thin films deposited by chemical bath at room temperature. In this paper, an attempt is made to report some of the dielectric properties of solution deposited PbS thin films for solar cell, charge storage/detection applications. In all the thin films used in this study, thickness thin film was kept at about 103 nm to minimize the inherent defects and pinholes.

METHODOLOGY

The chemical bath deposition technique was used. Glass substrate (microscope slides) which had been previously degreased in concentrated nitric acid for 24 h, cleaned in cold water with detergent, rinsed with di-ionized water and dried in clean dry air to provide better surface nucleation for growth of the films were used. A mixture of 1 M sodium hydroxide, 0.3 – 0.7 M lead nitrate solutions, 7.4 M triethanolamine (TEA), 14 M ammonia, 1 M thiourea, di-ionized and distilled water, microscopic glass slides and beaker were used. 5 ml of lead nitrate was poured into a 100 ml beaker followed by 5 ml of 1 M sodium hydroxide and then thoroughly stirred to obtain a milky solution. 6 ml of 1 M thiourea and 2 ml of 1 M tri-ethanolamine were immediately added, the mixture thoroughly stirred with a glass rod before glass slides was vertically introduced into the beaker. The dip time was kept at 120 min, and pH at 9 and at room temperature. Lead nitrate concentration was varied for the subsequent films from 0.4-0.7 M PbS as illustrated in Table 1. The grown samples were removed, rinsed with distilled water and allowed to dry before they were analyzed and characterized.

RESULTS

During deposition, cations and anions in the solution react to become neutral atoms, which precipitate slowly under the control of a complexing agent (TEA). With the addition of TEA, the reaction proceeded slowly so that PbS thin films of neutral atoms were formed on the substrate. The complexing agent slowed down precipitation action while ammonia served as a pH stabilizer. Sulphide ions were released by hydrolysis from thiourea and complexes formed were adsorbed onto the substrate as heterogeneous nucleation. Growth took place by ionic exchange reaction of S^{2-} with Pb^{2+} ions and by this process of ion-by-ion exchange, PbS thin films were deposited. The films were transparent, uniform and adherent though specularly reflecting. In discussing the dielectric properties of PbS thin films, a model to represent the dielectric property was used. A quantum–mechanical model to outline the characteristics of dielectrics of PbS thin films was used. The model predicts on the basis of classical mechanics. Based on the wave mechanical theory of matter, a dielectric is a material which is so constructed such that the lower bands of its allowed energy levels are completely full at the absolute zero of temperature (Exclusion Principle) and at the same time isolated from higher unoccupied bands by a large zone of forbidden energy levels. This is observed in PbS thin films (they have a dielectric constant of above 8). This shows that conduction in the lower fully occupied bands is impossible since there are no un-occupied energy levels to take care of the additional energy which would be acquired by the electrons from the applied field caused photons. The zone of forbidden energy levels is so wide that there is only a negligible probability that an electron in the lower band of allowed levels will acquire enough energy to make the transition to the unoccupied upper band where it could take part in conduction. That is why PbS thin films are poor solar cell absorber layers. When photons fall on PbS thin film layer, an electric field due to photons is impressed upon a PbS, positive and

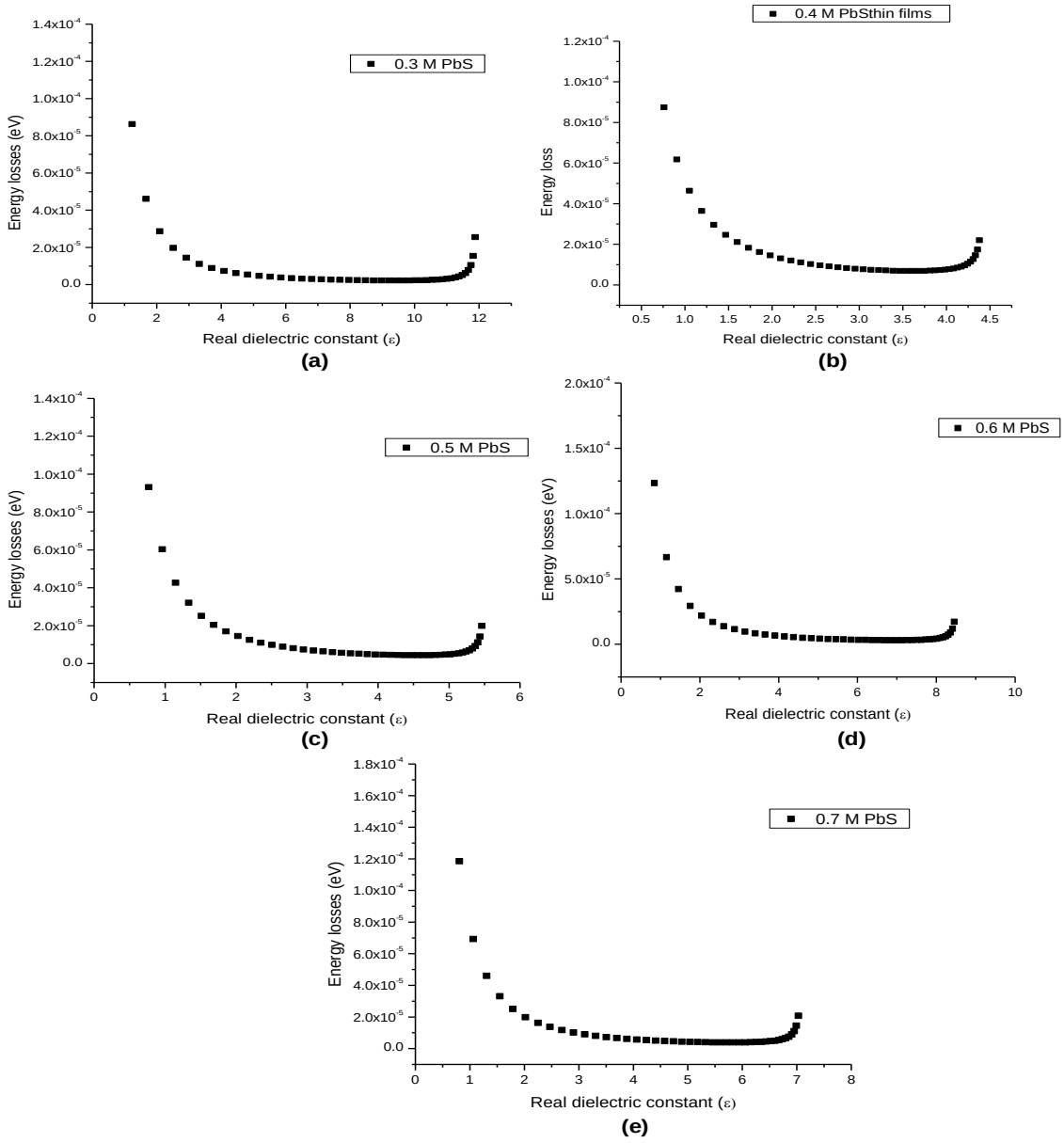

Figure 1. (a) Variation of real dielectric constant versus energy losses in 0.3 M PbS films; (b) Variation of dielectric constant against energy losses for 0.4 M PbS films; (c) Variation of real dielectric constant versus energy losses in 0.5 M PbS thin films; (d) Variation of real dielectric constant versus energy losses in 0.6 M PbS thin films; (e) Variation of real dielectric constant versus energy losses in 0.7 M PbS films.

negative charges in their atoms and molecules are displaced in opposite directions causing polarization. Since the motion of charges of opposite sign move in opposite directions, they constitute an electric current called a polarization current. This polarization causes energy losses in PbS thin films (Figure 1a to d). A charge accumulating in PbS thin film layer in an un-measurably short time referred to as the instantaneous dielectric constant or geometric dielectric constant describes the property of the medium giving rise to the effect called dielectric states (Figure 1 a-d). This is recognized by the modern theory that identifies two distinct types of charges and charging currents that rapidly results into forming instantaneous polarizations and absorptive polarizations. PbS thin films depends on this mechanism as shown in Figure 2. The effect of chemical and physical structures in PbS dielectric constant depend on two quantities; magnitude and relaxation-time which in turn determine many of the properties of dielectric polarizations of the absorptive type. The magnitude of the polarizability (*k*) of PbS can be expressed in terms of a directly measurable quantity or by simulation in relation to dielectric constant

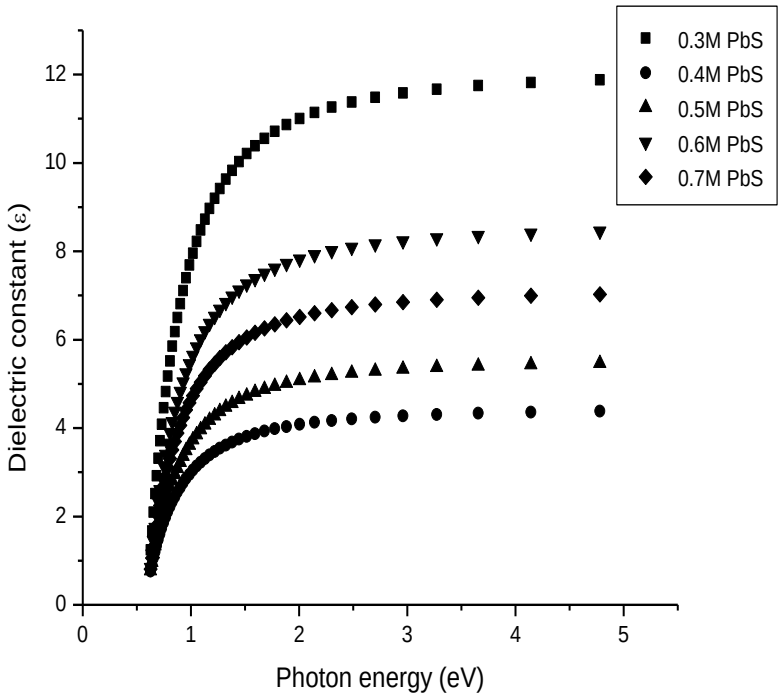

Figure 2. Variation of dielectric constants versus photon energy (eV) for PbS.

by the relation:

$$k = \frac{3(\varepsilon-1)}{4\pi(\varepsilon+2)} \quad (1)$$

A classification of dielectric polarization into absorptive polarization has been made based on this expression. Electronic polarizations are due to the displacement of charge within the atoms and are the most important of the instantaneous polarizations that determine the dielectric constant of PbS thin films. Polarizability per unit volume due to the electronic polarizations is considered to be a quantity which is proportional to the number of bound electrons in a unit volume and inversely proportional to the forces binding them to the nuclei of the atoms. This occurs in PbS molecules. This is depicted by the small band gap of about 0.4 eV for PbS thin films. It is known that the time required for any applied field to displace electrons within an atom to a new position with respect to their nuclei is so short that there is no observable effect of time or frequency upon the value of the dielectric constant. This is true only until frequencies corresponding to absorption lines in the visible or ultra-violet spectrum are attained (called the optical frequency range). The frequencies in the optical range corresponding to the absorption lines in the spectrum, the dielectric constant or better the refractive index changes rapidly with frequencies and till absorption starts to appears. This is why this report is justified to use refractive index (n) and dielectric constant (ε) interchangeably for the qualitative discussion of the properties of dielectric polarization that follows the relation $\varepsilon = n^2$, which is known as Maxwell's rule based on electromagnetic theory and only applicable whenever 'ε' and 'n' are measured at the same frequency no matter how high or low they may be. The refractive index (n) in the visible spectrum provides the means of determining the magnitude of electronic polarizations since other types of polarizations have negligible magnitude when frequency of the impressed field lies in the visible spectrum. For materials like PbS having only electronic polarizations, dielectric properties are simply independent of frequency in the electrical frequency range and are characterized by complex dielectric behaviours. PbS thin films also experience atomic polarizations. Atomic polarizations form part of the polarization of a molecule which can be attributed to the relative motion of the atoms in a molecule which it is composed. They are attributed to perturbation by any applied field causing vibrations on atoms due to energy gained from photons. Ions having their characteristics or resonance in the infra-red range experience them and thus PbS thin films that are sensitive to infra-red and atomic polarization begin to contribute to ε or n^2 at frequencies below approximately 10^{14} seconds; that is, in the near infrared and about 10^{10} cycles per second frequency where optical and electrical frequencies ranges merge. Atomic polarizations contribute a constant amount to ε and n^2 for any given material. It is taken as the difference between polarization (measured at some low infrared or high electric frequency) and the

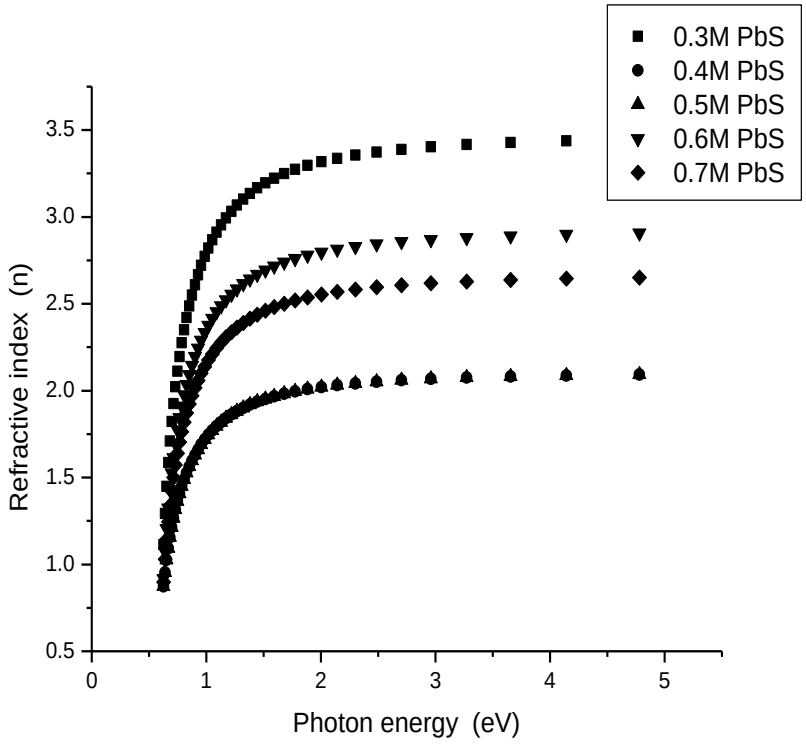

Figure 3. Variation of refractive index versus photon energy for PbS thin films.

electronic polarization as determined from refractive index measurements in the visible spectrum. When photoelectric effect causes a field to be applied, there is a tendency for molecules in a material to align themselves with their dipole axes in the direction of that filed. This dipole polarization is superimposed upon electronic and atomic polarizations induced by the field. Since dipole polarization depends upon the displacement of charges within an atom, rather than upon the displacement of charges within a molecule, time required for this type of polarization to form depends on internal frictions of the material. Debye expressed time of relaxation of the dipole polarization in terms of the internal frictional force by the equation:

$$\tau = \frac{\xi}{2kT} = \frac{8\pi\eta r^2}{2kT} \quad (2)$$

where ξ is the internal friction coefficient, η is the coefficient of viscosity, *r* is the radius of the molecule and T is the absolute temperature. Applying this equation to the calculation of the relaxation time for PbS thin films at room temperature, τ is found to be 10^{-10} seconds assuming that PbS molecular radius is 2 x 10^{-8} cm and taking viscosity as 0.01 poises as they form in the bath, the result agrees with the experimental studies extending from 10^{9} to10^{11} cycles. This is what causes the dielectric constant to decrease from its highest value to a value approximately equal to the square of their refractive index as seen in Figure 3.

Conclusion

Thin films of PbS were successfully deposited at room temperature using CBD at different lead ion concentrations. Their dielectric constant varied from a maximum value of 12 to a minimum value of 2.3 in the photon energy range of 1.0 to 4.8 eV. Energy loss was found to decrease as the dielectric constant of the thin film increases and it was concluded that the films could be used in photoconductivity, capacitor fabrication and solar cell absorber applications.

ACKNOWLEDGEMENTS

We acknowledge the assistance offered by the Department of Physics, Kenyatta University where this study was carried out and the Department of Material Science, University of Nairobi (Chiromo campus) for kindly providing UV-VIS-NIR spectrophotometer for spectral analysis.

REFERENCES

Bresser J, Fajinmi G, Sasusi Y (1996). Deposition time dependence on absorptivity of chemically deposited lead sulphide thin films. Res. J.

Appl. Sci. 9:931-937.
Chouldrury N, Sarma K (2008). Structural characterisation of nanocrystralline PbS thin films: synthesised by CBD method. Indian J. Pure. Appl. Phys. 46:261-265.
Dauoudi I, Ekpunobi A (1996). Optical properties and band offsets of CdS/PbS superlattice. The Pacific J. Sci. Technol, 11:404-407.
Glang M, Maisset A (1970). The influence of hydrazine hydrate in the preparation of lead sulphide thin film. Iranian J. Sci. Technol. 29:151-162.
Giuntini R, Pawar S, More P, Pawar A, Patil V (2010). Nanocrystalline PbS thin films: Synthesis, microstructural and optoelectronic properties. Scholars Res. Libr. 2:1-6.
Osherov A, makai J, Balasz J, Horvath Z., Gutman, N, Amir S, Golan Y (2010). Tenability of optical band edge in thin PbS films chemically deposited on GaAs(100). J. Condensed Matter. 22:1-7.
Patil R, Lisca M, Stancu V, Buda M, Pentia E, Botila A (2006). Crystalline size effect in PbS thin films grown on glass substrates by chemical bath deposition. J. Optoelectr. Advan. Mater. 1:43-45.
Pentia E, Pintilie L, Matei I, Botila T, Ozbay E (2001). Chemical prepared nanocrysalline PbS thin films. J. Optoelectr. Advan. Mater. 3:525-530.
Prakash V, Jumate N, Popescu G, Moldovan M, Prejmeriean C (2004). Studies of some electrical and photoelectrical properties of PbS films obtained by sonochemical methods. Chalcogenide Lett. 7:95-100.
Simashkevin S, Kamoun N, Brini R. Amara A (1994). Structural and optical properties of PbS thin films deposited by chemical bath deposition. Elsevier Mater. Chem. Phys. 97:71-80.
Sagbo A, Junghare A, Wadibhasme N, Darypurkar A, Mankar R, Sangawar V (1994). Thickness Dependent Structural, Electrical and Optical Properties of Chemically Deposited Nanopartical PbS Thin Films. Turk. J. Phys. 31:279-286.
Vidourek J, J´auregui R, Ram´ırez-Bon A, Mendoza-Galva´n, M, Sotelo-Lerma A (1995). Optical properties of PbS thin films chemically deposited at different temperatures. Thin Solid Films, 441:104–110.

academicJournals

Vol. 8(34), pp. 1722-1728, 16 September, 2013
DOI: 10.5897/IJPS09.146
ISSN 1992-1950 © 2013 Academic Journals
http://www.academicjournals.org/IJPS

International Journal of Physical Sciences

Full Length Research Paper

Second-order kinetic model for the adsorption of divalent metal ions on *Sida acuta* leaves

Oboh I. O.[1]*, Aluyor E. O.[2] and Audu T. O. K.[2]

[1]Department of Chemical and Petroleum Engineering, University of Uyo, Uyo, Nigeria.
[2]Department of Chemical Engineering, University of Benin, Benin city, Nigeria.

Accepted 4 September, 2013

The removal of metal ions from effluents is of importance to many countries of the world both environmentally and for water re-use. A comparison was made of the linear least-squares method of the widely used pseudo-second order kinetic model for the sorption of some divalent metal ions onto *Sida acuta* leaves. Four pseudo-second order kinetic linear equations were used for this study. The results obtained from the experimental data for *S. acuta* leaves of 1.0 g with particle size range of 0.25 to 0.5 mm and at 300 rpm with initial concentrations of 5.0, 4.0, 20 and 2.5 mg/dm^3 for Cu^{2+}, Ni^{2+}, Pb^{2+} and Zn^{2+} ions, respectively showed that when the four pseudo-second order kinetic linear equations were compared, the Type 2 model with regression values for Cu^{2+}, Ni^{2+}, Pb^{2+} and Zn^{2+} ions as 0.979, 0.995, 0.991 and 0.965 respectively showed best fit for the sorption onto *S. acuta* leaves. This provided the evidence that the divalent metal ions sorption unto *S. acuta* followed the pseudo-second – order kinetic expression.

Key words: *Sida acuta*, sorption, divalent metal ions, kinetic model, effluents.

INTRODUCTION

Elements in every group of the periodic table have been found to be stimulatory to animals. Most metals in the fourth period are carcinogenic. It can be assumed that the carcinogenicity is related to the electronic structure of transition and inner transitional metals (Luckey and Venugopal, 1977). Sorption of pollutants from wastewater has long been studied. The rate at which sorption takes place is of the utmost importance when designing batch sorption systems, consequently it is important to establish the time dependence of such systems under various process conditions (Ho, 2006).

The sorption of metal ions from aqueous solution plays an important role in water pollution control, and in recent years there has been considerable interest in the use of low-cost sorbents such as peat for this purpose. However, although the sorption kinetics of individual metal ions onto this type of material has been examined, the processes which occur are not completely understood, for instance, the rate limiting step and the bonding mechanism (Ho and McKay, 2000).

The application of low-cost sorbents including carbonaceous materials, agricultural products and waste by-products has been investigated. In recent years, agricultural by-products have been widely studied for metal removal from water. These include peat, wood, pine bark, banana pith, rice bran, soybean and cottonseed hulls, peanut shells, hazelnut shell, rice husk, sawdust, wool, orange peel and compost and leaves. Most of this work has shown that natural products can be good sorbents for heavy metals (Ho et al., 2002).

*Corresponding author. E-mail: obohio2009@yahoo.com.

Table 1. A comparison of the second order models.

References	Linear form	Plot
Sobkowsk and Czerwinski (1974)	$\frac{\theta}{1-\theta} = k_2 t$	$\frac{\theta}{1-\theta}$ vs. t
Ritchie (1977)	$\frac{q_\infty}{q_\infty - q} = \alpha t + 1$	$\frac{q_\infty}{q_\infty - q}$ vs. t
Blanchard et al. (1984)	$\frac{1}{n_0 - n} - \alpha_\beta = kt$	$\frac{1}{n_0 - n}$ vs. t
Ho (1995)	$\frac{t}{q_t} = \frac{1}{kq_e^2} + \frac{1}{q_e} t$	t/q_t vs. t

Sida acuta is a malvaceous weed that frequently dominates improved pastures, waste and disturbed places roadsides (Mann et al., 2003). The plant is native to Mexico and Central America but has spread throughout the tropics and subtropics (Holm et al., 1977). A comparison of the second order model is shown in Table 1. Sobkowsk and Czerwinski (1974) used a second-order rate equation based on the sorption capacity of a solid for a higher concentration of the solid for the rate of reaction of carbon dioxide sorption on a platinum electrode. Ritchie (1977) used a second-order empirical equation to test the sorption of gases onto a solid. The Ritchie equation has also been applied in solution/solid sorption systems. Blanchard et al. (1984) reported a similar rate equation for the overall exchange reaction of NH_4^+ ions fixed in zeolite by divalent metallic ions in solution. The second-order expression of Blanchard et al. (1984) was used to describe the kinetics of exchange processes between the sodium ions from zeolite A and cadmium, copper, and nickel ions from solutions. In recent years, Ho (2006) described sorption, which included chemisorption and provided a different idea to the second-order equation called a pseudo-second-order rate expression.

The purpose for this study is to know if the sorption of some divalent metal ions onto *S. acuta* leaves used as sorbent follows the pseudo-second –order kinetic expression.

MATERIALS AND METHODS

Preparation of *S. acuta* leaves

The leaves were dried at room temperature for a period of three days. The sorbent was screened to obtain a geometrical size of 0.25 - 0.5 mm. This was to allow for shorter diffusion path, thus allowing the sorbent to penetrate deeper into the effluent more quickly, resulting in a higher rate of adsorption (Adeyinka et al., 2007).

Phytochemical screening

Phytochemical tests were carried out on the powdered plant material employing standard phytochemical procedures to establish the presence or otherwise of secondary metabolites such as alkaloids, steroids, flavonoids, tannins and saponin glycosides (Sofowora, 1982; Evans, 1989).

Preparation of synthetic wastewater

Stock solutions of Nickel, Lead, Copper, Zinc and Aluminium were prepared with distilled water and Nickel (II) Sulphate, Lead (II) Nitrate, Zinc (II) Sulphate, and Copper (II) Sulphate respectively. All working solutions were obtained by diluting the stock solution with distilled water. The pH of the effluent was adjusted to a pH of 5 to prevent hydrolysis by the use of relevant acids and bases. The concentration of metal ions in effluent was analyzed by Atomic Absorption Spectrophotometer.

For quality control purpose, the diluted water were digested and analyzed with every sample group to track any possible contamination source. A duplicate was analyzed for every sample to track experimental error and show capability of reproducing results (Marshall and Champagne, 1995).

Adsorption experiment

The experiments were carried out in the batch mode for the measurement of adsorption capabilities. The bottles with 500 ml capacity were filled with 50 ml of the synthetic wastewater, and 1 g of *S. acuta* dried leaves (ground). The bottles were shaken for a predetermined period at room temperature in a reciprocating shaker for 2 h at 300 rpm.

The separation of the adsorbents and solutions was carried out by filtration with Whatman filter paper No. 42 and the filtrate stored in sample cans in a refrigerator prior to analysis. The residual metallic ion concentrations were also determined using an Atomic Absorption Spectrophotometer (AAS).

RESULTS AND DISCUSSION

Table 2 shows that *S. acuta* contained bioactive constituents such as alkaloids, flavonoids, cardiac and

Table 2. Results of phytochemical tests.

Test	Observation	Inference
Molisch's test for carbohydrates	Deep violet ring was observed at the interface	Carbohydrates present
Fehling's solution test for reducing sugar	A brick-red precipitate was observed	Glycoside present
Frothing test for saponin glycosides	Persistent frothing was observed	Saponin glycoside present
Blood haemolysis test for saponin glycoside	Clear zones of haemolysis was observed	Saponin glycoside confirmed
Borntrager's test for anthraquinone glycosides	No pink colouration was observed	Anthraquinone glycoside absent
Test for cyanogenetic glycosides	Yellow colour of sodium picrate paper retained.	Cyanogenetic glycoside absent
Keller-killiani test for deoxy-sugar	A brown ring was observed at the interface	Deoxy-sugar present in cardiac glycosides
Kedde's test for lactone ring	A violet colour that faded gradually with the deposition of whitish crystalline solid was observed	Lactone ring present in cardiac glycosides
Lieberman's test for steroidal ring	A colour change from violet to blue to green was observed	Steroidal ring present in cardiac glycosides
Salkowski's test for steroidal ring	A reddish-brown colour was observed at the interface	Steroidal ring present in cardiac glycosides
Tests for flavonoids	A yellow colour which turned to colourless was observed	Flavonoids present
Aqueous ferric chloride test for Tannins	No blue black, green or blue green precipitate or colouration observed	Tannins absent
Test for Phlobatannins	No red precipitate was observed	Phlobatanins absent
Test for alkaloids using water, methanol and chloroform as extracting solvents	Wagner's, Hager's and Dragendorff's reagent gave characteristic precipitates with methanol and chloroform extracts	Alkaloidal base present

saponin glycosides. An expression of the pseudo-second-order rate based on the solid capacity has been presented for the kinetics of sorption of divalent metal ions onto peat (Ho, 2006):

$$q_t = \frac{q_e^2 kt}{1 + q_e kt}, \quad (1)$$

where k is the pseudo-second-order rate constant (g/mg min), q_e is the amount of cadmium ion sorbed at equilibrium (mg/g), and q_t is amount of cadmium ion on the surface of the tree fern at any time, t,(mg/g). Equation 1 can be rearranged to obtain

$$q_t = \frac{t}{1/kq_e^2 + t/q_e}, \quad (2)$$

This has a linear form of

$$\frac{t}{q_t} = \frac{1}{kq_e^2} + \frac{1}{q_e} t. \quad (3)$$

If the initial sorption rate, as $h = q_t/t$ when t approaches 0, h (mg/g min), is

$$h = kq_e^2. \quad (4)$$

Table 3. Pseudo-second order kinetic model linear forms.

Type	Linear form	Plot	Parameter
Type 1	$\frac{t}{q_t} = \frac{1}{kq_e^2} + \frac{1}{q_e} t$	t/q_t vs. t	$q_e = 1/\text{slope}$ $k = \text{slope}^2/\text{intercept}$ $h = 1/\text{intercept}$
Type 2	$\frac{1}{q_t} = \left(\frac{1}{kq_e^2}\right)\frac{1}{t} + \frac{1}{q_e}$	$1/q_t$ vs $1/t$	$q_e = 1/\text{intercept}$ $k = \text{intercept}^2/\text{slope}$ $h = 1/\text{slope}$
Type 3	$q_t = q_e - \left(\frac{1}{kq_e^2}\right)\frac{q_t}{t}$	q_t vs q_t/t	$q_e = \text{intercept}$ $k = -1/\text{intercept x slope}$ $h = -\text{intercept/slope}$
Type 4	$\frac{q_t}{t} = kq_e^2 - kq_e^2 q_t$	q_t/t vs q_t	$q_e = -\text{intercept/slope}$ $k = \text{slope}^2/\text{intercept}$ $h = \text{intercept}$

Equation 2 can be rearranged to obtain

$$q_t = \frac{t}{1/h + t/q_e}, \quad (5)$$

and

$$\frac{t}{q_t} = \frac{1}{h} + \frac{1}{q_e} t. \quad (6)$$

In order to distinguish the kinetics equation based on the concentration of a solution from the sorption capacity of solids, this second-order rate equation has been called a pseudo-second-order one since it was represented.

The pseudo-second-order rate constants can be determined experimentally by plotting t/q_t against t. Although there are many factors which influence the sorption capacity, including the initial sorbate concentration, the reaction temperature, the solution pH value, the sorbent particle size and dose, and the nature of the solute, a kinetic model is concerned only with the effect of observable parameters on the overall rate (Ho, 2006). In this study, regression, r^2, was used to test the best-fitting of the kinetic model to the experimental data.

The least squares method is used for finding the parameters for kinetic models. The pseudo-second–order kinetic model has been linearized into four different types which were shown in Table 3 and a simple linear regression could result in different parameter estimates (Kinniburgh, 1986; Longhinotti, 1998; Ho, 2004). The most popular linear used is Type 1.

Figures 1 to 4 show experimental data with linear equations of the four pseudo-second–order kinetic models obtained by using the linear method for the sorption of the divalent metal ions under study onto *S. acuta*. Values of the pseudo-second – order kinetic model constant, k, the amount of the divalent metal ions under study sorbed at equilibrium, q_e, and the initial sorption rate, h, are listed in Table 4. The regression (r^2) values obtained for Type 3 indicated that there was a strong positive evidence that the divalent metal ions sorption unto *S. acuta* followed the pseudo-second –order kinetic expression. It is clear that transformations of non-linear pseudo-second –order kinetic models to linear forms implicitly alter their error structure and may also violate the error variance and normality assumptions of standard least-squares method (Longhinotti et al., 1998; Ho, 2004). In a linear analysis, different linear forms of the same model would significantly affect calculations of the parameters.

Conclusion

The following conclusion can be drawn as follows:

(1) The results show sorption of divalent metal ions used

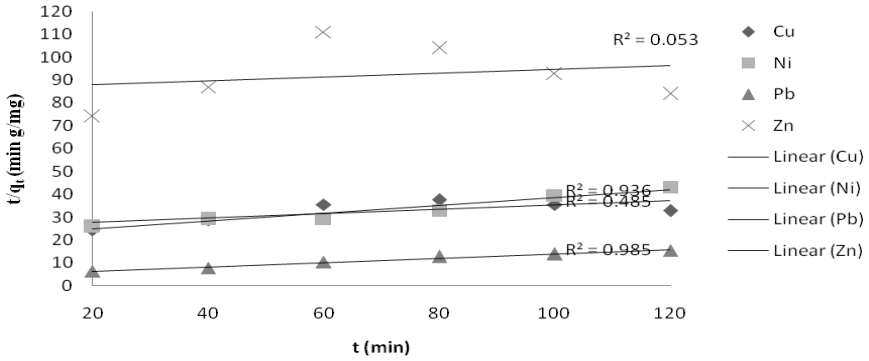

Figure 1. Type 1 pseudo-second- linear equations obtained by using the linear equations obtained from the linear method for the sorption of divalent metal ions onto sida acuta leaves.

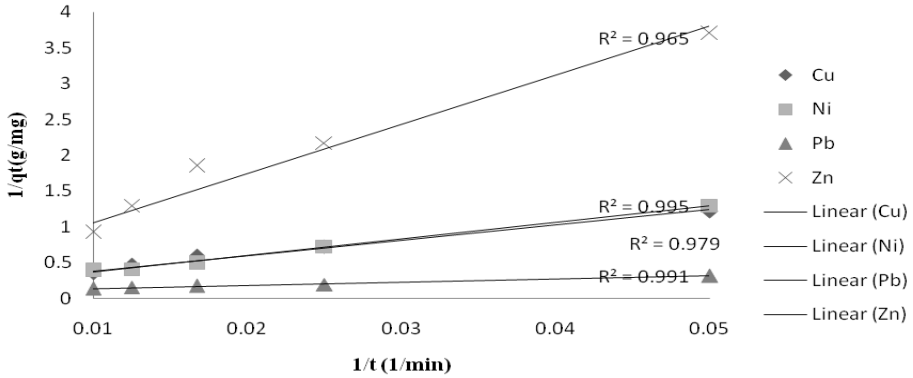

Figure 2. Type 2 pseudo-second- linear equations obtained by using the linear equations obtained from the linear method for the sorption of divalent metal ions onto sida acuta leaves.

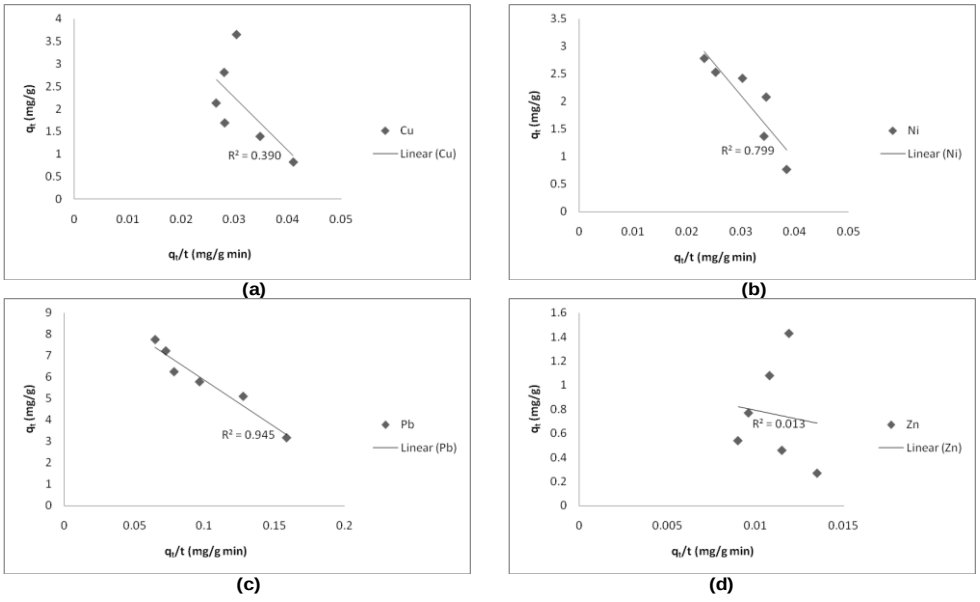

Figure 3. Type-3 pseudo-second- linear equations obtained by using the linear equations obtained from the linear method for the sorption of (a) Cu^{2+} ions, (b) Ni^{2+} ions, (c) Pb^{2+} ions, and (d) Zn^{2+} ions onto sida acuta leaves.

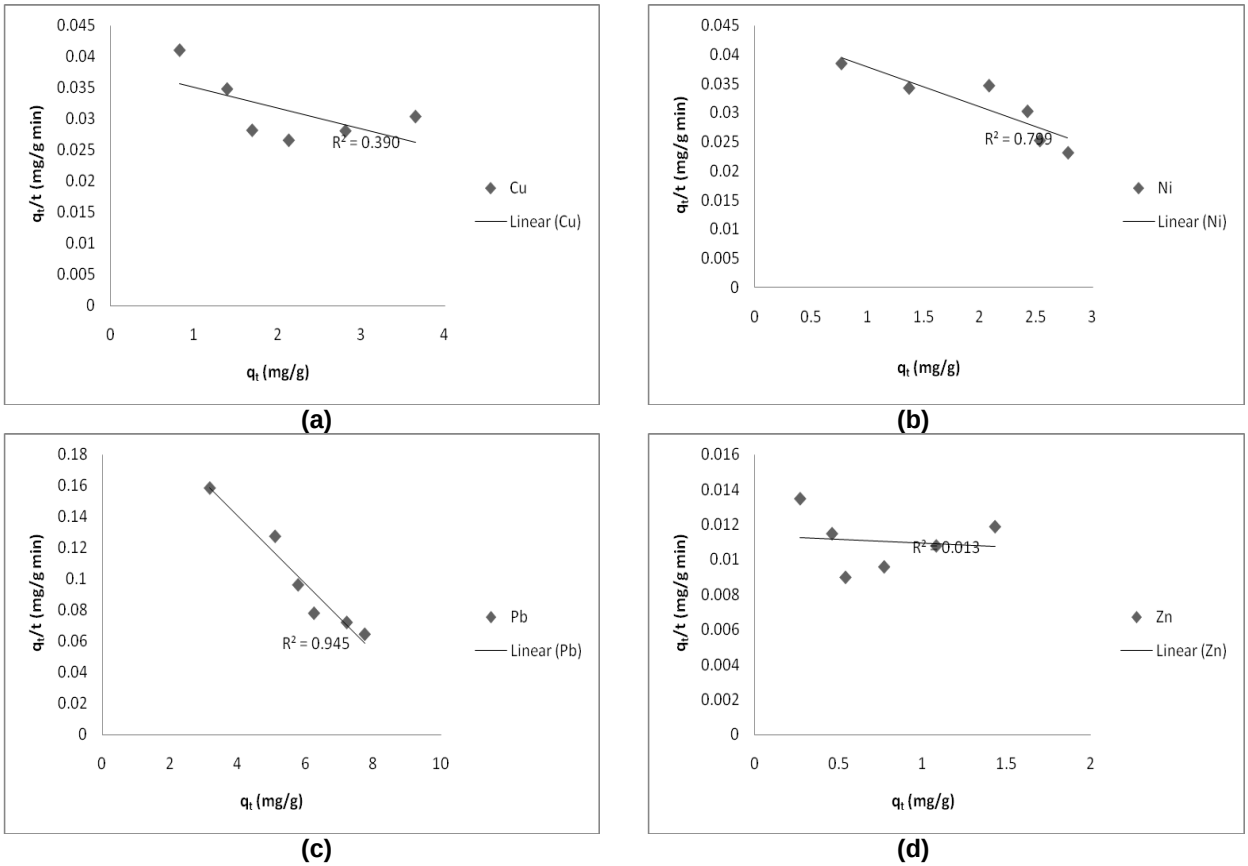

Figure 4. Type-4 pseudo-second- linear equations obtained by using the linear equations obtained from the linear method for the sorption of (a) Cu^{2+} ions, (b) Ni^{2+} ions, (c) Pb^{2+} ions, and (d) Zn^{2+} ions onto sida acuta leaves.

Table 4. Pseudo-second-order kinetic parameters obtained by using the linear methods for divalent metal ions.

Type	Parameter	Cu^{2+}	Ni^{2+}	Pb^{2+}	Zn^{2+}
Type 1	q_e (mg/g)	10.783	5.805	10.556	11.884
	k (g/mg min)	0.00033	0.00139	0.00200	0.00008
	h (mg/g min)	0.0385	0.0469	0.2232	0.0116
	r^2	0.485	0.985	0.936	0.053
Type 2	q_e (mg/g)	6.040	6.8630	10.315	2.668
	k (g/mg min)	0.00127	0.00093	0.00217	0.00205
	h (mg/g min)	0.0465	0.0436	0.2310	0.0146
	r^2	0.979	0.995	0.991	0.965
Type 3	q_e (mg/g)	5.770	5.620	10.206	1.099
	k (g/mg min)	0.00148	0.00152	0.00225	0.02955
	h (mg/g min)	0.0493	0.0481	0.2347	0.0357
	r^2	0.390	0.799	0.945	0.013
Type 4	q_e (mg/g)	11.522	6.529	10.456	25.850
	k (g/mg min)	0.00029	0.00105	0.00208	0.00002
	h (mg/g min)	0.0385	0.0447	0.2273	0.0114
	r^2	0.390	0.799	0.945	0.013

for the study on to *S. acuta* leaves by agitation; a pseudo-second order model can describe the sorption process. (2) The sorption equilibrium capacity, the sorption rate constant and the initial sorption rate can be a function of the metal ion present.

REFERENCES

Adeyinka A, Liang H, Tina G (2007). Removal of Metal Ion form Waste Water with Natural Waste, Sch. Eng. Technol. 33(4):1-8.

Blanchard G, Maunaye M, Martin G (1984). Removal of heavy metals from waters by means of natural zeolites, Water Res. 18(12):1501–1507.

Evans WC (1989). Trease and Evan's Pharmacognosy. English Language Book Society Bailliere Tindale, London. 13th edn., pp.39, 54-55, 131-132, 387, 546, 800-803.

Ho YS (1995). Adsorption of heavy metals from waste streams by peat. Ph.D. thesis, University of Birmingham, Birmingham, UK.

Ho YS, Mckay G (2000). The Kinetics of Sorption of Divalent Metal Ions onto Sphagnum Moss Peat, *Wat. Res.* 34(3):735-742.

Ho YS, Huang CT, Huang HW (2002). Equilibrium sorption isotherm for metal ions on tree fern. Process Biochem. 37:1421-1430.

Ho YS (2004). Selection of optimum sorption isotherm. Carbon 42(10): 2115-2116.

Ho YS (2006). Second-order kinetic model for the sorption of cadmium onto tree fern: A comparison of linear and non-linear Methods. Water Res. 40:119-125.

Holm LG, Plucknett DL, Pancho JV, Herberger JP (1977). The Worlds Worst Weeds: distribution and biology (University Press of Hawaii, Honolulu, USA).

Kinniburgh DG (1986). General purpose adsorption isotherms, Environ. Sci. Technol. 20(9):895-904.

Longhinotti E, Pozza F, Furlan L, Sanchez MDND, Klug M, Laranjeira MCM, Favere VT (1998). Adsorption of anionic dyes on the biopolymer chitin. J. Brazilian Chem. Soc. 9(5):435-440.

Luckey TD, Venugopal B (1977). Metal Toxicity in Mammals, Physiologic and Chemical Basis for Metal Toxicity, New York: Plenum Press, Vol. 1.

Mann A, Gbate M, Umar AN (2003). *Sida acuta* subspecie *acuta*. *Medicinal and economic plant of Nupeland.* Jube Evans Books and Publication, P. 241.

Marshall WE, Champagne TE (1995). Agricultural Byproducts as Adsorbents for Metal Ions in Laboratory Prepared Solutions and in Manufacturing Wastewater, *Journal of Environmental Science and Health, Part A:* Environ. Sci. Eng. 30(2):241-261.

Ritchie AG (1977). Alternative to the Elovich equation for the kinetics of adsorption of gases on solids. J. Chem. Soc. Faraday Trans. I 73(10):1650-1653

Sobkowsk J, Czerwinski A (1974). Kinetics of carbon dioxide adsorption on a platinum electrode, J. Electroanal. Chem. 55(3):391-397.

Sofowora A (1982). Medicinal Plants and Traditional Medicine in Africa. John Wiley and Sons, Chichester. pp. 142-145.

academicJournals

Vol. 8(34), pp. 1729-1737, 16 September, 2013
DOI: 10.5897/IJPS2013.3988
ISSN 1992 - 1950 © 2013 Academic Journals
http://www.academicjournals.org/IJPS

International Journal of Physical Sciences

Full Length Research Paper

Influence of fuel in the microwave assisted combustion synthesis of nano α-alumina powder

Ramesh G.[1]*, Mangalaraja R. V.[2], Ananthakumar S.[3] and Manohar P.[1]

[1]Department of Ceramic Technology, A.C Tech. Campus, Anna University, Chennai, India.
[2]Department of Materials Engineering, University of Concepcion, Concepcion, Chile.
[3]Materials and Minerals Division, National Institute for Interdisciplinary Science and Technology (NIIST), Trivandrum, India.

Accepted 4 September, 2013

Microwave assisted combustion synthesis is used for fast and controlled processing of advanced ceramics. Single phase and sinter active nano crystalline alpha alumina powders were successfully synthesized by different fuel-to-oxidant molar ratios using aluminium nitrate as an oxidiser, glycine as a reducing agents and millipore water as a solvent by microwave assisted combustion synthesis. Thermodynamic modelling of the combustion reaction shows that as the fuel-to-oxidant ratio increases, the amount of gases produced and adiabatic flame temperature also increases. The precursor powders were investigated by thermogravimetry (TG) analyses. The as prepared precursors calcined at 900 to 1200°C in air atmosphere were characterized for their structure and morphology. The thermal analyses (TG/DSC), X-ray diffraction (XRD) and Fourier transform infra red (FT-IR) results demonstrate the effectiveness of the microwave assisted combustion synthesis. The transmission electron microscopy (TEM) observations show the different morphologies of as-prepared powders and shows the particle sizes in the range of <50 nm. The results confirm that the homogeneous, nano scale alumina powders derived by microwave assisted combustion have high crystalline quality and the morphology of the as-prepared precursor powders.

Key words: Synthesis, microwave, glycene-gel, decomposition, alumina, nano crystalline.

INTRODUCTION

Alumina as an excellent ceramic material, finds potential application because of its high melting point (2400°C) with excellent chemical stability, high corrosion resistivity and low volatility in vacuum. Synthesis of fine-grained ceramic products has been the topic of many recent investigations on account of their beneficial properties over coarse-grained ceramics (Yi-quan and Yu-feng, 2001; Edrissi and Norouzbeigi, 2007; Shojaie-Bahaabad and Taheri-Nassaj, 2008; Robert et al., 2009; Mimani and Patil, 2001; Ananthapadmanabhan et al., 2004).

Over the last few decades, a great variety of techniques have been developed to synthesize highly reactive and high-purity materials to fabricate fine-grained ceramic products. The techniques including spray pyrolysis, precipitation (Shaoyan et al., 2008), sol-gel (Mirjalili et al., 2010), hydrothermal and combustion synthesis (Robert et al., 2009; Chyi-Ching et al., 2004; Ganesh and Ferreira, 2007) have been employed to synthesise ultra fine Al_2O_3 powders. Mechanical synthesis of α-Al_2O_3 requires extensive mechanical ball milling and easily introduces impurities. Vapour phase reaction for the preparation fine α-Al_2O_3 powder from a gas phase precursor demands high temperature above 1200°C. Sol-gel method based on molecular precursors

*Corresponding author. E-mail: rameshsrirangam@rediffmail.com.

usually makes use of metal alkoxides as raw material. However, the high prices of alkoxides and long gelation periods limit the application of this method. The precipitation method suffers from its complexity and time consuming (long washing times and aging time). The direct formation of α-Al_2O_3 via the hydrothermal method needs high temperature and pressure. Most of these techniques involve expensive raw materials and are associated with unmanageable processing steps.

Fortunately, the drawbacks of these methods as mentioned above could be partially eliminated by the so called combustion synthesis (also known as self-propagating high-temperature synthesis). It is emerged as effective powder synthesis route as it is a simple and economic process and yields high-purity powders with excellent homogeneity and fine particle sizes (Singanahally and Alexender, 2008; Edrissi and Mohammad, 2008). Combustion synthesis is not only simple, but safe and rapid process wherein the main advantages are energy and time savings. This quick, straightforward process can be used to synthesize homogeneous, high-purity, crystalline oxide ceramic powders including ultrafine alumina powders with broad range of particle sizes.

The basis for the combustion synthesis comes from the thermo-chemical concepts used in the field of propellants and explosives. This technique involves the exothermic chemical reaction of a fuel (for example, citric acid, urea, glycine, oxalic acid or glycol, etc.) and an oxidizer (for example, nitrates) (Tianyou et al., 2006; Jiang et al., 2007). The exothermicity sometime appears in the form of flame, which temperature can be in excess of 1500°C. The large amount of gases generated during combustion synthesis rapidly cools the product leading to nucleation of crystallites without any substantial growth. The gas generated also can disintegrate the large particles or agglomerates; therefore, the resulted product consists of very fine particles of friable agglomerates or nanoparticles (Xiujing and Yan, 2006).

Actually, the mechanism of the combustion reaction is quite complex. The main parameters influencing the reaction include type of the main fuel, fuel to oxidizer ratio, the amount of oxidizer in excess, ratio of fuels, pH of the solution and rate of calcinations. In general, a good fuel should not react violently nor produce toxic gases, and must act as a complexing agent for metal cations.

In the present research, we have proposed a new method called 'microwave-assisted glycene-gel decomposition technique' to prepare nonocrystalline alumina powders. Compared to conventional heating, microwave heating leads to a more uniform microstructure. In the microwave process, heat will be generated internally within the material, instead of originating from external sources. Because of the rapid heating of the microwave process, lower processing temperatures are needed which in turn provides a suitable condition for the formation of nano-sized powders. Microwave synthesis of alumina powder reduces the sintering temperature and thereby reducing the particle size.

The use of microwave energy for the synthesis of ceramic oxide powders using a few fuels has been earlier reported (Ganesh et al., 2005; Mangalaraja et al., 2009). The powders synthesized by this technique are ultrafine, pure and more homogeneous and less-agglomerated. The present work reports the synthesis of alumina nano powders using varied fuel to oxidant ratio and heating. Microwave assisted glycene-gel decomposition technique under normal atmospheric pressure has not been studied so far thoroughly. Decomposition of the glycene precursor, phase transformations and morphology of the synthesized alumina powder are investigated. Also in this synthesis, Millipore water is used as a solvent to dissolve aluminium nitrate and fuel to synthesis process for producing alumina nano powders.

Generally, natural water contains soft particulates (vegetable debris) and hard particulates (sand, rock) as well as colloidal matters that can interfere in processing factors. Natural water contains dissolved gases such as nitrogen, oxygen and carbon dioxide. The concentrations of oxygen and nitrogen may affect the products. Inorganic ions (such as sodium, calcium, magnesium or iron, and anions, such as bicarbonate, chloride and sulphate) even at trace levels, may affect chemical reactions by acting as catalysts. Milli-Q system has three-step purification in one unit. Secondary purification via high-recovery reverse osmosis cartridge removes 95 to 99% of inorganic ions, 99% of dissolved organics, bacteria, and particulates. The purifications of Millipore process gives the water resistivity 18.2 MΩ-cm at 25°C and the particulate level is <1 particulate/ml.

The extent of conversion to the α-Al_2O_3 phase depends on the temperature and the time of calcinations. Generally, it exists in a number of meta-stable polymorphs before a complete transformation to thermodynamically stable α–alumina. These polymorphs include γ (gamma), Θ (theta), η (eta), δ (delta), χ (chi), k (kappa) and β(beta). The formation of one, two or more of above mentioned transient aluminas before the complete transformation to the final stable α–alumina depends upon the processing conditions, the degree of crystallinity and the presence of impurities in the starting materials. The powders obtained through combustion synthesis were characterized by Fourier transform infra red (FT-IR), X-ray diffraction, thermo gravimetric analysis (TG), and Transmission electron microscopy (TEM).

EXPERIMENTAL

In a typical experiment, a solid mixture containing indispensable quantities of aluminium nitrate (Merck, GR grade), and glycene (Merck, GR grade) was taken in a Pyrex glass dish and was irradiated with microwaves in a modified domestic microwave over (ONIDA, POWER BARBEQUE 28, India, Model No. 28CJS14, microwave 900 W, input range 230 V ac 50 Hz, microwave

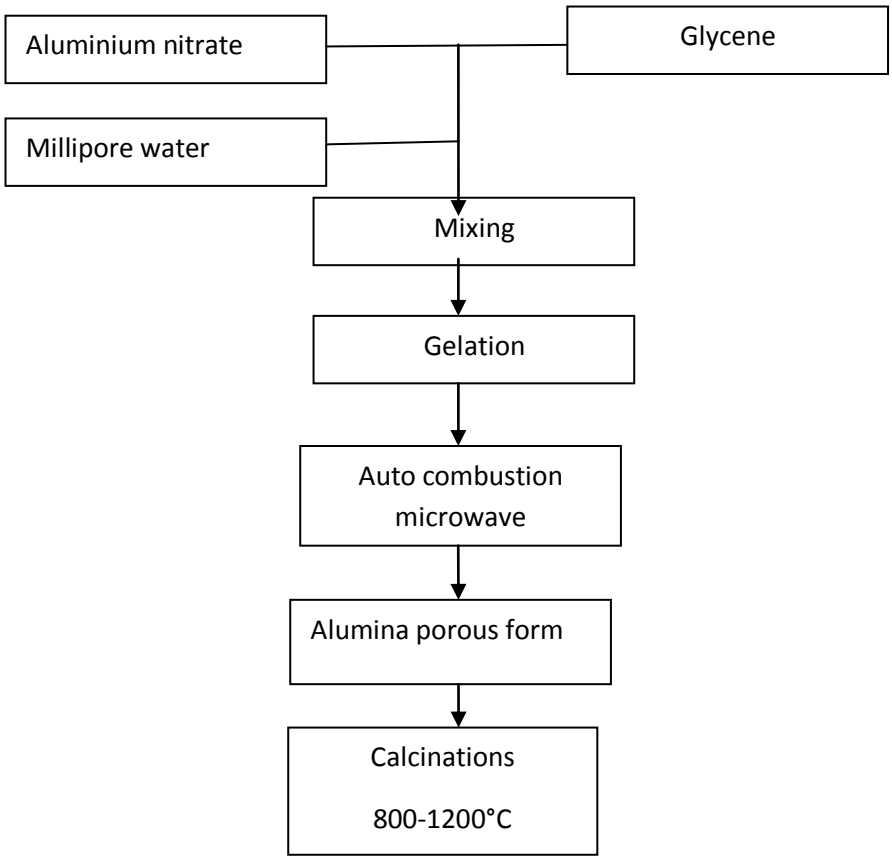

Figure 1. Schematic of the Nitrate-Glycene combustion process.

frequency 2.45 GHz) to produce alumina material. A provision was made for the escape of combustion gases by providing an exhaust of the microwave oven.

In general, the raw materials must be readily available and convenient. In addition, it should react non-violently and produce non-toxic gases. The molar ratio of glycene (combustion aid) to aluminium nitrate (main oxidizer) was selected in the amounts of 0.51 (high level), 0.60 (stiochiometric) and 0.71 (low level). The initial composition of the solution containing aluminium nitrate, $Al(NO_3)_3.9H_2O$ and glycene was derived from the total oxidizing and reducing valences of the oxidizer and fuel using the concepts of propellant chemistry. Carbon, hydrogen and aluminium were considered as reducing elements with the corresponding valences of +4, +1 and +3 respectively. Oxygen was considered as an oxidizing element with the valence of 2, the valence of nitrogen was considered to be 0 because of its conversion to molecular nitrogen (N_2) during combustion. The total calculated valence of metal nitrated by arithmetic summation of oxidizing and reducing valences was -15. The calculated valence of glycene was +9. The stoichiometric composition of the redox mixture demanded that 2(-15) + n (+9) = 0, or n = 3.33 mol. This calculation was done for mixture of aluminium nitrate and glycene.

The products were synthesized by an amount of 15 gm per batch. The meticulous process is given in the form of flowchart as shown in Figure 1. The aluminium nitrate and glycene were dissolved in a required amount of Millipore water and mixed thoroughly to ensure a molecular level mixing to form a homogeneous solution. Metal nitrates possess hygroscopicity; consequently, they easily absorb moisture and become slurry. Therefore, the reactants can be mixed homogeneously during the stirring process. The mixture solution was transferred to a Pyrex glass dish and later introduced into a microwave oven to undergo decomposition in the microwave field of 2.45 GHz. Initially, the solution was boiled to transform to a honey like consistency, that escort to a transparent sticky gel and then the gel was immediately decomposed by a self-combustion accompanied by the evolution of a brown fume and finally yielded a fluffy precursor which did not contain crystalline phases. During decomposition of gel, a large amount of gaseous products N_2, CO_2 and H_2O evolved without the necessity of getting oxygen from outside.

In fact, on all fuel-to-oxidant ratios evaluated, upon auto-ignition, it resulted in a brownish voluminous product identified by XRD as an amorphous structure, which indicates the incomplete combustion probably due to characteristics of fuel employed. Subsequently, these powders were calcined at 800, 900, 1000 and 1200°C at a heating rate of approximately 10°C/min., during 2 h of soaking time. The prepared powders were characterised by X-ray diffraction (XRD), Fourier transform infra red (FT-IR) and thermal analysis (TG and DSC) techniques. The as prepared powders were also investigated by the thermal analysis (TG/DSC) and Fourier transform infra red (FT-IR) studies.

X-ray diffraction was executed on combustion synthesized powders for phase characterization, at a rate of 60/min., using Cu Ka radiation on a General Engineering X-ray diffractometer (model GE-110T). Silicon was also employed as an external standard for correction due to instrumental broadening. The phase structure and crystallite size of the prepared Al_2O_3 powder was estimated from X-ray peak broadening using Scherer formula.

Table 1. Effect of fuel ratio on phase and crystallite size of calcined alumina.

Temperature (°C)	Phase			Crystallite size (nm)			Crystallite size*		
	G/N =0.51	G/N =0.60	G/N =0.71	G/N=0.51(H)	G/N=0.60(S)	G/N=0.71(L)	G/N =0.51	G/N =0.56	G/N =0.69
800	-	-	-	Amorphous	Amorphous	Amorphous			
900	γ , δ	γ	γ , δ , α	49	49	38	90.3	96.8	123.2
1000	γ , δ	γ , δ , α	γ , δ , α	50	46	46			
1200	α	α	α	52	51	45			

*Effect of crystallite size at 1100°C for different glycine-to-nitrate ratios- report of Toniolo et al. (2005).

The theoretical chemical reaction equation of the stoichiometric combustion reaction can be written as follows:

Stoichiometry

$$1.0\ Al(NO_3)_3.9H_2O + 1.67\ NH_2CH_2COOH \longrightarrow 0.5\ Al_2O_3 + 2.33\ N_2 + 3.33\ CO_2 + 13.17\ H_2O$$

Fuel-rich (+ 17.62%)

$$1.0\ Al(NO_3)_3.9H_2O + 1.96\ NH_2CH_2COOH + 1.32O_2 \longrightarrow 0.5\ Al_2O_3 + 4.96\ N_2 + 3.92\ CO_2 + 13.9\ H_2O$$

Fuel-lean (-15.54%)

$$1.0\ Al(NO_3)_3.9H_2O + 1.41\ NH_2CH_2COOH \longrightarrow 0.5\ Al_2O_3 + 4.41\ N_2 + 2.82\ CO_2 + 12.52\ H_2O + 1.155\ O_2$$

RESULTS AND DISCUSSION

Powder X-ray analysis

The average crystallite size values were estimated using the following equation of Scherrer.

$$D = \frac{0.9\lambda}{\sqrt{B2 - b2\cos\Theta}}$$

Where D is the average crystallite size, λ the wavelength of the radiation, Θ the Bragg's angle and B and b are the FWHMs observed for the sample and standard, respectively. Silicon powder was used to measure the instrumental peak broadening. Terms B and 2Θ were obtained from each XRD pattern and PC-APD (X-manager) software that uses information of ICDD (international center of diffraction data) to recognize alumina phases. The average crystallite size for each sample was calculated from the above formula.

Toniolo et al. (2005) studied the crystallite size of the powder for the fuel-to-oxidant ratio varied by the combustion synthesis technique using glycine as fuel and aluminium nitrate as an oxidizer to produce alumina powders through conventional heating process. In this present work, comparison was made between variation in the powder characteristics obtained through microwave assistance for different fuel-to-oxidant ratios with Toniolo et al. (2005). The phase structure and crystallite size of the prepared Al_2O_3 powder estimated from X-ray peak broadening using Scherrer formula is shown in Table 1.

As can be observed from Figure 2 (G/N=0.50), the fuel rich batch powders obtained by the combustion of aluminium nitrate and glycene mixture in a domestic microwave oven for 4 min. exhibited significantly broad XRD peaks indicative of excess quantity of heat generated and radiated from inner atom to outer surface of the material. The sample 1d shows at temperature higher than 1000°C high intensities of α-Al_2O_3 peaks are observed, indicating crystallite growth of the grains. With the increase of calcinations temperature up to 1000°C, the crystallinity of α-Al_2O_3 improved as shown in the samples 1b and 1c. At 1200°C, rather weak peaks of α-Al_2O_3 disappear, indicating γ to α-Al_2O_3 transition. The γ-Al_2O_3 peaks, except for the strongest one disappear, indicating the γ to α-Al_2O_3 phase transition is almost completed. At temperature higher than 1000°C, high intensities of α-Al_2O_3 peaks are observed, indicating crystallite growth of the grains.

As can be observed from Figure 2 (G/N=0.60), the stoichiometric batch powders obtained by the combustion of aluminium nitrate and glycene mixture in a domestic microwave oven for 4 min. exhibited a few broad XRD peaks indicatives of crystallite size growing up and α-Al_2O_3 crystallite rapidly grew up to 51 nm as transformation was completed. XRD patterns show that samples 2a has more amorphous particles than the others. Also the crystallinities of sample 2d are better than those of other samples. Furthermore, samples 2b and 2c are mixtures of δ and γ phases and a sample 2d is a pure α-alumina. The results show that when an XRD profile has broad peaks, the crystallite sizes are small and the crystallinity is poor but when the peaks are narrow, the corresponding crystals are large.

From Figure 2 (G/N=0.71), the fuel rich batch material obtained from the identical reaction mixture in a domestic microwave oven shows in sample 3d, the complete transformation to α-phase took place after calcinations temperature of 1200°C. This result illustrates an advantage of microwave heating since the formation time and temperature are significantly reduced compared to conventional heating. The formation of γ-Al_2O_3 was first detected in sample 3b after increase in calcinations temperature: γ-Al_2O_3 was still the main constituent for this heating amount. Some δ and α-Al_2O_3 the intermediate

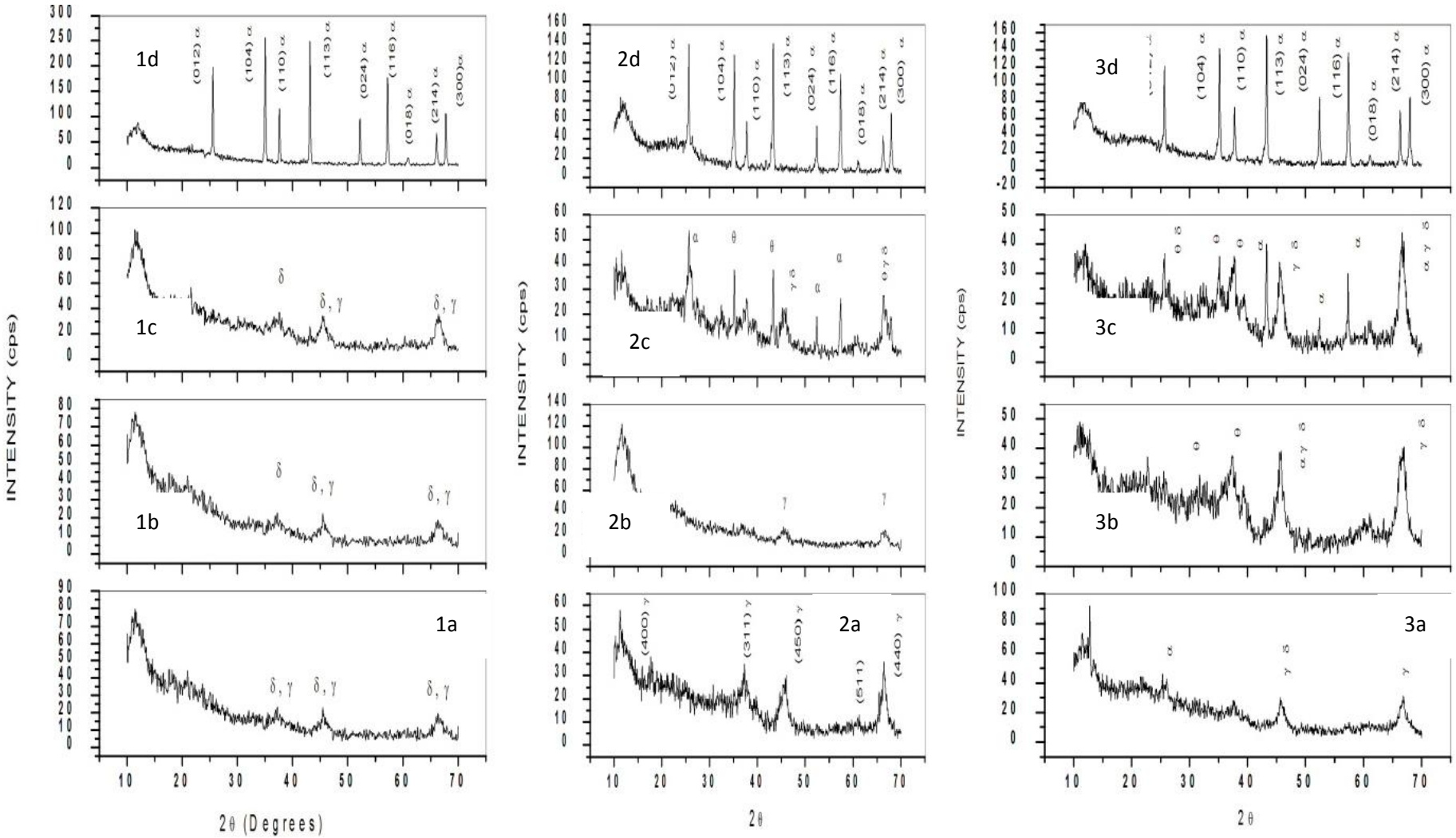

Figure 2. XRD patterns of as-synthesized precursors G/N=0.51,0.60 and 0.71 calcined at a) 800°C (b) 900°C (c) 1000°C (d) 1200°C.

phases were detected before α-Al_2O_3 formation. The amount of gases released during the exothermic reaction is very high, so it cools the reaction environment. These results in poor crystallinity in some prepared powders also control the growth of crystal size. Figure 3 shows the variation of crystallite size with different G/N ratios.

The particle size of α-Al_2O_3 was obtained about

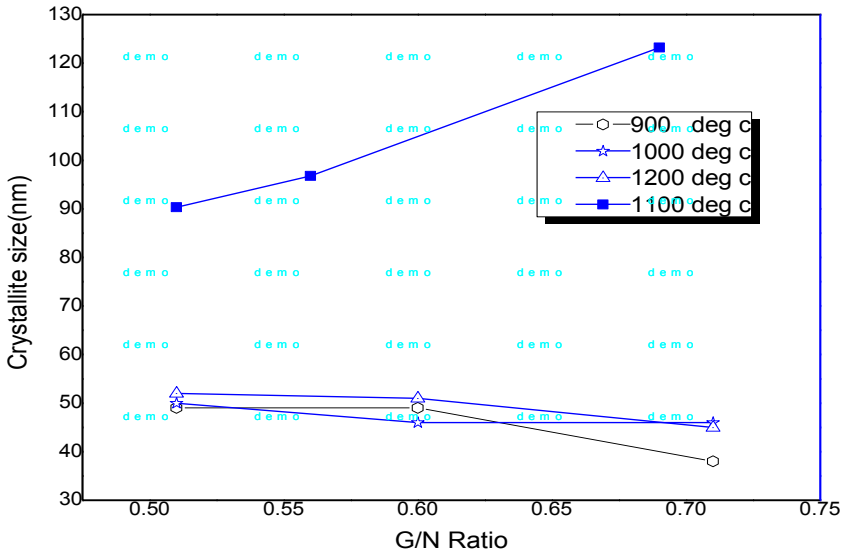

Figure 3. Different molar ratio and crystallite size at different calcined temperature.

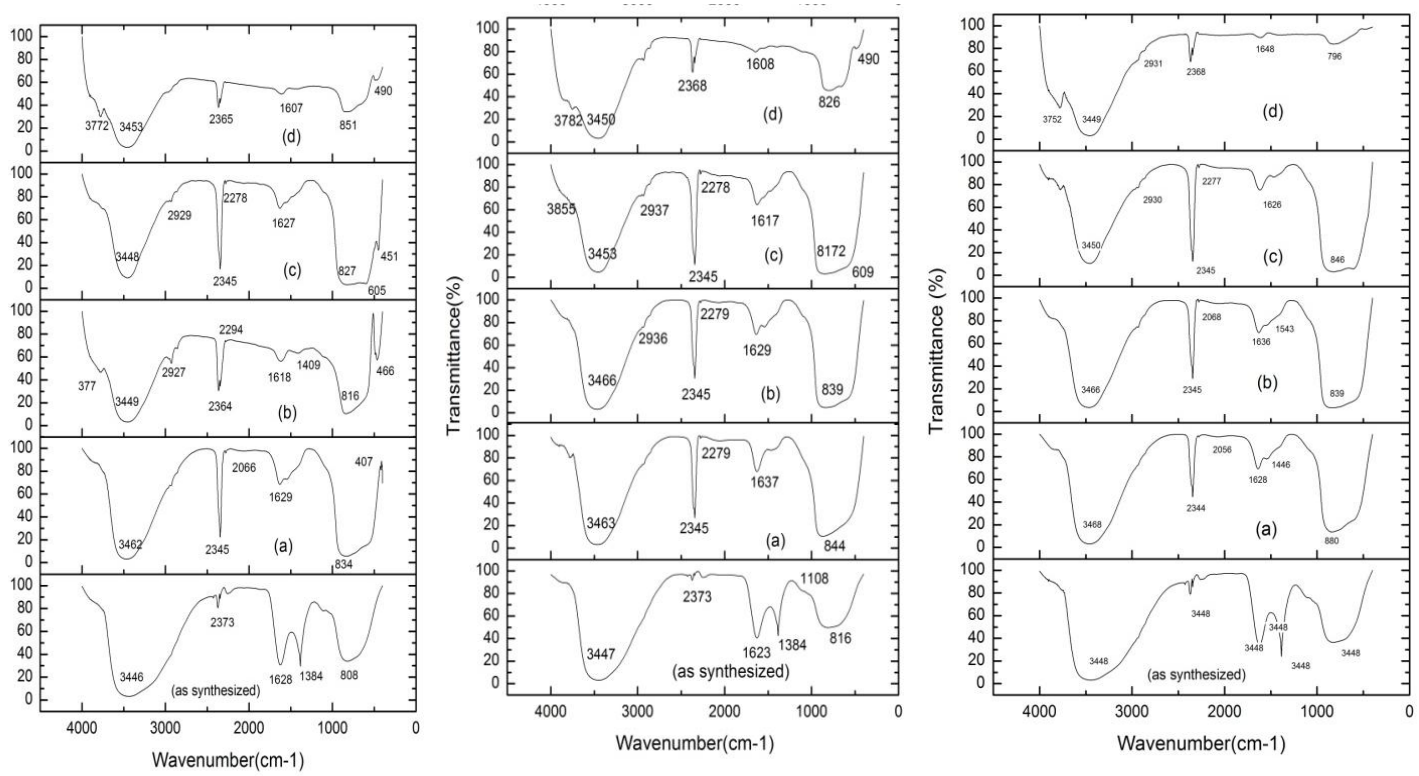

Figure 4. FTIR Spectrum of as-synthesized precursors G/N=0.51,0.60 and 0.71 calcined at 1)as synthesized a) 800°C, (b) 900°C, (c) 1000°C and (d) 1200°C.

38 nm in the case of lean fuel, 46 nm in the case of stoichiometric and 49 nm for fuel rich, and there was prominent change obtained by comparing this microwave assistance and Millipore water usage with respect to conventional process with ordinary distilled water.

FTIR analysis

The FTIR at 4000-400 cm^{-1} for the precursor (G/N=0.51, 0.60 and 0.71) calcined at different temperatures are shown in Figure 4. This clearly shows a broad absorption

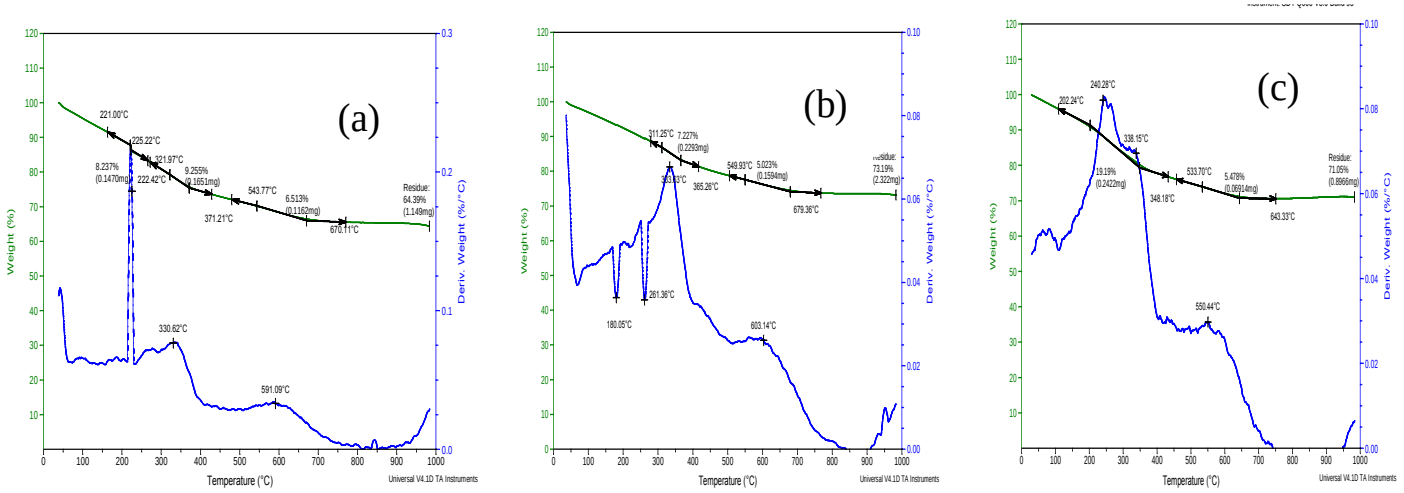

Figure 5. Simultaneous DSC-TGA curves of the as prepared powder of (a)G/N=0.51, (b) G/N=0.60 and (c) G/N=0.71.

at around 3400 cm^{-1} and a small absorption at 654 cm^{-1}, which are characteristic stretching vibration and deformation vibration of hydroxyl group (O-H), respectively. The characteristic bands of nitrate ions in the region of 1385 cm^{-1} indicate its incomplete decomposition during heat-treating process of the gel in the microwave synthesis. Peaks localized at 1623 cm^{-1} are assigned to asymmetrical stretching vibration of carboxyl ions (COO^-). In the FTIR spectra of powder calcined at 800°C and above, the absorption bands of NO_3^- group disappear because of the complete decomposition of nitrate. At different calcined G/N ratios reveals the appearance of ammonium ions in the regions of 2365 cm^{-1}.

DSC-TGA analysis

As shown in Figure 5a (0.51), the most weight loss 9% occurs between 321 to 371°C due to evaporation of volatile components. The weight loss of the as synthesized powder is less than 6.5% between 543 to 670°C. So the volatilization does not occur obviously. From 670 to 983°C, a weight loss occurs due to volatilization of carbon which corresponds to an endothermic reaction. However, there was an exothermic reaction due to crystallization of transition phases of alumina in this range. Above 983°C, an exothermic reaction occurs due to transformation of transition phases of alumina to α-alumina. With TG analysis, it was possible to confirm phase transformation into thermodynamically stable crystallographic alpha alumina which starts at about 983°C. This result agrees with that obtained by XRD analyses.

In Figure 5b (0.6), the TG curve demonstrates two weight loss steps. First, it was verified on a significant fall by about 7.2% at 311°C. The second drop was slight by about 5% at 550 to 750°C. Afterwards the curve became horizontal. In Figure 5c (0.71), the TG curve demonstrates two weight loss steps. First, it was verified on an important fall by about 19.19% at 202°C; it shows exothermic behaviour of auto-ignition. The second drop was slight by about 5.47% between 240 to 534°C. Above 643°C the curve became horizontal.

Between 533 to 643°C is expected and observed weight losses may be attributed to the remained carbon contamination, which can be inferred from the fact that a grayish product was obtained. The total weight loss above 643°C of TGA curve also indicates that the remaining carbon is slowly decomposed. However, compared to three molar ratios processed precursor through microwave synthesis, it inferred that fuel lean is suitable for synthesis of high purity and crystallite particles due to electric induction of atom to produce sufficient temperature for the reactions. The thermal characteristic of the synthesized alumina precursor powder is shown in Table 2.

TEM data

Figure 6 is a TEM photograph taken after the as-synthesized product had been calcined at different temperature of 900, 1000 and 1200°C. The sizes of the spherical particles are dispersed with negligible agglomeration and are homogeneously distributed ranging from 38 to 46 nm, which is about the same as the sizes estimated by using XRD method.

Conclusions

Nanocrystalline Al_2O_3 powders were prepared with crystallite sizes ranging between 38 and 52 nm using

Table 2. Thermal characteristics of the Al_2O_3 precursor materials.

Stages	G/N=0.51		G/N=0.60		G/N=0.71	
	Decomposition Temperature (°C)	Mass loss%	Decomposition Temperature (°C)	Mass loss%	Decomposition Temperature (°C)	Mass loss%
First	222	8.237	311	7.227	202	19.19
Second	371	9.255	550	5.023	534	5.478
Third	670	6.519	---	---	---	--
Stability	983	64.40	983	73.19	983	71.05

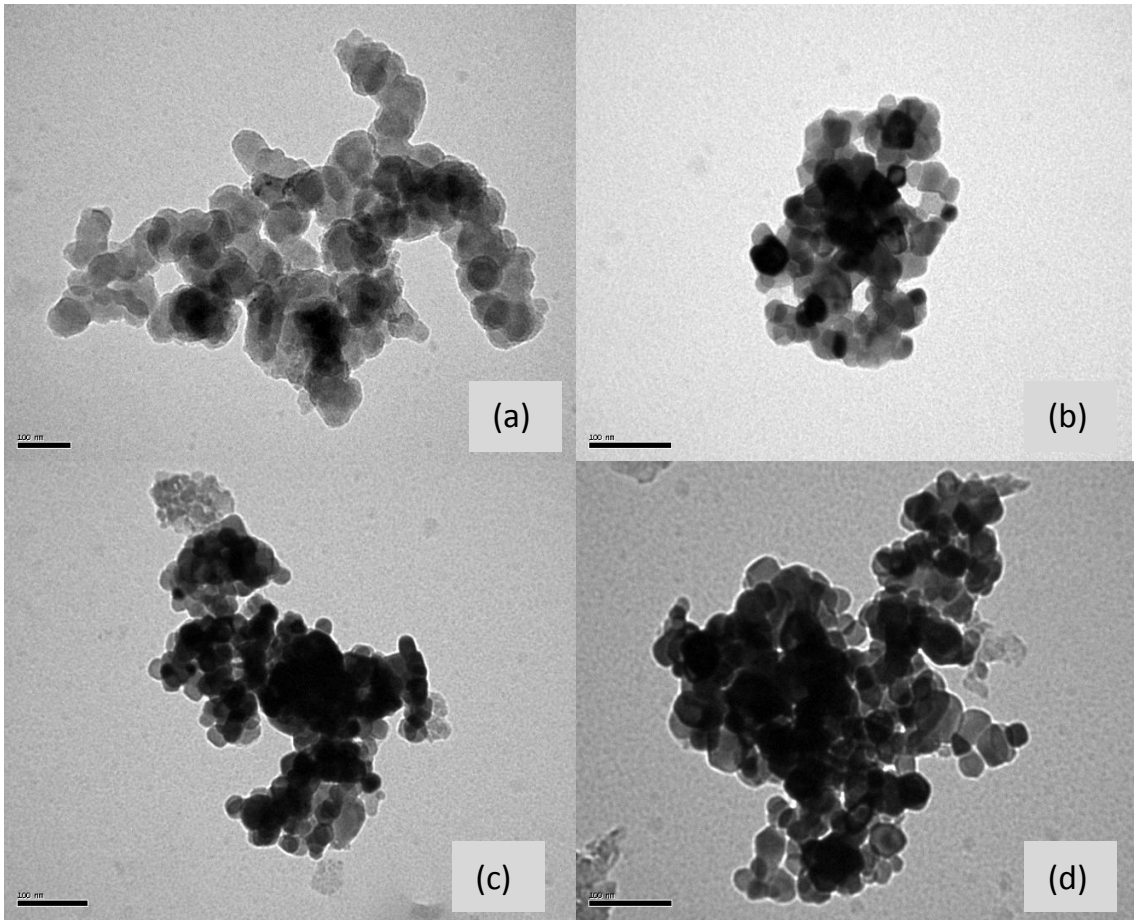

Figure 6. TEM picture of as-synthesized precursors a) G/N= 0.71 calcined at 900°C, (b) G/N= 0.71 calcined at 1000°C, (c) G/N= 0.60 calcined at 1000°C and (d) G/N= 0.71 calcined at 1200°C.

microwave assisted self-ignition process. Microwave assisted glycene – nitrate gel combustion synthesis has outstanding potential for producing nanocrystalline alumina powders. The technique produced pure, homogeneous and nanocrystalline Al_2O_3 particles, which are essential and beneficial to sintering and also to make transparent alumina ceramics.

The γ-Al_2O_3 crystallites appeared at 900°C with particle size of about 38 nm, and there was only a slight increase in grain size with the increase of calcination temperature, γ-Al_2O_3 crystallite almost disappeared and α-Al_2O_3 crystallite rapidly grew up to 52 nm at 1200°C when the transformation was just completed. The increasing molar ratio of G/N was found to be in favour of γ- to α-Al_2O_3 phase transition, whereas the precursor with G/N=0.71 at 900°C yielded a relatively well dispersed ultrafine α-Al_2O_3 powder with particle size of 38 nm. The mechanism of the combustion reaction is quite complex and fuel-to-oxidizer ratios and Millipore water is one of the most important parameters that influence the reaction. The

combustion of glycene-nitrate mixture appears to undergo a self-propagating and non explosive exothermic reaction.

REFERENCES

Yi-quan W, Yu-feng Z (2001). “Preparation of plate like nanoalpha alumina particle”, Ceramic Int. 27:265-268.

Edrissi M, Norouzbeigi R (2007). “Synthesis and characterization of alumina nanopowders by combustion of nitrate-amino acid gels”, Mater. Science-Poland. 25(4).

Shojaie-Bahaabad M, Taheri-Nassaj E (2008). ” Economical synthesis of nano alumina powder using an aqueous sol–gel method”, Mater. Lett. 62:3364–3366.

Robert I, Ioan L, Cornelia P (2009). “The influence of combustion synthesis conditions on the *a*-Al_2O_3 powder preparation”, J. Mater. Sci. 44:1016–1023.

Mimani T, Patil KC (2001). “Solution combustion synthesis of nanoscale oxides and their composites”, Mater. phys. mech. 4:134-137.

Ananthapadmanabhan PV, Thiyagarajan TK, Sreekumar KP, Venkatramani N (2004). “Formation of nano-sized alumina by in-flight oxidation of aluminium powder in a thermal plasma reactor”, Scripta Materialia, 50:143–147.

Shaoyan W, Xiaoan L, Shaofeng W, Yang L, Yuchun Z (2008). “Synthesis of γ-alumina via precipitation in ethanol” Mater. Lett. 62:3552–3554.

Mirjalili F, Hasmaliza MB, Chuah AL (2010). ”Size-controlled synthesis of nano α- alumina particles through the sol–gel method”, Ceramics Int. 36:1253–1257.

Chyi-Ching H, Tsung-Yung W, Jun W, Jih-Sheng T (2004). ”Development of a novel combustion synthesis method for synthesizing of ceramic oxide powders”, Mater. Sci. Eng. B, 111:49-56.

Ganesh I, Ferreira JMF (2007). “Influence of Phase Composition on Sintered Microstructure of Combustion Synthesized Oxides”, Research Letters in Materials Science, Vol.2007, Article ID 91376, P. 5.

Singanahally TA, Alexander SM (2008). “Combustion Synthesis and Nano materials”,Current opinion in solid state and Materials Science, 12(3-4):44-50.

Edrissi M, Norouzbeigi R (2008). Taguchi optimization for combustion synthesis of aluminium oxide Nano-particles, Chinese J. Chem. 26:1401-1406.

Tianyou P, Xun L, Ke D, Jiangrong X, Haibo S (2006). ” Effect of acidity on the glycine–nitrate combustion synthesis of nanocrystalline alumina powder”, Mater. Res. Bulletin. 41:1638–1645.

Jiang L, Yusong W, Yubai P, Jingkun G (2007). ”Alumina precursors produced by gel combustion”, Ceramics Int. 33:361–363.

Xiujing Z, Yan FGC (2006). Combustion Synthesis of the nano-structured alumina powder, Nano Science. 11(4):286-292.

Ganesh I, Johnson R, Rao GVN, Mahajan YR, Madavendra SS, Reddy BM (2005). Microwave assisted combustion synthesis of nanocrystalline MgAl2O4 spinel powder. Ceramic Int. 31:67-74.

Mangalaraja RV, J. Mouzon, Hedström P, Carlos CP, Ananthakumar S, Odén M (2009). “Microwave assisted combustion synthesis of nanocrystalline yttria and its powder Characteristics”, Ceramic Int. 35(3):1173-1179.

Toniolo JC, Lima MD, Takimi AS, Bergmann CP (2005). “Synthesis of alumina powders by the glycine-nitrate combustion process”, Mater. Res. Bulletin. 40:561-571.

UPCOMING CONFERENCES

14th International Conference on Accelerator and Large Experimental Physics Control Systems. The Hyatt Regency Embarcadero Center San Francisco, California October 6-11, 2013

December 6-7, 2013 Sydney, Australlia 2013 5th International Conference on Signal Processing Systems

Conferences and Advert

October 2013
14th International Conference on Accelerator and Large Experimental Physics Control Systems. The Hyatt Regency Embarcadero Center San Francisco, California October 6-11, 2013

December 2013
5th International Conference on Signal Processing Systems Sydney, Australlia, December 6-7, 2013

International Journal of Physical Sciences

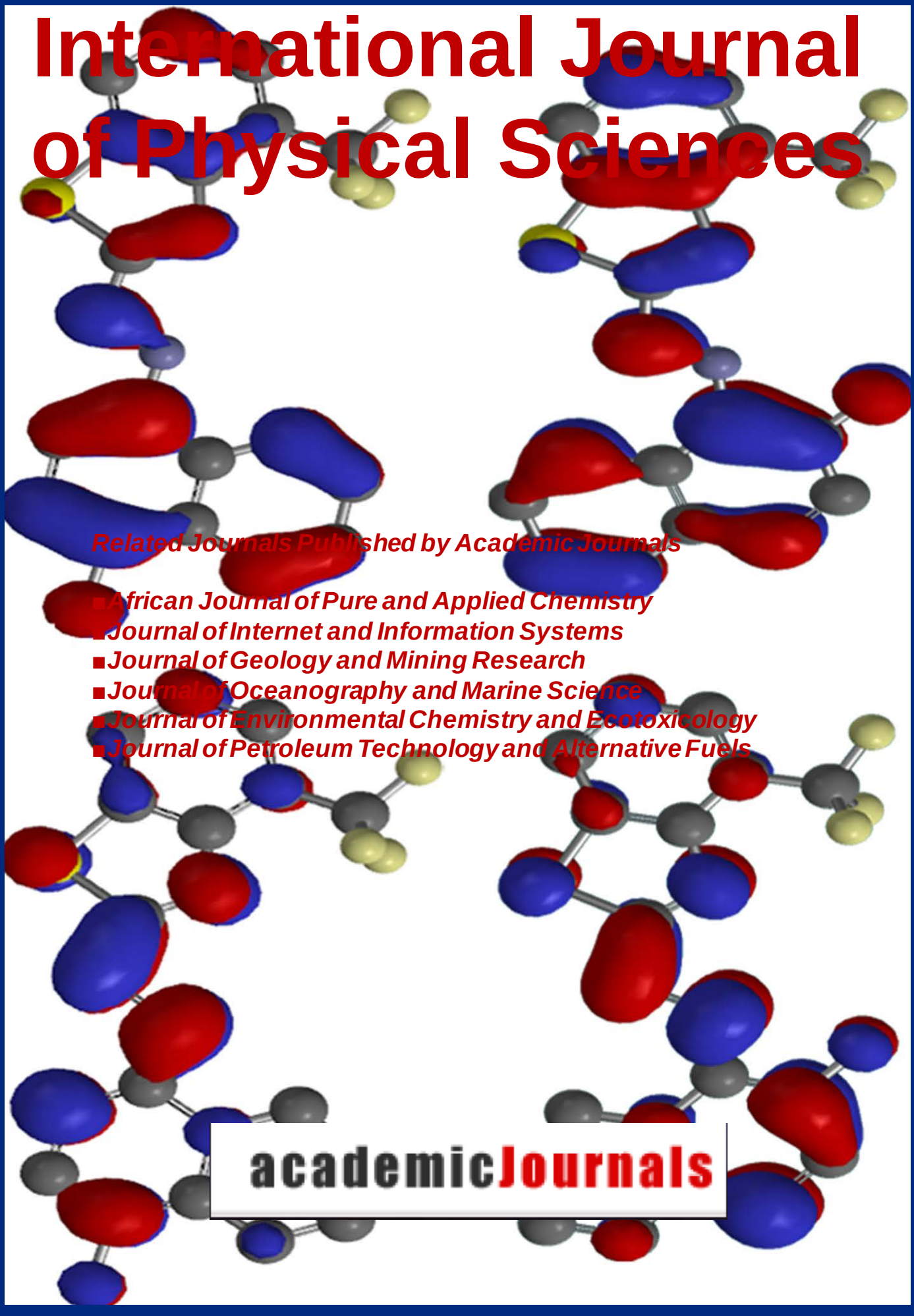

Related Journals Published by Academic Journals

- *African Journal of Pure and Applied Chemistry*
- *Journal of Internet and Information Systems*
- *Journal of Geology and Mining Research*
- *Journal of Oceanography and Marine Science*
- *Journal of Environmental Chemistry and Ecotoxicology*
- *Journal of Petroleum Technology and Alternative Fuels*

academicJournals